Mechanistic and Structural Insights into the Chemical Modulation of Amyloid Aggregation

By

Kyle J. Korshavn

A dissertation submitted in partial fulfillment
of the requirements for the degree of
Doctor of Philosophy
(Chemistry)
in the University of Michigan
2017

Doctoral Committee:

Professor Mi Hee Lim, Ulsan National Institute of Science and Technology, Co-Chair
Professor Ayyalusamy Ramamoorthy, Co-Chair
Professor Carol A. Fierke
Professor Brandon T. Ruotolo
Professor Anna A. S. Schwendeman

2017

ii

a researcher and have become part of my family here at Michigan. From the Ramamoorthy lab, my thanks are extended to Dr. Kazutoshi Yamamoto, Dr. Rongchun Zhang, Dr. Kamal Mroue, Dr. Rongchung Zhang, Dr. Rui Huang, Dr. Meng Zhang, Dr. Elke Prade, Dr. Thirupati Ravula, Joshua Damron, and Katie Gentry. I must give an extra thanks to the RAMyloid team members who have been a joy to work with over the years, Dr. Jeff Brender, Dr. Patrick Walsh, Dr. Sam Kotler, Dr. Amit Pithadia, Kian Kamgar-Parsi, Sarah, Cox, and Chris MacDonald. Amyloid proteins are frustrating to work with on their best days and unbearable at their worst. Having such amazing people to share my office, frustrations, and daily caffeine with made all of those frustrations bearable.

My work brought me to questions that were difficult to answer independently and thus I was privileged to work with many wonderful collaborators. Dr. Stefano Manfredini was gracious enough to provide me with a new suite of small molecules to investigate. Dr. Anirban Bhunia was vital in my studies investigating the structural transitions of membrane-peptide interactions. Much of what I know about NMR was learned by working side by side for a year and on long car rides between Ann Arbor and Lansing. Finally, Dr. Young-Ho Lee and Dr. Carmelo La Rosa have provided invaluable conversations regarding my studies of the mechanisms behind membrane-protein interactions and aggregation.

My family has always supported me throughout my time at Michigan. My parents, Stuart and Tina, have always been my support, tolerating phone calls or texts at random times of day and night to either celebrate my accomplishments or commiserate together against protein that had aggregated either to quickly or not quickly enough. All that I have been able to accomplish in my life is because of their love, support, and belief in my ability to do anything; I continue to strive daily to become the type of person of whom they can be proud. My brothers, Evan and

Drew, have finally accepted me into the cool, older kids club. Despite being the youngest, they have treated me as their equal and supported me in all that I have tried to do. My grandparents, who are no longer with us, have inspired much of what I have set out to do with my life. Grammy Marie and Papa Martin were a source of constant love and support, reminding me that no matter what happened, there would always be a Werther's butterscotch and a hug waiting for me. My Grandpa Sherman's long fight with dementia initially inspired me to pursue a career in science. Growing up watching an amazing and accomplished man slowly lose himself, I was driven to understand why and how in order to help prevent other children and other families from feeling what I felt during that time. My Grandma Fran was the strongest person I have ever or will ever have the pleasure of meeting. Through multiple successful fights against cancer, she was the rock of our family. She was the head chef, the event coordinator, and my biggest fan. Watching her persevere through both her own struggles while always caring for my grandfather taught me a strength that does not exist outside of love. That strength continues on within our family and has held me fast when I have felt myself falling away. It will continue to drive me on.

Finally, my source of constant joy (and occasional consternation) throughout my time at Michigan has been my fiancée Cassie. Despite my quirks, my flaws, and my annoying habit to quote nerdy movies and the Hamilton soundtrack at all hours of the day and night, she continues to put up with me and has stood by my side. She is my best friend that I am excited to spend the rest of my life with. She continues to amaze and inspire me, motivating me to constantly be the best version of myself that I can be.

Table of Contents

List of Figures

List of Appendices

Abstract

The aggregation of amyloid-beta (Abeta) is implicated in the etiology of Alzheimer's disease (AD). Aggregation *in vivo* permits interactions with transition metal ions and lipids of the cell membrane. Abeta-metal interactions are suggested to induce metal ion dyshomeostasis and promote oxidative stress while Abeta-membrane interactions catalyze the formation of specific oligomers which destabilize and permeabilize the lipid bilayer. Oxidative stress may also modulate bilayer integrity through acyl chain peroxidation which causes membrane thinning. The structural and mechanistic effects of these interactions on the aggregation of Abeta remain unclear. Multiple glycosidic polyphenol natural products and their esterified derivatives were investigated for their ability to function as molecular probes against metal-Abeta. The interactions between Abeta and thin model membranes were also investigated through a combination of NMR spectroscopy, fluorescence spectroscopy, and atomic force and transmission electron microscopies.

The natural products **Phlorizin**, **Verbascoside**, and **Rutin** were all evaluated for their ability to modulate metal-Abeta aggregation. **Verbascoside** effectively inhibited aggregation while its esterified derivative, **VPP**, showed similar efficacy *in vitro*. Both compounds were also capable of disaggregating preformed fibrils, though they bound to both the monomeric and fibrillar forms of Abeta through distinct mechanisms. Esterification greatly reduced **VPP**'s ability to inhibit metal-Abeta cytotoxicity, however.

Subsequently, the interaction and aggregation of Abeta with both thick (DOPC or POPC) and thin (DLPC) model membranes was evaluated. tr-NOESY and relaxation based NMR experiments probed monomer interaction on the bilayer surface; folding was conserved regardless of bilayer thickness, suggesting that the preliminary interaction is exclusively driven by surface contacts. Additionally, the work provides the first experimentally derived structural constraints for membrane-associated Abeta. The progression of Abeta from its conserved, folded, monomeric state to its aggregated state was monitored in the presence of thick and thin membranes. DLPC bilayers uniquely stabilized membrane associated oligomers while simultaneously destabilizing the bilayer. DLPC also remodeled preformed fibrils into a pseudo-unfolded state which resembles protofibrillar aggregates.

These results provide a new reagent with potential applications as a probe against metal-Abeta *in vitro* and insights into early structures of membrane-associated Abeta and mechanisms by which membrane structure can modulate the Abeta aggregation.

Chapter 1

Introduction to Proteins, Metals, and Membranes in Alzheimer's Disease

Portions of this chapter were adapted from the following publications:

> Lee, H. J., Korshavn, K. J., Kochi, A., Derrick, J. S., Lim, M. H. Cholesterol and Metal Ions in Alzheimer's Disease. *Chem. Soc. Rev.* **43**, 6672-6682 (2014); Beck, M. W., Pithadia, A. S., DeToma, A. S., Korshavn, K. J., Lim, M. H. in *Ligand Design in Medicinal Inorganic Chemistry*, Storr, T., Ed.; John Wiley & Sons, Ltd: Chinchester, West Sussex, **2014**, 257-286.

1.1.   Introduction to Alzheimer's disease

In November of 1906, Dr. Alois Alzheimer first presented the case of a 50 year old female patient who had presented paranoia, sleep disruptions, memory loss, and mood changes. Upon examining the brain of this patient postmortem, he observed the presence of proteinaceous aggregates with in the brain's histology.[1] This marked the first discussion of a disease which now bears its discoverer's name, Alzheimer's. In the 110 years since this initial discussion, Alzheimer's disease (AD) has become one of the most widely recognized mental disorders to the lay public. As of 2015, an estimated 46.8 million individuals were believed to be living with AD worldwide; it is expected that the number of afflicted individuals will increase to at least 130 million by the year 2050.[2] Within the United States of America, between 2000 and 2013, deaths caused by AD have increased by 71%, from 17.6 individuals per 100,000 in 2000 to 26.8 individuals per 100,000 in 2013 (Fig. 1.1).[3] In contrast, the five other leading causes of death, breast cancer, prostate cancer, heart disease, stroke, and HIV, have all seen their mortality rates decrease over the same time period (Fig. 1.1b). Despite over a century of research into the

1
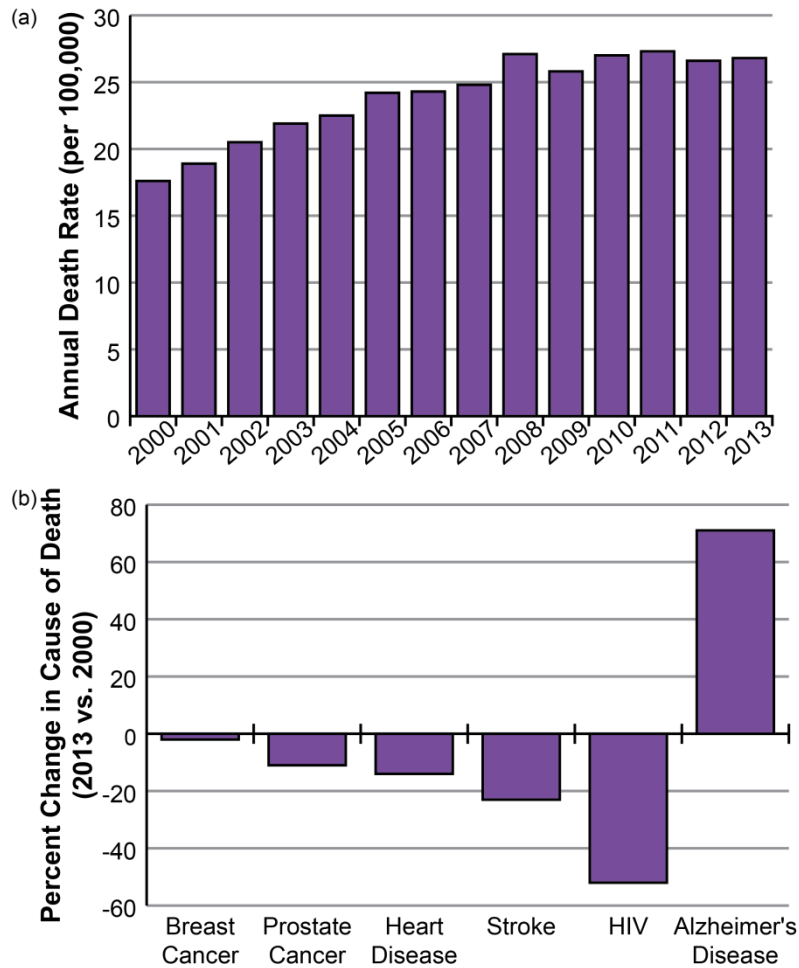
Figure 1.1. Mortality rates associated with AD. (a) The death rate associated with AD has gradually increased since 2000. (b) From 2000 to 2013, of the 6 leading causes of death in the United States, only AD has seen an increase in disease associated deaths. Figures adapted from reference 3.

causes, effects, and potential treatments of AD, we remain unable to effectively regulate the disease.

1.2.   Molecular pathology of AD

A major hindrance to the development of effective therapeutics against AD progression and death is the complex pathology which underlies the disease. This complexity has obfuscated the identification of a singular mechanism by which neuronal damage and death occur in AD and has subsequently prevented the development of effective and targeted biological or chemical

2

interventions. Due to the initial observation by Dr. Alzheimer of proteinaceous aggregates in the brains of diseased patients, AD is commonly discussed as a protein folding disease, involving both the peptide amyloid-β (Aβ) found within senile plaques and hyperphosphorylated tau protein observed in neurofibrillary tangles.[4-6] Along with the misregulation of protein folding, it has also been suggested that metal ion dyshomeostasis may be culpable in AD-related toxicity; defects in metal ion regulation have also been suggested to foster and environment of heightened oxidative stress in the brain.[7,8] Disruption of neuronal lipid bilayers, caused by protein dyshomeostasis, has also been suggested to facilitate cellular death.[9] Finally, it was proposed that reductions in the levels of the neurotransmitter acetylcholine could be causative in AD progression.[10,11] While most current FDA approved drugs against AD are targeted against this hypothesis, it has become more widely accepted that this misregulation is the result of disease progression, as opposed to causative.[10-12] With the multitude of pathways implicated in cellular malfunction in AD, it is unsurprising that an effective therapy continues to be elusive. While it remains to be seen what role each of these individual mechanisms plays in disease pathogenesis and progression, consensus is growing that many of these factors and pathways are interrelated. The modulation of one may result in changes in others aspects of the disease as well, and therapeutically targeting a single pathway may be minimally efficacious.[4,6,7,9,13]

1.2.1. Amyloid hypothesis of AD

As one of the two protein aggregates initially observed in the brains of AD patients, Aβ was associated very early on with AD pathogenesis.[6,13] The implication of Aβ as a key component of AD related neurotoxicity rose to prominence with the introduction of the amyloid cascade hypothesis first proposed in the early 1990s.[14,15] Aβ, encompassing a variety of peptide isoforms ranging from 38 to 43 residues, results from the proteolysis of the transmembrane

3

amyloid precursor protein (APP) by β- and γ-secretase enzymes (Fig. 1.2a).[4,6,13] However, APP is also capable of creating a non-amyloidogenic, truncated peptide when it is cleaved by α-secretase instead of β-secretase. Despite the many isoforms of Aβ which have been observed, the 40 and 42 residue isoforms are the most prevalent in the brains of AD patients.[6,13] It is also thought that $A\beta_{42}$ is the more toxic of the two predominant species while $A\beta_{40}$ is the most common product of APP cleavage.[4]

As a monomeric peptide, Aβ is relatively inert and non-toxic; it has been proposed that Aβ may possess some neuroprotective functions, though the extent of these protective roles remains controversial.[16-18] It is suggested that Aβ only enacts its toxic function during and after its transformation into an amyloidogenic fiber.[4,6,13,19] Like other amyloid forming peptides and proteins, Aβ is proposed to undergo a nucleation dependent polymerization mechanism to form amyloid fibrils(Fig. 1.2b).[20,21] In this aggregation pathway, monomers interact to form small oligomers. These oligomers then combine with each other and/or monomeric subunits to generate larger oligomers, eventually forming a large protofibrillar species. Once the protofibril is generated, it is able to rapidly elongate and generate mature fibrils.[21] These fibers are able to subsequently fragment into shorter segments which are capable of catalyzing additional elongation and subsequently generate additional fibrils.[22] While the initial amyloid hypothesis has suggested that the end stage fibrils were the principle toxic species, a more recent shift within the field now posits that intermediate oligomers are the culprit.[14,19,23] It remains unclear, however, at what point these purported toxic oligomers are formed during aggregation. It is possible that they are either on pathway towards aggregation or off-pathway variants that result from improper amyloid formation.[23]

A leading hindrance to better understanding the identity and function of toxic Aβ oligomers is a lack of structural insight into distinct oligomeric species. The monomeric state of Aβ is well established to be predominantly unstructured and random coil, though some studies have identified a lowly populated partially helical structure in solution which can be stabilized by the presence of detergents (Fig. 1.2c).[24-27] The end stage fibrils are also well characterized due to their extreme stability.[28-33] The wealth of structural data has revealed the ability of Aβ to generate a variety of stable polymorphs which depend on the peptide isoform and the aggregation conditions (Fig. 1.2d).[34] It remains unclear, however, how end stage fiber polymorphism is controlled by aggregation conditions and whether the intermediates formed on the way to distinct polymorphs are similarly unique or whether polymorphism is only dictated at the end of Aβ aggregation. Meanwhile, the relatively transient nature of intermediate oligomers has rendered them a black box; while it is known that they exist and that there are varieties, details about the kinetics of their formation or their structure are unknown for the most part.

Some initial investigations have begun to probe oligomer structure, though they often rely on low resolution techniques or additional chemical modification to stabilize the intermediate species. Conformation specific antibodies have provided the most rudimentary tool to distinguish amyloid aggregate structures.[35] A11 is capable of binding globular, prefibrillar oligomers while OC binds to the cross-β strand structure common to many amyloids.[36,37] While these tools are useful in histological examination and some high throughput studies, they lack insight at the molecular level. Methods such as AFM have had better luck at distinguishing distinct oligomeric species. While molecular dynamics (MD) simulation has been used to augment these investigations, there is still little experimental data exploring the atomic resolution of oligomeric structure.[38]

Higher resolution methodologies such as crystallography and NMR have had recent success in providing constraints on some unique oligomeric species. Crystallographic investigations continue to require short peptide fragments, however, and predominantly generate fibrillar or prefibrillar structures.[34,39-41] NMR based studies, meanwhile, benefit from their ability to utilize full length Aβ peptide. However, these studies require extremely high concentrations of peptide to generate their stable intermediates, raising questions about the relevance of the observed intermediates and whether they are the result of traditional amyloid aggregation or are the result of artificially high peptide concentration.[42,43] These preliminary investigations of Aβ oligomers emphasize the technical difficulty which accompanies the study of lowly populated and transient oligomeric states. What is more, these studies show that the potential oligomers likely possess a diversity similar to that already observed in end stage fibers, which poses a great challenge to the community as it works to fully characterize the aggregation of Aβ from its freshly cleaved, monomeric state all the way to its terminal fiber. It should also be noted that the majority of these structural studies exploring the monomer, intermediate aggregates, and fibrils all occur *in vitro* and, almost always, in the absence of additional biomolecules. It is known that Aβ interacts with a variety of other molecules *in vivo* and that these interactions are capable of further modulating the aggregation of Aβ.[6,7,9,44,45] Investigations of the impact of these heterogeneous environments are occurring in parallel with the studies of Aβ alone described above.
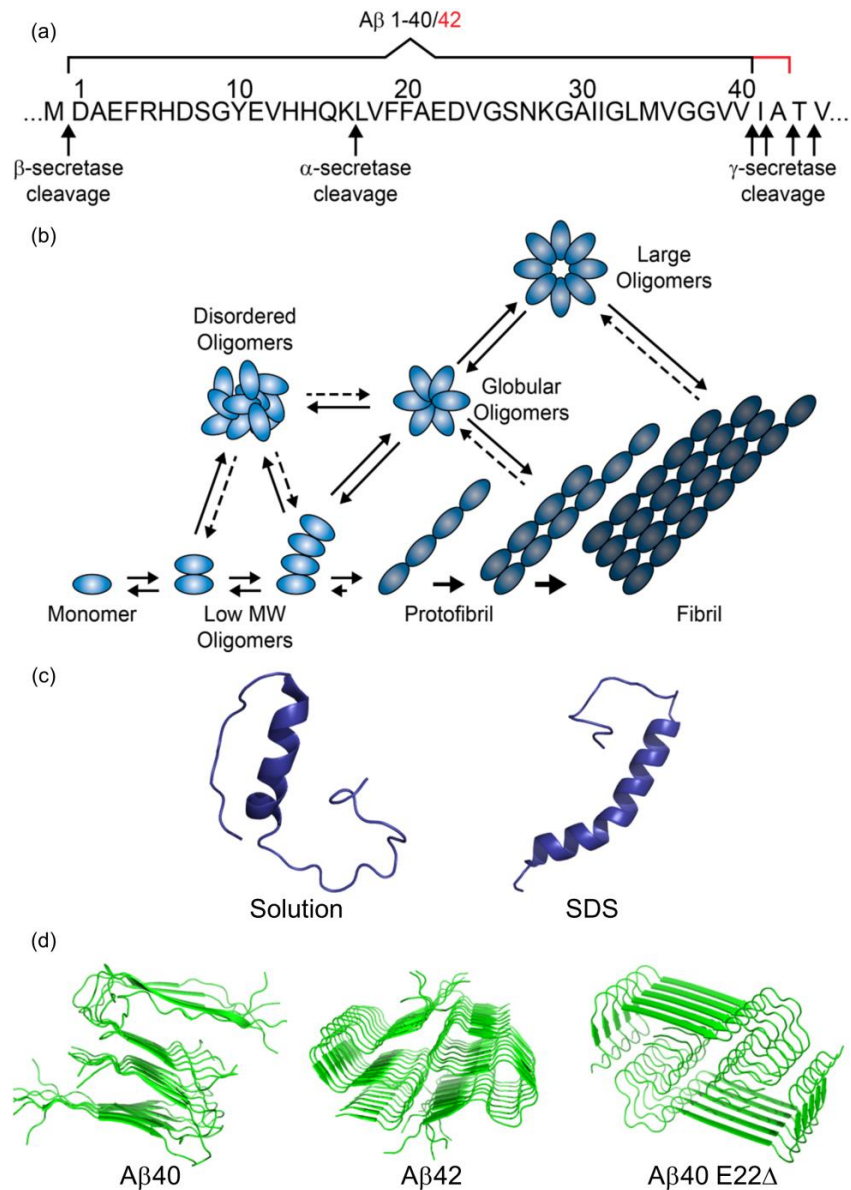
Figure 1.2. Amyloid formation by Aβ. (a) Monomeric Aβ is derived via the proteolytic cleavage of the transmembrane protein APP. Cleavage by β- and γ-secretase produces the full length, amyloidogenic peptide. A lack of specificity in γ-secretase cleave is partly responsible for the generation of various isoforms like Aβ40 and Aβ42. (b) After monomeric Aβ is generated, it undergoes a nucleation-dependent polymerization reaction to eventually form fibrils. During its aggregation, it is able to form both on- and off-pathway aggregates whose presence and structure is dependent upon solution conditions. (c) While monomeric Aβ is traditionally considered an intrinsically disordered peptide, devoid of structure, solution NMR studies have observed structured species in solution as well as in the presence of the detergent SDS.[25,26] (d) Amyloid fibrils have an array of polymorphs which are dependent upon their solution conditions as well as their sequence. Variations in both their C-terminal sequence and mutations such as the Osaka mutation (E22Δ) can dramatically alter the final structure.[30-32]

7

1.2.2. Metal ion hypothesis of AD

Just as proteostasis is proposed to be disrupted in AD due to the aggregation of Aβ and hyperphorphorylated tau protein, so too are metal ions suggested to be misregulated.[4,7] Metals serve a wide range of functions within the brain, including acting as secondary messengers in cellular signaling, stabilizing protein structure, acting as enzymatic cofactors, and transporting dioxygen (O_2).[7,46,47] Within AD, however, metal ions such as Zn(II), Cu(I/II), and Fe(II/III) enter a state of dyshomeostasis. In this diseased state, metal ions become miscompartmentalized and the cell is susceptible to entering a state of heightened oxidative stress.[7,46] The altered distribution of metals can induce non-native conformations in metalloproteins and deactivate metalloproteins through a loss of metal active sites or cofactors.[4,7,48,49] Loss of functional native proteins, such as the antioxidants Cu/Zn superoxide dismutase (SOD1) and cytochrome *c* oxidase (C*c*O), coupled with the coordination of redox active metals like Cu(I/II) and Fe(II/III) in non-native environments is also capable of generating reactive oxygen species (ROS) and promoting oxidative stress.[7,47] The increased presence of ROS may, in turn, promote oxidative damage of both proteins and lipids which further destabilizes proteins and the cellular membranes.[4,7,50,51] Prolonged exposure to oxidative stress is damaging to the mitochondria and one mechanism by which metal ion dyshomeostasis is capable of directly mediating cellular death in AD.[52,53]

Along with disrupting normal functions within the brain, aberrant metal behavior is capable of exacerbating the aggregation of Aβ.[4,7,13,44,54] The transition metal ions Zn(II), Cu(I/II), and Fe(II/III) were all observed to be present in the senile plaques of AD patients at concentrations 3-5 times higher than the sounding tissue.[54,55] Subsequent *in vitro* studies have shown that all three metals can coordinate with Aβ, generating metal–Aβ complexes;

furthermore, it has been suggested that coordination of Aβ to either Cu(I/II) or Zn(II) can alter the aggregation of the peptide (Fig. 1.3).[4,7,46] The redox inactive Zn(II)-Aβ complex is coordinated through either four or six donor atoms originating from histidine side chains and amide backbone heteroatoms within the first sixteen residues of the peptide sequence.[44,56] The coordination of Cu–Aβ is dynamic and pH dependent.[7,46,57] The predominant coordination at physiologically relevant pH (i.e., 7.4) for Cu(II) is 3N1O (three nitrogen donor atoms and one oxygen donor atom; believed to be His6, His13/14, N-terminal amine, and Asp1 carboxylate) while Cu(I) adopts a 2N (two nitrogen donor atoms; suggested to be His13 and His14) coordination sphere.[58] Along with altering the aggregation of Aβ, Cu–Aβ species have a redox potential = 0.30 V versus normal hydrogen electrode (NHE).[7,46,58] Few structural studies have been reported for iron coordination to Aβ due to the propensity of Fe(II) to oxidize to Fe(III) and
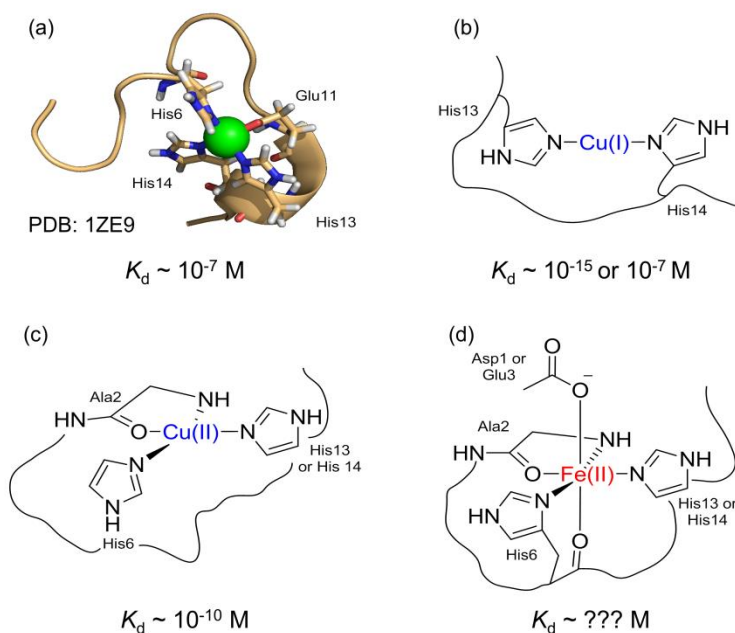
Figure 1.3. Metal ion coordination by monomeric Aβ. Monomeric Aβ is able to coordinate to (a) Zn(II), (b) Cu(I), (c) Cu(II), and (d) Fe(II) *via* the first 16 residues of the sequence. Current estimates for the affinity of the complexes range from high nM to low pM.[7,44,46]

precipitate as $Fe(OH)_3$ and other complexes.[58] Preliminary results propose that Asp1, Glu3, and His6/13/14 may be involved in Fe(II) coordination by Aβ.[58] Like Cu–Aβ, Fe–Aβ is redox active; in the Aβ–iron–nitriloacetic acid complex the redox potential was measured to be 0.23 V versus NHE.[59]

1.2.3. Membranes and Aβ in AD

As a disease of systemic dyshomeostasis and perturbation, AD extends beyond the changes in protein folding and metal ion distribution discussed above and disrupts many aspects of cellular metabolism.[60,61] Lipid metabolism is particularly impacted.[62-65] Because lipids play a crucial role in maintaining cellular homeostasis across the neuronal bilayer, facilitate the transport of materials throughout the cell, and mediate the production and aggregation of Aβ their modulation has wide ranging impacts on AD pathology.[64-66]

Many toxic mechanisms have been proposed for Aβ aggregates in AD.[23] A prominent model proposes that the interaction of various Aβ aggregates with the surface of the neuronal membrane is capable of disrupting bilayer integrity.[9,65] Ionic depolarization across neuronal bilayers has long been associated with AD which implicates a potential pathway of membrane permeabilization.[67,68] A structural basis for these toxic interactions remains unclear, however. Studies have suggested that Aβ is capable of forming pore-like structures which span the neuronal bilayer and facilitate the influx of Ca^{2+}.[68-70] Such pores have been detected for both $Aβ_{40}$ and $Aβ_{42}$, the Osaka mutant $Aβ_{40}(ΔE22)$ as well as a D-enantiomer sequence of $Aβ_{40}$ which suggests a highly conserved aggregation intermediate.[68,69,71-73] Common to many of these observed channels is a specificity to Ca^{2+}; other metal ions, such as Zn^{2+} and Al^{3+}, are unable to traverse these channels while also blocking the influx of Ca^{2+}.[68,69,73]

The transient and inhomogeneous formation of these proposed pore-like structures has made them difficult to characterize structurally. Atomic force microscopy (AFM) based measurements have observed pore like structures on synthetic bilayers which vary in their size and subunit arrangement.[38,74,75] MD simulations based around these observed pores, coupled with solid-state NMR structures of the cross-β-strand fiber structures, have produced initial β-barrel models which seek to explain the formation of these transmembrane pores.[38] These models are incomplete, however, because they base their structural modeling on the assumption of a β-strand peptide with minimal experimental evidence. More recent exploration of membrane-associated Aβ aggregates has observed another β-barrel structure by NMR using peptide trapped in detergent micelles.[76] While this lends credence to the ability of Aβ to form β-barrels in hydrophobic environments, the use of detergent-based membrane mimetics reduces the value of comparing the NMR-based model with that derived from AFM performed on bilayers. Additional exploration is certainly required to better define the structural arrangement of membrane-associated Aβ pores.

Accompanying pore formation, large scale membrane permeabilization has been reported to result from Aβ aggregation on the lipid bilayer surface.[69] As opposed to pore formation which allows the specific influx of Ca^{2+}, membrane permeabilization results in the unconstrained transit of both ions and larger biomolecules across the membrane. In this way, the cell is not just depolarized, but loses all internal equilibria. Combined, these two distinct modes of disruption pose a two-step mechanism by which lipid bilayers may be permeabilized (Fig. 1.4). It remains unclear whether pore formation must precede membrane disruption or if the two mechanisms are decoupled from each other.[69] Additionally, while pore formation has been found to be a consistent mechanism across various peptide sequences and membrane model systems,
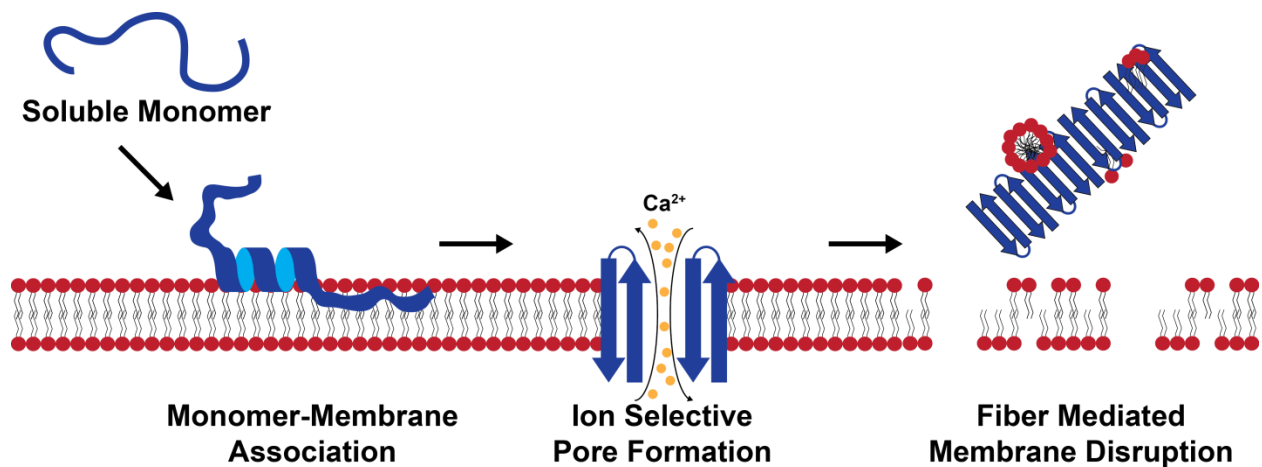
Figure 1.4. Modes of membrane disruption by Aβ. Aβ is able to interact with lipid bilayers through a variety forms. Disruption by aggregates has been proposed to predominantly occur through pore formation and fiber-associated permeabilization.[69]

membrane permeabilization by Aβ has been suggested to be specific for bilayers which contain the lipid GM1 ganglioside within *in vitro* model systems.[69] This requirement does not preclude permeabilization from occurring *in vivo*. GM1 ganglioside is known to incorporate into lipid rafts and GM1 ganglioside clusters while fulfilling a variety of functions within cellular bilayers.[77] Additionally, Aβ oligomers have been isolated from mouse interstitial fluid which contain stabilized GM1 ganglioside clusters. [78] Coupled with *in vitro* results suggesting that GM1 gangliosides are able to specifically catalyze toxic modes of Aβ aggregation, it suggests that GM1 is able to play a crucial physiological role in the membrane-associated aggregation of Aβ.[45] Thus, while the general aggregation pathways of Aβ in solution are dependent upon the isoforms of peptide, aggregation upon lipid bilayers is seemingly equally dependent upon the bilayer composition. This complicates the search for structural and mechanistic insights into the roles of membrane-mediated Aβ aggregation in AD. Not only must all relevant peptide sequences be interrogated, but relevant lipid bilayer compositions must also be considered.

1.3. Molecular probes of amyloid misfolding

Current therapeutic interventions against AD provide temporary symptomatic relief; the five USA Food and Drug Administration (FDA) approved compounds for AD treatment are either acetylcholinesterase (AChE) inhibitors or *N*-methyl-D-aspartate (NMDA) receptor inhibitors (Fig. 1.5).[7,20,79] Meanwhile, therapeutics targeting what are believed to be the causative aspects of AD have experienced limited clinical success.[80-84] While potential drugs fail in clinical trials for a variety of reasons, it seems likely that AD therapeutics often fail due to a lack of understanding regarding the underlying molecular pathologies.[67,83,84] Thus, the development of tools which are capable of interrogating individual aspects of AD, such as amyloid formation or metal ion dyshomeostasis, as well as multifunctional tools which are capable of simultaneously exploring the link between pathological factors is beneficial.[85-93] Through the application of molecular probes it may be possible to better identify viable sites for therapeutic intervention within AD.
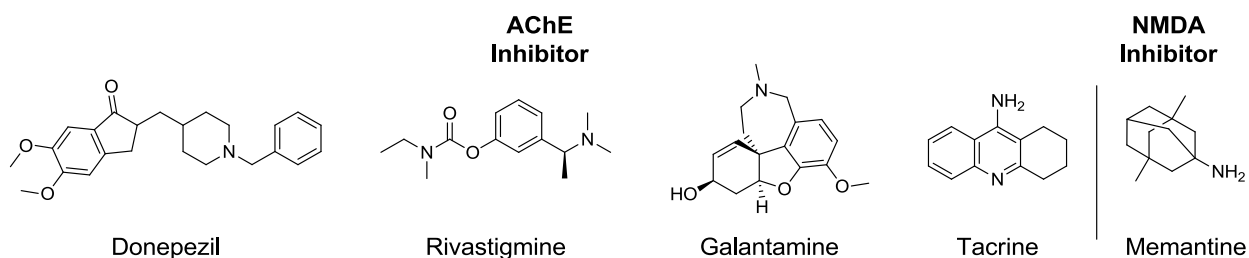
Figure 1.5. FDA approved drugs for the treatment of AD. Four currently approved therapeutics act as AChE inhibitors: donepezil, rivastigmine, galantamine, and tacrine. Memantine acts as an NMDA inhibitor.

1.3.1. Chemical modulators of amyloid aggregation

While it is highly advantageous to develop chemical agents capable of selectively modulating the aggregation of Aβ, the identification and characterization of such tools is a daunting task. Amyloid formation by Aβ can be modulated by a variety of chemicals common to protein biochemistry, including detergents, like sodium dodecyl sulfate (SDS), and chemical

denaturants, such as guanidinium chloride.[26,76,94-99] These reagents are extremely non-selective in their action, however. They are capable of intervening at many different steps in the aggregation of Aβ, are non-selective for Aβ aggregation, and are unsuitable for application in *in vivo* systems. Thus, the development of specific molecular and biomolecular tools is essential.[100]

1.3.1.1. Peptide-based tools

Early exploration of molecular modulation of Aβ aggregation took advantage of the self-recognition sequence in the middle of the Aβ sequence.[89] It is known that $Aβ_{16-20}$ (KLVFF) acts as a nucleating site for early aggregation events towards fibrillation.[4,89] It was observed that the pentapeptide derived from this central sequence is capable of inhibiting fibril formation by full length $Aβ_{40}$ and $Aβ_{42}$.[101,102] However, because the pentapeptide was derived from the amyloidogenic sequence of full length Aβ the truncated construct was also capable of forming fibrillar structures, though the kinetics of their formation are much slower than for $Aβ_{40}$ and $Aβ_{42}$.[101,103] Based on this initial success, peptide variants have subsequently been explored. Proline mutations were scanned through fragments of the central sequence of Aβ, and the substitutions were observed to reduce the propensity of the peptide to form fibrillar aggregates while maintaining the ability to modulate fibrillation by full length Aβ.[104,105] The mechanistic success of peptide fragments as amyloid modulators has spurred advances in stabilized peptides and peptidomimetics which have the advantage of increased stability and bioavailability *in vivo*.[106,107] Cyclization of the KLVFF sequence generated a more stable variant of the fragment which successfully stabilized small oligomers of reduced toxicity.[108] The appendage of the KLVFF sequence onto a branched dendrimer framework similarly increased the reagent's stability while maintaining the anti-amyloidogenic activity of the sequence.[109] The overall success of these peptide-based tools has led to the development of a whole class of reagents

termed β-sheet breakers which have subsequently been implemented in a variety of amyloid-related protein folding problems.[89,110] While these β-sheet breakers initially were peptide sequences exclusively, they are now a mix of both peptide-based and small molecule tools.[110]

1.3.1.2. Natural products

Small organic molecules offer an attractive alternative to peptide-based molecular tools; they possess an enhanced diversity of chemical space and can be more readily synthetically modified to improve various aspects of function. The lack of structural information regarding points of interest at which small molecules may intervene in Aβ aggregation makes natural products attractive; these compounds can be readily screened to identify effective hits without a need for well characterized targets which are traditionally required for rational design of synthetic molecules. Natural products possess a range of stable scaffolds which have been shown to effectively modify a variety of biological systems, including enzyme activity, protein-protein and protein-DNA interactions, and membrane protein function.[111] Additionally, because they are derived from natural sources, small molecule natural products often exhibit improved pharmacological characteristics, improved absorption, and reduced inherent toxicity relative to their synthetic counterparts.[111]

Polyphenolic compounds have become a leading class of small molecules in the study of Aβ modulation (Fig. 1.6).[112,113] Curcumin, a prototypical polyphenol derived from turmeric, has been reported to possess a wide range of beneficial properties, including an ability to block amyloid formation.[114,115] When incubated with monomeric Aβ, curcumin prevents the formation of soluble oligomers *in vitro* and decreases amyloid plaque load in AD model APP transgenic mice *in vivo*.[114] It is believed that curcumin successfully inhibits fibrillation, in part, through interaction with C-terminal residues which subsequently prevents the formation of the D23-K28

salt bridge responsible for stabilizing the cross β-strand structure of Aβ fibrils.[116] Resveratrol, a potent antioxidant found in red wine, has also been reported to reduce the toxicity of Aβ species.[117,118] Initially, it was suggested that the principle mode of protection was as an antioxidant and through reduction of the inflammatory response to the presence of Aβ.[117-119] Along with this antioxidant behavior, resveratrol is capable of binding to both monomeric and aggregated forms of both $A\beta_{40}$ and $A\beta_{42}$ with dissociation constants (K_d) of 10-50 μM.[120] Additionally, the association of resveratrol with monomeric Aβ promotes the formation of non-toxic, soluble oligomers.[121] These results suggest that resveratrol is capable of modulating Aβ associated toxicity through multiple distinct mechanisms. (-)-Epigallocatechin-gallate (EGCG), a polyphenolic extract from green tea, is a potent antiamyloidogenic compound with activity against a broad spectrum of aggregation-prone proteins and peptides.[122-126] Along with inhibiting Aβ fibrillation, EGCG is capable of remodeling preformed Aβ fibrils, suggesting an ability to intervene at a variety of stages of aggregation.[123]

Despite the availability of these and other antiamyloidogenic natural products, they are not without their drawbacks. As observed in the study of resveratrol, many natural products are capable of interacting with a variety of proteins and multiple cellular processes. While these issues are minimized in simplified *in vitro* analysis of protein aggregation, it reduces the utility of the tools in cell-based and *in vivo* systems designed to investigate the broader functions of Aβ aggregation.[113] Additionally, the *in vitro* activity of polyphenolic natural products does not always translate to more complex systems due to a combination of small molecule instability and off target effects.[127] Additionally, natural products often possess pharmacophores which are susceptible to oxidation (such as quinones and catechols) or covalent modification, obscuring the identity of the active molecule.[128] Thus, while natural products provide a range of exciting and

valuable tools for the study of Aβ aggregation, their applications are inherently limited in the absence of medicinal chemistry-inspired modifications.
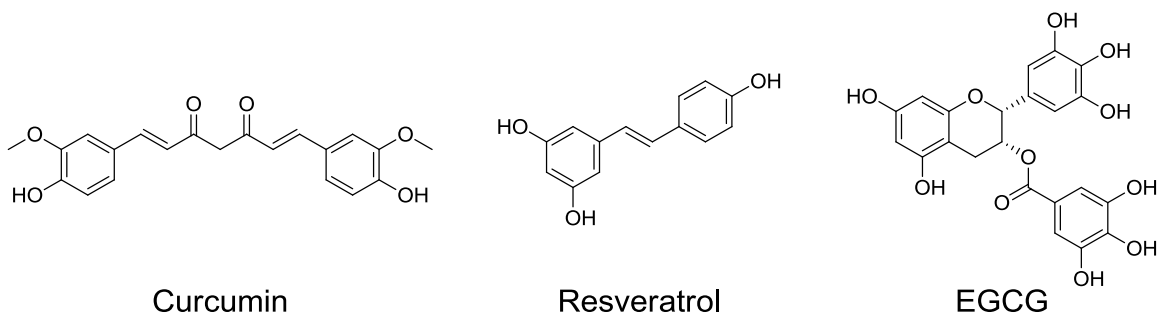
Figure 1.6. Antiamyloidogenic natural products. A variety of polyphenolic natural products, including curcumin, resveratrol, and EGCG, have demonstrated an ability to modulate the aggregation and toxicity of Aβ *in vitro* and *in vivo*.

1.3.1.3. Synthetic antiamyloidogenic small molecules

Given the limitations which both peptide and natural product amyloid inhibitors possess, synthetic small molecule modulators have also been extensively explored.[129,130] Some of the early successes in synthetic small molecule probes were organic dyes due to their high solubility and stability and relatively low toxicity (Fig. 1.7a).[129] Congo red has long been used in the histological detection of amyloid plaques in tissue.[131-133] Exploring Congo red's ability to bind to Aβ aggregates, it was observed to block peptide fibril formation and subsequently block aggregate associated toxicity.[134,135] It was also observed that, at low peptide concentrations, Congo red stabilizes monomeric Aβ$_{40}$ and prevents early oligomer formation in cell culture media.[136] As the peptide and Congo red concentration are increased, the two are capable of forming small oligomeric complexes at a 1:1 ratio of peptide to ligand; the addition of higher concentrations of Congo red promotes larger oligomers with a peptide to ligand ratio of 1:2.[137] These stabilized oligomers are proposed to be off-pathway from conventional amyloid fibrillation. Orange G is another dye traditionally used to stain proteinaceous aggregates, and it
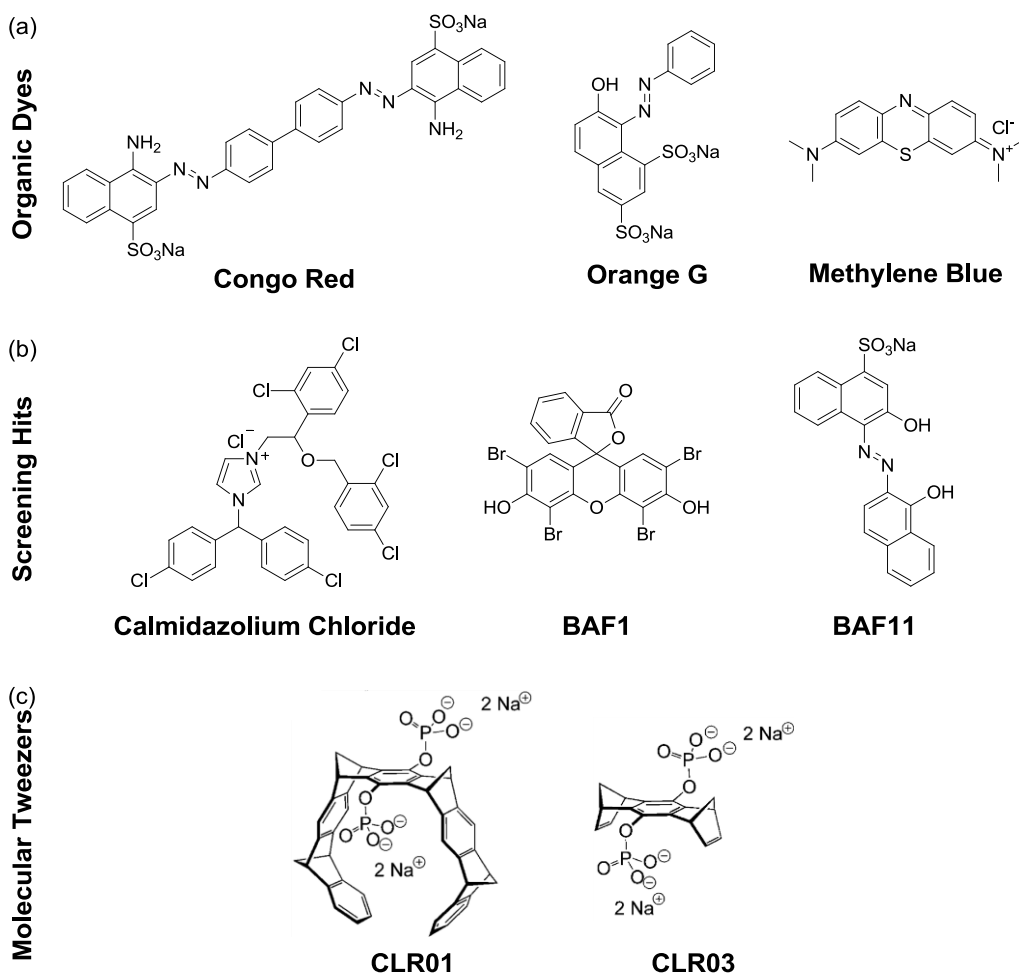
Figure 1.7. Non-natural organic small molecule modulators of Aβ aggregation. (a) Organic dyes like Congo red, orange G, and methylene blue were some of the early probes of Aβ amyloid formation. (b) High throughput screening has helped identify unexpected scaffolds like calmidazolium chloride, BAF1, and BAF11 which possess antiamyloidogenic activity. (c) With more recent understanding of the amyloid formation pathway, it has become possible to rationally select synthetic molecules like CLR01 and CLR03 which may possess unique modulatory behavior.[138]

has been proposed to be a broad scope inhibitor of Aβ aggregation.[139,140] However, follow up studies revealed that, similar to Congo red, orange G inhibits the formation of fibrillar aggregates by stabilizing on pathway oligomers.[90] Crystallographic analysis has revealed that orange G is also capable of binding to fibrillar Aβ species through positively charged lysine residues, despite its inability to block fibril formation.[141] Methylene blue is another dye which has found applications in a wide range of fields, serving as an antiseptic, chemotherapy agent, and

antibiotic among many other functions.[142] Unlike Congo red and orange G, methylene blue has been proposed to inhibit oligomer formation while promoting fibrillation.[143] Additionally, preformed Aβ fibrils are susceptible to remodeling by methylene blue; they were observed to be converted into amorphous aggregates, suggesting that the fibrils promoted by the presence of methylene blue during aggregation differ from the fiber structure formed by free Aβ in solution.[144] The antiamyloidogenic activity of methylene blue has also been shown to be neuroprotective in a transgenic mouse model of AD.[145]

While the dyes described above have provided valuable insights into how Aβ aggregation may be modulated, their applications have been driven more by their long history in histology and medicine than any structure- or mechanism-based rationale. The lack of defined structures along the amyloidogenic pathway of Aβ makes conventional rational design of antiamyloidogenic small molecules difficult as there are few targets to base designs upon. However, screening approaches are able to provide valuable insight into pharmacophores which have value as specific amyloid inhibitors through a discovery-focused approach rather than a validation-focused approach as was used with the dyes (Fig. 1.7b). The Library of Pharmacologically Active Compounds (LOPAC) was screened for modulators by affixing fibrils to a plate and incubating the compounds with biotin-tagged Aβ; the extent of fibrillation was subsequently measured with a streptavidin-europium fluorescent probe.[146] The screen yielded no potent inhibitors of aggregation. However, one compound, calmidazolium chloride, was found to promote the formation of protofibrillar aggregates. The stabilized protofibrils were observed to be structurally distinct from conventional fibers formed in solution. Residues 22-29 were found to have increased structure and rigidity indicative of a unique polymorph.[146] A small library of previously identified amyloid modulators was also evaluated to determine distinct mechanisms

of inhibition.[90] From the small library, three distinct classes of modulators were observed. Class 1 compounds destabilize oligomer formation but had no impact upon fibrillation by Aβ. Class 2 compounds were found to inhibit both oligomer and fiber formation. Class 3 compounds were found to block fibrillation but not oligomerization.[90] Recent advances in both the understanding of amyloid fiber structure and *in silico* screening technologies have also facilitated computational analysis of small molecule probes against Aβ aggregation.[141,147-149] Following the *in silico* screen of ~18,000 distinct compounds, 25 hits were explored experimentally, and 5 were found to reduce the toxicity of Aβ aggregates.[150] Two of these active compounds, BAF1 and BAF11, bind to preformed fibrils with low μM dissociation constants. It is proposed that this relatively tight affinity for the fibril stabilizes the end stage aggregate and decreases the concentration of toxic intermediate oligomers.

In parallel with repurposing known molecules and utilizing screening to identify functional amyloid modulators, rational selection and design of active molecules is expanding. A powerful example is the implementation of "molecular tweezers" (MTs) to specifically target charged lysine and arginine side chains of amyloidogenic sequences (Fig. 1.7c).[138,151] The MT CLR01 and its truncated derivative CLR03 were both analyzed for their ability to inhibit a range of amyloidogenic peptides and proteins, including $A\beta_{40}$ and $A\beta_{42}$.[138] While CLR01 was a potent inhibitor of aggregation by $A\beta_{40}$ and successfully attenuated the aggregation of $A\beta_{42}$, CLR03 demonstrated no efficacy, suggesting that it was unable to engage the charged side chains. Additionally, CLR01 successfully decreased the toxicity of Aβ aggregates in cell culture.[138] A follow up study employing ion-mobility spectroscopy-mass spectrometry (IM-MS) found that CLR01 promoted the formation of small, compact oligomeric species while CLR03 promoted the formation of on pathway oligomers.[152] CLR01 was also observed to inhibit $A\beta_{40}$ fibrillation

on lipid bilayers and the membrane perturbation associated with amyloid formation.[153] Because of its efficacy against amyloid aggregation, the pharmacological impact of CLR01 was investigated and the compound was observed to be non-toxic with minimal side effects in mouse models. It was also observed to be blood-brain barrier permeable, showing promising signs as a lead candidate in therapeutic optimization.[154]

1.3.2. Multifunctional small molecules against amyloid formation

While the development of antiamyloidogenic molecular probes continues, the multifactorial nature of AD makes it important to possess tools which can simultaneously interrogate multiple aspects of disease pathology.[4,7,155] Towards this end, researchers have pursued multifunctional small molecules which are able to interact with multiple components associated with AD, including Aβ aggregation, misregulated metal ions, and AChE inhibition.[85,86,155] There are two primary approaches to the development of multifunctional small molecules. Two distinct pharmacophores which are known to modulate distinct aspects of AD biology can be connected via a short, flexible tether using the linkage approach. Alternatively, a moiety responsible for one mode of action can be installed within a functional framework known to regulate a second parameter through the incorporation approach (Fig. 1.8a).[155]

An early effort at a bifunctional metal−Aβ modulator was XH1 (Fig. 1.8b).[156] Two molecules of a derivative of the amyloid binding dye thioflavin-T (ThT) were combined with a linker capable of metal chelation. XH1 was found to decrease Zn(II)−Aβ aggregation and decrease the amyloid plaque load in a PS1/APP transgenic mouse model which models AD pathology. Another bifunctional probe, Cyc-KLVFF, was designed by combining the cyclic metal chelator cyclen with the known β-sheet breaker peptide sequence KLVFF.[157] Similar to the

effect of XH1 on Zn(II)−Aβ, Cyc-KLVFF successfully attenuated the aggregation of Cu(II)−Aβ species while also reducing cellular apoptosis induced by toxic Cu(II)−Aβ aggregates.
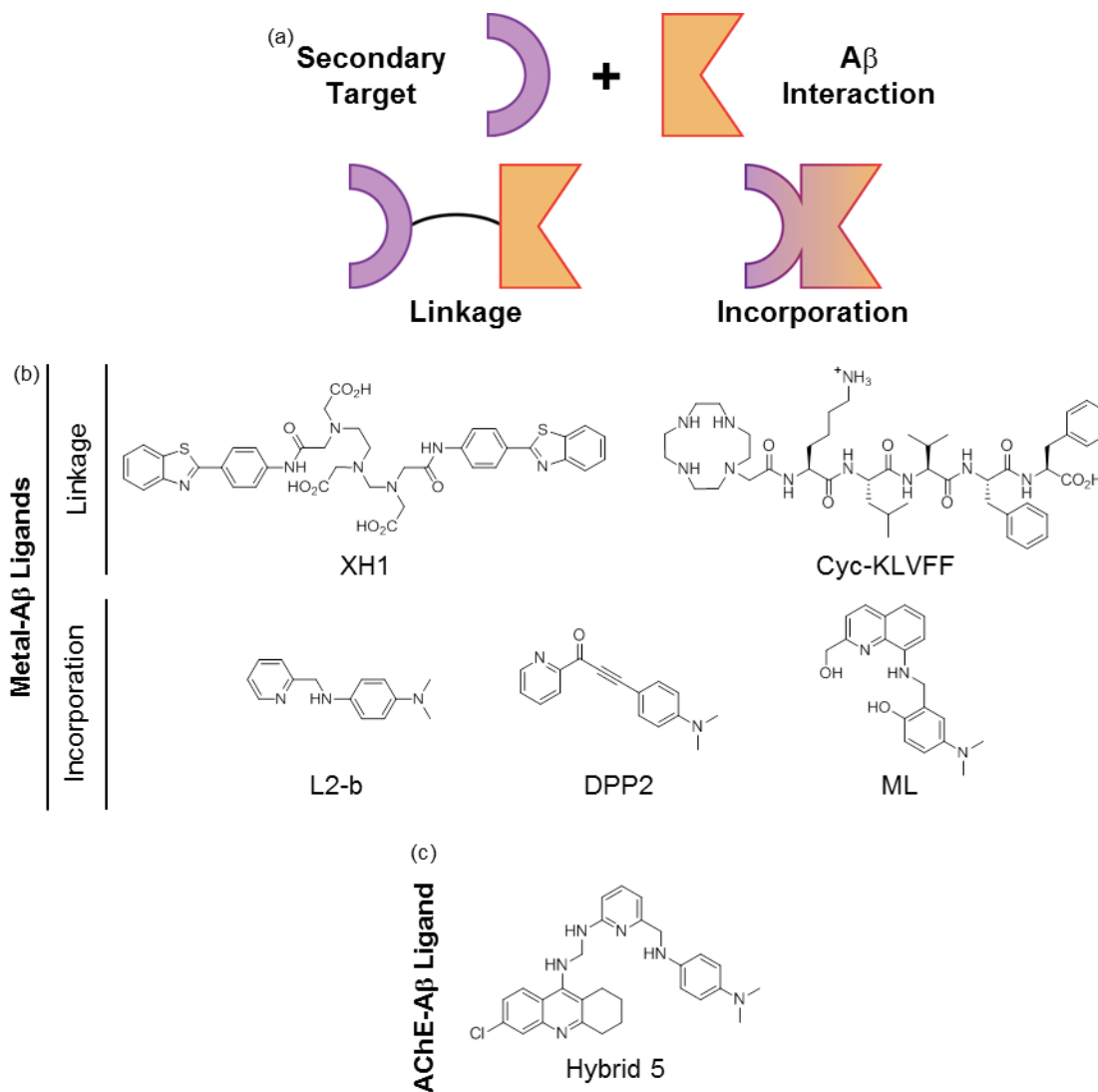
Figure 1.8. Multifunctional ligand design. (a) Multifunctional probes may be developed by combining frameworks which individually interrogate a single aspect of AD pathology using a flexible linker (linkage approach) or by incorporating one pharmacophore into the framework of the other. (b) XH1 and Cyc-KLVFF are metal−Aβ probes generated using the linkage approach while clioquinol, L2-b, DPP2, and ML were all produced using the incorporation method. (c) Hybrid 5 was developed to simultaneously interact with metal−Aβ species and modulate AChE activity.

The incorporation method has also produced a range of effective metal−Aβ modulators.[85,86,155] L2-b was initially developed by installing a metal chelation moiety similar to that found in the metal chelator clioquinol into the stilbene framework common to imaging agents used to interrogate plaque load *in vivo* (Fig. 1.8b).[158-160] L2-b was observed to successfully attenuate the aggregation of both Cu(II)−Aβ and Zn(II)−Aβ and rescued cell viability that was decreased as a result of metal-Aβ aggregation. Additionally, it was found that the inclusion of the dimethylamino moiety in L2-b was important for the framework's function.[158] Another bifunctional probe, DPP2, was developed using a similar approach as was employed in the design of L2-b; the diphenylpropynone scaffold, a known Aβ binding agent, was equipped with a bidentate metal chelation moiety.[155,161] Like L2-b, DPP2 successfully modulated the aggregation of both Zn(II)− and Cu(II)−Aβ. Unlike L2-b, however, DPP2 was toxic to cells, likely due to its ability to act as a Michael acceptor. This suggests that DPP2 is best suited as an *in vitro* probe of metal associated protein aggregation while L2-b has more promise as an in cell or *in vivo* probe.[162] A more recent advance in multifunctional Aβ modulation is the ligand ML.[163] The stilbene framework used in the development of L2-b was coupled with L2-b itself to promote metal−Aβ interaction while also expanding the metal chelation ability via the addition of two additional donor atoms. The tetradentate metal binding was also suggested to have antioxidant capabilities by reducing the redox cycling of chelated metal ions. It was observed that ML effectively modulates the aggregation of Aβ both in the presence and absence of metal ions while reducing the toxicity of a range of Aβ aggregates and functioning as a potent antioxidant. The success of ML suggests that our understanding of Aβ aggregation and its interaction with the molecular pathologies of AD has expanded to a point where rational design of modulators is possible, though still difficult.

This progress is further evident in the trifunctional compound Hybrid 5 which is capable of modulating metal−Aβ and AChE activity (Fig. 1.8c).[164] In order to generate Hybrid 5, the metal-Aβ modulator L2-b was combined with a derivative of the FDA approved AChE inhibitor tacrine. Despite the presence of the linker, Hybrid 5 possessed stronger AChE inhibition behavior than tacrine. Hybrid 5 also maintained its ability to modulate both Zn(II)− and Cu(II)−Aβ aggregation while successfully inhibiting the aggregation of metal-free Aβ in solution. While tacrine has fallen out of favor clinically due to extreme hepatotoxicity, the *in vitro* success of Hybrid 5 suggests that it is possible to generate compounds which simultaneously modulate multiple, unassociated aspects of AD molecular pathology.[165] This holds great promise for the immediate development of molecular probes and the eventual generation of more efficacious therapeutic interventions.

1.4. Methods to investigate aspects of Aβ aggregation

Due to the highly heterogeneous nature of Aβ aggregation, it is essential to possess a technical toolbox which contains a wide range of methodologies and probes capable of characterizing aggregating species that span from the monomeric peptide up to the mature fibril and all intermediates in between. A prominent probe of the amyloid community is the amyloid-specific dye ThT.[97] ThT fluorescence increases based on the presence of β-strand structures in solution and provides indirect evidence of fibril formation.[166,167] With recent advances in kinetic modeling based on ThT-based aggregation monitoring, it is also now possible to infer a variety of mechanistic distinctions which provides insight into potential intermediate aggregate steps.[168-170] Despite the prevalence of ThT in the field of amyloid research it still suffers from a number of limitations. Because of its charge, ThT preferentially interacts with charged surfaces and is therefore susceptible to changes in solution pH.[171] Additionally, it has been demonstrated that

24

small molecule modulators of amyloid formation sometimes possess fluorescence profiles which overlap with that of ThT or are capable of competing with ThT for the same binding site, resulting in dye displacement and a reduction in fluorescence despite no structural alteration.[172-174] Finally, some peptide sequences form fibers which are incapable of binding to ThT, a deficiency that can be induced by both polymorphic idiosyncrasies and intrinsic charge repulsion.[175,176] Given these restrictions inherent to ThT assays, fluorescence analysis is often coupled with circular dichroism spectroscopy (CD).[177] CD is able to confirm the fibrillation that is observed as a result of ThT fluorescence increases, but it is also capable of distinguishing non-fibrillar changes in structure. Helical intermediates of Aβ have been observed in the presence of negatively charged lipid bilayers while helical species of amylin, an amyloidogenic peptide associated with type II diabetes, have been stabilized by the presence of a synthetic derivative of curcumin.[178,179] These non fibrillar states are invisible to ThT and thus highlight the complimentary power of CD.

Both static and dynamic light scattering (SLS and DLS, respectively) are able to further distinguish distinct aggregation intermediates, though become less useful as the heterogeneity of the sample increases or extremely large particles form.[180,181] Both of these limitations are common in the later stages of amyloid formation making these tools best suited for the investigation of early oligomeric species. Aggregate size can also be estimated through either size exclusion chromatography (SEC) or analytical ultracentrifugation (AUC) though these disruptive techniques do not allow for high temporal resolution and can disrupt transient oligomeric complexes.[182,183] Large aggregates, intractable by SLS, DLS, or SEC can be monitored and quantified through both transmission electron microcopy (TEM) and atomic force microscopy (AFM) as complimentary methods. Negative stain TEM, which relies on contrasting

stains, is capable of distinguishing aggregate sub-types while cryogenic TEM (Cryo-EM) has made advances in determining atomic level structures of model amyloid fibrils.[184-187] AFM is similarly able to quantitatively distinguish amyloid fibril polymorphs while also being capable of monitoring a single sample over time with minimal disruption.[188,189]

Higher resolution structural insights are capable through the application of IM-MS. Advancements in ion-mobility spectrometry, initially used to study single subunit proteins, have enabled the study of much larger protein complexes.[190-193] Because of this ability, IM-MS is an ideal tool for the investigation of amyloid peptide structure and organization. The sensitivity of collisional cross-section measurements to modest shifts in monomer structure due to small molecule and metal interactions has made it a valuable method for the characterization of early folding changes both on and off the pathway of amyloid formation.[194,195] IM-MS has also proven powerful at identifying unique oligomeric intermediates which occur during the lab phase of amyloid formation.[196-198] The ion-mobility component allows multiple oligomers of the same mass to be distinguished and has helped to identify some potentially key on pathway oligomeric intermediates for amyloid formation by Aβ.[196] When coupled with computational modeling and MD simulation, IM-MS is capable of providing high resolution insights into potential structural changes underlying amyloid formation. However, the lack of atomic level experimental constraints within these measurements makes complementation with additional biophysical tools, such as NMR and crystallography, advantageous.

As detailed earlier, end stage amyloid fibers are the most structurally well characterized Aβ aggregate. The extreme stability of mature fibers makes them ideal candidates for rigorous characterization by solid-state NMR.[28-33] This work has revealed some of the details which underlie aggregate polymorphism and has begun to reveal distinctions between patient

phenotypes.[29] Additionally, crystallographic studies of amyloidogenic peptide fragments have illuminated some of the chemical underpinnings of polymorphism and clarified fiber packing motifs.[34,39-41] Recent advances in amyloid crystallography have also elucidated small, oligomeric structures formed by fragments of the Aβ sequence.[39,40,199-201] These intermediate aggregates, ranging from small trimers to higher order, pore-like aggregates, have revealed some commonalities in β-strand formation by Aβ which exist in both these stabilized oligomers and the mature fibril, though their morphologies differ dramatically. While fibers remain the predominant subject for structural analysis, the recent paradigm shift within the amyloid community emphasizes the fundamental role of non-fibrillar intermediates as the predominant toxic species in AD.[19] Thus, structural investigation of those intermediates has begun to take center stage, though the tools to fully characterize these intermediates formed by full length peptide remain in their relative infancy.

The propensity for Aβ to aggregate in solution makes rapid acquisition of NMR data highly advantageous. 1D ^{19}F NMR has been applied to monitor the aggregation propensity of various amyloidogenic peptides and distinguish their oligomeric intermediates.[174,202] This method takes advantage of the minimal background afforded by the non-natural ^{19}F atoms incorporated into a synthetic methionine derivative which improves the signal to noise ratio and shortens the time necessary to acquire each spectrum. However, due to the single site labeling, this method provides minimal structural insight, though it is an extremely valuable approach for investigating the general pathways of aggregation. A recent 2D [1]H-^{15}N correlation experiment, SOFAST-HMQC (band-Selective Optimized-Flip-Angle Short-Transient Heteronuclear Multiple Quantum Coherence), provides residue specific resolution in a matter of minutes while conventional HMQC experiments can require multiple hours for to acquire a single, well

resolved spectrum.[203] This allows for the monomeric peptide to be monitored as a function of time while also making it possible to monitor the interaction of the peptide with a variety of ligands and protein binding partners.[163,204] Relaxation and exchange based solution NMR experiments also allow us to characterize the interaction of monomeric peptide with larger structures (such as lipid bilayers or amyloid fibrils).[205-209] Despite these methodologies, it remains difficult to characterize the intermediate aggregates of Aβ in the absence of chemical modifications due to both the large size of the species and the inherent heterogeneity.[76,210,211] The largest hurdle to the further characterization of intermediate aggregates is the validation of non-disruptive preparation methods which can reproducibly generate stable and more homogeneous oligomeric species.

Solid-state NMR, while commonly applied to the study of fibrillar aggregates, is also capable of probing structural details of intermediate oligomers through a combination of careful sample preparation and selective labeling. Kotler *et al.* have recently applied radio frequency driven dipolar recoupling (RFDR) based ^{1}H-^{1}H experiments to investigate a stabilized, unstructured, off pathway oligomer of Aβ$_{40}$. The method took advantage of the abundance of protons inherent in the peptide and selective filtering of NMR signals using magic angle spinning (MAS) to only investigate structural parameters of a moderately sized aggregate. While the isolated aggregate was found to be relatively unstructured, the method is a viable approach for the future study of other intermediates. Solid-state NMR has also proved useful in exploring the mechanisms of Aβ aggregation on lipid bilayers. By mixing selectively ^{13}C labeled Aβ$_{40}$ with zwitterionic liposomes, it was possible to monitor different stages of peptide insertion into the lipid bilayer and subsequent membrane perturbation with atomic level resolution.[212] A follow up study allowed for the observation of distinct aggregation pathways that are dependent upon both

peptide concentration and preexisting aggregate species.[43] While not as developed as the solid-state methods applied for the study of fibrillar aggregates, solid-state NMR has already proven itself invaluable in the investigation of amyloid intermediates and will continue to be a vital tool as the field explores new chemical and biological means by which aggregation intermediates may be stabilized.

1.5.   Dissertation objectives

While many studies have examined individual aspects of AD pathology in *in vitro* settings, there remains a substantial gap in our understanding of how various contributors to cytotoxicity, including Aβ aggregation, metal dyshomeostasis, oxidative stress, and membrane disruption, are interrelated.[4,9,86] The objectives of this thesis are to explore connections which bridge these individual facets of the disease and explore their relationships to one another. I first explore a new set of natural products (**Phlorizin**, **Verbascoside**, and **Rutin**) and their synthetically esterified derivatives (**F2**, **VPP**, and **R2**) for their ability to modulate metal-associated Aβ aggregation (Chapter 2). While natural products have been previously examined for their ability to modulate metal–Aβ aggregation, little work has explored how natural product frameworks may be synthetically modified to tune their reactivity.[195,204,213,214] Then, in order to explore the effects of oxidative stress on membrane-mediated amyloid formation by Aβ, I examine the effect of lipid bilayer thinning on the structure of monomeric Aβ upon interaction with a synthetic membrane (Chapter 3) that the effect which thin bilayers have upon the progression of Aβ$_{40}$ from its monomeric state to a fibrillar aggregate (Chapter 4). It has been documented that, as a result of the increased oxidative stress in the AD brain, polyunsaturated lipid molecules may be truncated due to peroxidation. These shortened lipids can subsequently incorporate into the neuronal bilayer and alter the chemical and mechanical properties of the

membrane with which Aβ interacts and aggregates.[50,51,215-218] Despite the pathological link between bilayer thinning, Aβ aggregation, and AD, the role of pathologically thinned bilayers has yet to be investigated in protein aggregation.

1.6.   References

1.   Hippius, H. & Neundorfer, G. The discovery of Alzheimer's disease. *Dialogues Clin. Neurosci.* **5**, 101-108 (2003).

2.   Alzheimer's Disease International, *World Alzheimer's Report 2015: An Analysis of Prevalence, Incidence, Cost and Trends.* (2015).

3.   Alzheimer's Association. 2016 Alzheimer's disease facts and figures. *Alzheimers Dement.* **12**, 459-509 (2016).

4.   Savelieff, M. G., Lee, S., Liu, Y. & Lim, M. H. Untangling amyloid-beta, tau, and metals in Alzheimer's disease. *ACS Chem. Biol.* **8**, 856-865 (2013).

5.   Iqbal, K., Liu, F. & Gong, C. X. Tau and neurodegenerative disease: the story so far. *Nat. Rev. Neurol.* **12**, 15-27 (2016).

6.   Rauk, A. The chemistry of Alzheimer's disease. *Chem. Soc. Rev.* **38**, 2698-2715 (2009).

7.   Kepp, K. P. Bioinorganic chemistry of Alzheimer's disease. *Chem. Rev.* **112**, 5193-5239 (2012).

8.   Markesbery, W. R. Oxidative stress hypothesis in Alzheimer's disease. *Free Radic. Biol. Med.* **23**, 134-147 (1997).

9.   Kotler, S. A., Walsh, P., Brender, J. R. & Ramamoorthy, A. Differences between amyloid-beta aggregation in solution and on the membrane: insights into elucidation of the mechanistic details of Alzheimer's disease. *Chem. Soc. Rev.* **43**, 6692-6700 (2014).

10.   Francis, P. T., Palmer, A. M., Snape, M. & Wilcock, G. K. The cholinergic hypothesis of Alzheimer's disease: a review of progress. *J. Neurol. Neurosurg. Psychiatry* **66**, 137-147 (1999).

11.   Craig, L. A., Hong, N. S. & McDonald, R. J. Revisiting the cholinergic hypothesis in the development of Alzheimer's disease. *Neurosci. Biobehav. Rev.* **35**, 1397-1409 (2011).

12. Terry, A. V., Jr. & Buccafusco, J. J. The cholinergic hypothesis of age and Alzheimer's disease-related cognitive deficits: recent challenges and their implications for novel drug development. *J. Pharmacol. Exp. Ther.* **306**, 821-827 (2003).

13. Hamley, I. W. The amyloid beta peptide: a chemist's perspective. Role in Alzheimer's and fibrillization. *Chem. Rev.* **112**, 5147-5192 (2012).

14. Hardy, J. A. & Higgins, G. A. Alzheimer's disease: the amyloid cascade hypothesis. *Science* **256**, 184-185 (1992).

15. Selkoe, D. J. The molecular pathology of Alzheimer's disease. *Neuron* **6**, 487-498 (1991).

16. Castellani, R. J. *et al.* Reexamining Alzheimer's disease: evidence for a protective role for amyloid-beta protein precursor and amyloid-beta. *J. Alzheimers. Dis.* **18**, 447-452 (2009).

17. Lee, H. G. *et al.* Challenging the amyloid cascade hypothesis: senile plaques and amyloid-beta as protective adaptations to Alzheimer disease. *Ann. N. Y. Acad. Sci.* **1019** (2004).

18. Kumar, D. K. *et al.* Amyloid-beta peptide protects against microbial infection in mouse and worm models of Alzheimer's disease. *Sci. Transl. Med.* **8**, 340ra372 (2016).

19. Hardy, J. & Selkoe, D. J. The amyloid hypothesis of Alzheimer's disease: progress and problems on the road to therapeutics. *Science* **297**, 353-356 (2002).

20. Jakob-Roetne, R. & Jacobsen, H. Alzheimer's disease: from pathology to therapeutic approaches. *Angew. Chem. Int. Ed. Engl.* **48**, 3030-3059 (2009).

21. Harrison, R. S., Sharpe, P. C., Singh, Y. & Fairlie, D. P. Amyloid peptides and proteins in review. *Rev. Physiol. Biochem. Pharmacol.* **159**, 1-77 (2007).

22. Knowles, T. P. *et al.* An analytical solution to the kinetics of breakable filament assembly. *Science* **326**, 1533-1537 (2009).

23. Benilova, I., Karran, E. & De Strooper, B. The toxic Abeta oligomer and Alzheimer's disease: an emperor in need of clothes. *Nat. Neurosci.* **15**, 349-357 (2012).

24. Roche, J., Shen, Y., Lee, J. H., Ying, J. & Bax, A. Monomeric Abeta(1-40) and Abeta(1-42) Peptides in Solution Adopt Very Similar Ramachandran Map Distributions That Closely Resemble Random Coil. *Biochemistry* **55**, 762-775 (2016).

25. Vivekanandan, S., Brender, J. R., Lee, S. Y. & Ramamoorthy, A. A partially folded structure of amyloid-beta(1-40) in an aqueous environment. *Biochem. Biophys. Res. Commun.* **411**, 312-316 (2011).

26. Coles, M., Bicknell, W., Watson, A. A., Fairlie, D. P. & Craik, D. J. Solution structure of amyloid beta-peptide(1-40) in a water-micelle environment. Is the membrane-spanning domain where we think it is? *Biochemistry* **37**, 11064-11077 (1998).

27. Crescenzi, O. *et al.* Solution structure of the Alzheimer amyloid beta-peptide (1-42) in an apolar microenvironment. Similarity with a virus fusion domain. *Eur. J. Biochem.* **269**, 5642-5648 (2002).

28. Meier, B. H. & Bockmann, A. The structure of fibrils from 'misfolded' proteins. *Curr. Opin. Struct. Biol.* **30**, 43-49 (2015).

29. Lu, J. X. *et al.* Molecular structure of beta-amyloid fibrils in Alzheimer's disease brain tissue. *Cell* **154**, 1257-1268 (2013).

30. Petkova, A. T., Yau, W. M. & Tycko, R. Experimental constraints on quaternary structure in Alzheimer's beta-amyloid fibrils. *Biochemistry* **45**, 498-512 (2006).

31. Colvin, M. T. *et al.* Atomic Resolution Structure of Monomorphic Abeta42 Amyloid Fibrils. *J. Am. Chem. Soc.* **138**, 9663-9674 (2016).

32. Schutz, A. K. *et al.* Atomic-resolution three-dimensional structure of amyloid beta fibrils bearing the Osaka mutation. *Angew. Chem. Int. Ed. Engl.* **54**, 331-335 (2015).

33. Tycko, R. Physical and structural basis for polymorphism in amyloid fibrils. *Protein Sci.* **23**, 1528-1539 (2014).

34. Colletier, J. P. *et al.* Molecular basis for amyloid-beta polymorphism. *Proc. Natl. Acad. Sci. U.S.A.* **108**, 16938-16943 (2011).

35. Glabe, C. G. Structural classification of toxic amyloid oligomers. *J. Biol. Chem.* **283**, 29639-29643 (2008).

36. Kayed, R. *et al.* Common structure of soluble amyloid oligomers implies common mechanism of pathogenesis. *Science* **300**, 486-489 (2003).

37. Kayed, R. *et al.* Fibril specific, conformation dependent antibodies recognize a generic epitope common to amyloid fibrils and fibrillar oligomers that is absent in prefibrillar oligomers. *Mol. Neurodegener.* **2**, 18 (2007).

38. Jang, H. *et al.* Disordered amyloidogenic peptides may insert into the membrane and assemble into common cyclic structural motifs. *Chem. Soc. Rev.* **43**, 6750-6764 (2014).

39.   Kreutzer, A. G., Hamza, I. L., Spencer, R. K. & Nowick, J. S. X-ray Crystallographic Structures of a Trimer, Dodecamer, and Annular Pore Formed by an Abeta17-36 beta-Hairpin. *J. Am. Chem. Soc.* **138**, 4634-4642 (2016).

40.   Pham, J. D., Demeler, B. & Nowick, J. S. Polymorphism of oligomers of a peptide from beta-amyloid. *J. Am. Chem. Soc.* **136**, 5432-5442 (2014).

41.   Pham, J. D., Spencer, R. K., Chen, K. H. & Nowick, J. S. A fibril-like assembly of oligomers of a peptide derived from beta-amyloid. *J. Am. Chem. Soc.* **136**, 12682-12690 (2014).

42.   Kotler, S. A. *et al.* High-resolution NMR characterization of low abundance oligomers of amyloid-beta without purification. *Sci. Rep.* **5**, 11811 (2015).

43.   Delgado, D. A. *et al.* Distinct Membrane Disruption Pathways Are Induced by 40-Residue beta-Amyloid Peptides. *J. Biol. Chem.* **291**, 12233-12244 (2016).

44.   Faller, P., Hureau, C. & Berthoumieu, O. Role of metal ions in the self-assembly of the Alzheimer's amyloid-beta peptide. *Inorg. Chem.* **52**, 12193-12206 (2013).

45.   Matsuzaki, K. How do membranes initiate Alzheimer's Disease? Formation of toxic amyloid fibrils by the amyloid beta-protein on ganglioside clusters. *Acc. Chem. Res.* **47**, 2397-2404 (2014).

46.   Faller, P. & Hureau, C. A bioinorganic view of Alzheimer's disease: when misplaced metal ions (re)direct the electrons to the wrong target. *Chemistry* **18**, 15910-15920 (2012).

47.   Que, E. L., Domaille, D. W. & Chang, C. J. Metals in neurobiology: probing their chemistry and biology with molecular imaging. *Chem. Rev.* **108**, 1517-1549 (2008).

48.   Bleackley, M. R. & Macgillivray, R. T. Transition metal homeostasis: from yeast to human disease. *Biometals* **24**, 785-809 (2011).

49.   Greenough, M. A., Camakaris, J. & Bush, A. I. Metal dyshomeostasis and oxidative stress in Alzheimer's disease. *Neurochem. Int.* **62**, 540-555 (2013).

50.   Montine, T. J. *et al.* Lipid peroxidation in aging brain and Alzheimer's disease. *Free Radic. Biol. Med.* **33**, 620-626 (2002).

51.   Butterfield, D. A. & Lauderback, C. M. Lipid peroxidation and protein oxidation in Alzheimer's disease brain: potential causes and consequences involving amyloid beta-

peptide-associated free radical oxidative stress. *Free Radic. Biol. Med.* **32**, 1050-1060 (2002).

52.   Moreira, P. I., Carvalho, C., Zhu, X., Smith, M. A. & Perry, G. Mitochondrial dysfunction is a trigger of Alzheimer's disease pathophysiology. *Biochim. Biophys. Acta.* **1802**, 2-10 (2010).

53.   Wang, X. *et al.* Oxidative stress and mitochondrial dysfunction in Alzheimer's disease. *Biochim. Biophys. Acta.* **1842**, 1240-1247 (2014).

54.   Lovell, M. A., Robertson, J. D., Teesdale, W. J., Campbell, J. L. & Markesbery, W. R. Copper, iron and zinc in Alzheimer's disease senile plaques. *J. Neurol. Sci.* **158**, 47-52 (1998).

55.   Miller, L. M. *et al.* Synchrotron-based infrared and X-ray imaging shows focalized accumulation of Cu and Zn co-localized with beta-amyloid deposits in Alzheimer's disease. *J. Struct. Biol.* **155**, 30-37 (2006).

56.   Damante, C. A. *et al.* Metal loading capacity of Abeta N-terminus: a combined potentiometric and spectroscopic study of zinc(II) complexes with Abeta(1-16), its short or mutated peptide fragments and its polyethylene glycol-ylated analogue. *Inorg. Chem.* **48**, 10405-10415 (2009).

57.   Tiiman, A., Palumaa, P. & Tougu, V. The missing link in the amyloid cascade of Alzheimer's disease - metal ions. *Neurochem. Int.* **62**, 367-378 (2013).

58.   Hureau, C. Coordination of redox active metal ions to the amyloid precursor protein and to amyloid-β peptides involved in Alzheimer disease. Part 1: An overview. *Coord. Chem. Rev.* **256**, 2164-2174 (2012).

59.   Jiang, D. *et al.* Ternary complexes of iron, amyloid-beta, and nitrilotriacetic acid: binding affinities, redox properties, and relevance to iron-induced oxidative stress in Alzheimer's disease. *Biochemistry* **48**, 7939-7947 (2009).

60.   Cai, H. *et al.* Metabolic dysfunction in Alzheimer's disease and related neurodegenerative disorders. *Curr. Alzheimer. Res.* **9**, 5-17 (2012).

61.   Blesa, R. *et al.* Cerebral metabolic changes in Alzheimer's disease: neurobehavioral patterns. *Dementia* **7**, 239-245 (1996).

62.   Hazel, J. R. & Williams, E. E. The role of alterations in membrane lipid composition in enabling physiological adaptation of organisms to their physical environment. *Prog. Lipid. Res.* **29**, 167-227 (1990).

63. Prasad, M. R., Lovell, M. A., Yatin, M., Dhillon, H. & Markesbery, W. R. Regional membrane phospholipid alterations in Alzheimer's disease. *Neurochem. Res.* **23**, 81-88 (1998).

64. Lim, W. L., Martins, I. J. & Martins, R. N. The involvement of lipids in Alzheimer's disease. *J. Genet. Genomics* **41**, 261-274 (2014).

65. Butterfield, D. A. & Abdul, H. M. in *Handbook of Neurochemistry and Molecular Neurobiology* (eds A. Lajtha, G. Tettamanti, & G. Goracci) Ch. 22, 563-582 (Springer US, 2010).

66. Di Paolo, G. & Kim, T. W. Linking lipids to Alzheimer's disease: cholesterol and beyond. *Nat. Rev. Neurosci.* **12**, 284-296 (2011).

67. Jang, H. *et al.* Alzheimer's disease: which type of amyloid-preventing drug agents to employ? *Phys. Chem. Chem. Phys.* **15**, 8868-8877 (2013).

68. Arispe, N., Rojas, E. & Pollard, H. B. Alzheimer disease amyloid beta protein forms calcium channels in bilayer membranes: blockade by tromethamine and aluminum. *Proc. Natl. Acad. Sci. U.S.A.* **90**, 567-571 (1993).

69. Sciacca, M. F. *et al.* Two-step mechanism of membrane disruption by Abeta through membrane fragmentation and pore formation. *Biophys. J.* **103**, 702-710 (2012).

70. Quist, A. *et al.* Amyloid ion channels: a common structural link for protein-misfolding disease. *Proc. Natl. Acad. Sci. U.S.A.* **102**, 10427-10432 (2005).

71. Jang, H. *et al.* Familial Alzheimer's disease Osaka mutant (DeltaE22) beta-barrels suggest an explanation for the different Abeta1-40/42 preferred conformational states observed by experiment. *J. Phys. Chem. B* **117**, 11518-11529 (2013).

72. Capone, R. *et al.* All-d-Enantiomer of beta-Amyloid Peptide Forms Ion Channels in Lipid Bilayers. *J. Chem. Theory Comput.* **8**, 1143-1152 (2012).

73. Rhee, S. K., Quist, A. P. & Lal, R. Amyloid beta protein-(1-42) forms calcium-permeable, Zn2+-sensitive channel. *J. Biol. Chem.* **273**, 13379-13382 (1998).

74. Jang, H. *et al.* beta-Barrel topology of Alzheimer's beta-amyloid ion channels. *J. Mol. Biol.* **404**, 917-934 (2010).

75. Connelly, L. *et al.* Atomic force microscopy and MD simulations reveal pore-like structures of all-D-enantiomer of Alzheimer's beta-amyloid peptide: relevance to the ion channel mechanism of AD pathology. *J. Phys. Chem. B* **116**, 1728-1735 (2012).

76. Serra-Batiste, M. *et al.* Abeta42 assembles into specific beta-barrel pore-forming oligomers in membrane-mimicking environments. *Proc. Natl. Acad. Sci. U.S.A.* **113**, 10866-10871 (2016).

77. Schnaar, R. L. Gangliosides of the Vertebrate Nervous System. *J. Mol. Biol.* **428**, 3325-3336 (2016).

78. Hong, S. *et al.* Soluble Abeta oligomers are rapidly sequestered from brain ISF in vivo and bind GM1 ganglioside on cellular membranes. *Neuron* **82**, 308-319 (2014).

79. Francis, P. T., Parsons, C. G. & Jones, R. W. Rationale for combining glutamatergic and cholinergic approaches in the symptomatic treatment of Alzheimer's disease. *Expert. Rev. Neurother.* **12**, 1351-1365 (2012).

80. Sevigny, J. *et al.* The antibody aducanumab reduces Abeta plaques in Alzheimer's disease. *Nature* **537**, 50-56 (2016).

81. Rosenblum, W. I. Why Alzheimer trials fail: removing soluble oligomeric beta amyloid is essential, inconsistent, and difficult. *Neurobiol. Aging* **35**, 969-974 (2014).

82. Greenberg, B. D. *et al.* Improving Alzheimer's disease phase II clinical trials. *Alzheimers Dement.* **9**, 39-49 (2013).

83. Becker, R. E. & Greig, N. H. Fire in the ashes: can failed Alzheimer's disease drugs succeed with second chances? *Alzheimers Dement.* **9**, 50-57 (2013).

84. Carter, M. D., Simms, G. A. & Weaver, D. F. The development of new therapeutics for Alzheimer's disease. *Clin. Pharmacol. Ther.* **88**, 475-486 (2010).

85. Savelieff, M. G., DeToma, A. S., Derrick, J. S. & Lim, M. H. The ongoing search for small molecules to study metal-associated amyloid-beta species in Alzheimer's disease. *Acc Chem Res* **47**, 2475-2482 (2014).

86. Derrick, J. S. & Lim, M. H. Tools of the trade: investigations into design strategies of small molecules to target components in Alzheimer's disease. *Chembiochem* **16**, 887-898 (2015).

87. Liu, D. *et al.* Inhibitor discovery targeting the intermediate structure of beta-amyloid peptide on the conformational transition pathway: implications in the aggregation mechanism of beta-amyloid peptide. *Biochemistry* **45**, 10963-10972 (2006).

88. Findeis, M. A. Approaches to discovery and characterization of inhibitors of amyloid beta-peptide polymerization. *Biochim. Biophys. Acta.* **1502**, 76-84 (2000).

89. Sciarretta, K. L., Gordon, D. J. & Meredith, S. C. Peptide-based inhibitors of amyloid assembly. *Methods Enzymol.* **413**, 273-312 (2006).

90. Necula, M., Kayed, R., Milton, S. & Glabe, C. G. Small molecule inhibitors of aggregation indicate that amyloid beta oligomerization and fibrillization pathways are independent and distinct. *J. Biol. Chem.* **282**, 10311-10324 (2007).

91. Ryan, T. M. *et al.* Small amphipathic molecules modulate secondary structure and amyloid fibril-forming kinetics of Alzheimer disease peptide Abeta(1-42). *J. Biol. Chem.* **287**, 16947-16954 (2012).

92. Zhu, M. *et al.* Identification of small-molecule binding pockets in the soluble monomeric form of the Abeta42 peptide. *J. Chem. Phys.* **139**, 035101 (2013).

93. Walsh, D. M. *et al.* Certain inhibitors of synthetic amyloid beta-peptide (Abeta) fibrillogenesis block oligomerization of natural Abeta and thereby rescue long-term potentiation. *J. Neurosci.* **25**, 2455-2462 (2005).

94. Noda, S. *et al.* Thioflavin T-Silent Denaturation Intermediates Support the Main-Chain-Dominated Architecture of Amyloid Fibrils. *Biochemistry* **55**, 3937-3948 (2016).

95. Coalier, K. A., Paranjape, G. S., Karki, S. & Nichols, M. R. Stability of early-stage amyloid-beta(1-42) aggregation species. *Biochim. Biophys. Acta.* **1834**, 65-70 (2013).

96. Fezoui, Y. & Teplow, D. B. Kinetic studies of amyloid beta-protein fibril assembly. Differential effects of alpha-helix stabilization. *J. Biol. Chem.* **277**, 36948-36954 (2002).

97. LeVine, H., 3rd. Thioflavine T interaction with synthetic Alzheimer's disease beta-amyloid peptides: detection of amyloid aggregation in solution. *Protein Sci.* **2**, 404-410 (1993).

98. Shabestari, M. H., Meeuwenoord, N. J., Filippov, D. V. & Huber, M. Interaction of the amyloid beta peptide with sodium dodecyl sulfate as a membrane-mimicking detergent. *J. Biol. Phys.* **42**, 299-315 (2016).

99. So, M. *et al.* Supersaturation-Limited and Unlimited Phase Spaces Compete to Produce Maximal Amyloid Fibrillation near the Critical Micelle Concentration of Sodium Dodecyl Sulfate. *Langmuir* **31**, 9973-9982 (2015).

100. Nie, Q., Du, X. G. & Geng, M. Y. Small molecule inhibitors of amyloid beta peptide aggregation as a potential therapeutic strategy for Alzheimer's disease. *Acta. Pharmacol. Sin.* **32**, 545-551 (2011).

101.   Tjernberg, L. O. *et al.* Arrest of beta-amyloid fibril formation by a pentapeptide ligand. *J. Biol. Chem.* **271**, 8545-8548 (1996).

102.   Zhang, L. *et al.* Kinetic studies of inhibition of the amyloid beta (1-42) aggregation using a ferrocene-tagged beta-sheet breaker peptide. *Anal. Biochem.* **434**, 292-299 (2013).

103.   Tjernberg, L. O. *et al.* Controlling amyloid beta-peptide fibril formation with protease-stable ligands. *J. Biol. Chem.* **272**, 12601-12605 (1997).

104.   Wood, S. J., Wetzel, R., Martin, J. D. & Hurle, M. R. Prolines and amyloidogenicity in fragments of the Alzheimer's peptide beta/A4. *Biochemistry* **34**, 724-730 (1995).

105.   Soto, C. *et al.* Beta-sheet breaker peptides inhibit fibrillogenesis in a rat brain model of amyloidosis: implications for Alzheimer's therapy. *Nat. Med.* **4**, 822-826 (1998).

106.   Vagner, J., Qu, H. & Hruby, V. J. Peptidomimetics, a synthetic tool of drug discovery. *Curr. Opin. Chem. Biol.* **12**, 292-296 (2008).

107.   Hatahet, F. & Ruddock, L. W. Modulating proteostasis: peptidomimetic inhibitors and activators of protein folding. *Curr. Pharm. Des.* **15**, 2488-2507 (2009).

108.   Arai, T. *et al.* A cyclic KLVFF-derived peptide aggregation inhibitor induces the formation of less-toxic off-pathway amyloid-beta oligomers. *Chembiochem* **15**, 2577-2583 (2014).

109.   Chafekar, S. M. *et al.* Branched KLVFF tetramers strongly potentiate inhibition of beta-amyloid aggregation. *Chembiochem* **8**, 1857-1864 (2007).

110.   Adessi, C. & Soto, C. Beta-sheet breaker strategy for the treatment of Alzheimer's disease. *Drug. Develop. Res.* **56**, 184-193 (2002).

111.   Beghyn, T., Deprez-Poulain, R., Willand, N., Folleas, B. & Deprez, B. Natural compounds: leads or ideas? Bioinspired molecules for drug discovery. *Chem. Biol. Drug. Des.* **72**, 3-15 (2008).

112.   Porat, Y., Abramowitz, A. & Gazit, E. Inhibition of amyloid fibril formation by polyphenols: structural similarity and aromatic interactions as a common inhibition mechanism. *Chem. Biol. Drug. Des.* **67**, 27-37 (2006).

113.   Lakey-Beitia, J., Berrocal, R., Rao, K. S. & Durant, A. A. Polyphenols as therapeutic molecules in Alzheimer's disease through modulating amyloid pathways. *Mol. Neurobiol.* **51**, 466-479 (2015).

114. Yang, F. *et al.* Curcumin inhibits formation of amyloid beta oligomers and fibrils, binds plaques, and reduces amyloid in vivo. *J. Biol. Chem.* **280**, 5892-5901 (2005).

115. Hamaguchi, T., Ono, K. & Yamada, M. REVIEW: Curcumin and Alzheimer's disease. *CNS Neurosci. Ther.* **16**, 285-297 (2010).

116. Mithu, V. S. *et al.* Curcumin alters the salt bridge-containing turn region in amyloid beta(1-42) aggregates. *J. Biol. Chem.* **289**, 11122-11131 (2014).

117. Jang, J. H. & Surh, Y. J. Protective effect of resveratrol on beta-amyloid-induced oxidative PC12 cell death. *Free Radic. Biol. Med.* **34**, 1100-1110 (2003).

118. Conte, A., Pellegrini, S. & Tagliazucchi, D. Synergistic protection of PC12 cells from beta-amyloid toxicity by resveratrol and catechin. *Brain Res. Bull.* **62**, 29-38 (2003).

119. Savaskan, E. *et al.* Red wine ingredient resveratrol protects from beta-amyloid neurotoxicity. *Gerontology* **49**, 380-383 (2003).

120. Ge, J. F., Qiao, J. P., Qi, C. C., Wang, C. W. & Zhou, J. N. The binding of resveratrol to monomer and fibril amyloid beta. *Neurochem. Int.* **61**, 1192-1201 (2012).

121. Feng, Y. *et al.* Resveratrol inhibits beta-amyloid oligomeric cytotoxicity but does not prevent oligomer formation. *Neurotoxicology* **30**, 986-995 (2009).

122. Ehrnhoefer, D. E. *et al.* EGCG redirects amyloidogenic polypeptides into unstructured, off-pathway oligomers. *Nat. Struct. Mol. Biol.* **15**, 558-566 (2008).

123. Bieschke, J. *et al.* EGCG remodels mature alpha-synuclein and amyloid-beta fibrils and reduces cellular toxicity. *Proc. Natl. Acad. Sci. U.S.A.* **107**, 7710-7715 (2010).

124. Kocisko, D. A. *et al.* New inhibitors of scrapie-associated prion protein formation in a library of 2000 drugs and natural products. *J. Virol.* **77**, 10288-10294 (2003).

125. Meng, F., Abedini, A., Plesner, A., Verchere, C. B. & Raleigh, D. P. The flavanol (-)-epigallocatechin 3-gallate inhibits amyloid formation by islet amyloid polypeptide, disaggregates amyloid fibrils, and protects cultured cells against IAPP-induced toxicity. *Biochemistry* **49**, 8127-8133 (2010).

126. Chandrashekaran, I. R., Adda, C. G., MacRaild, C. A., Anders, R. F. & Norton, R. S. Inhibition by flavonoids of amyloid-like fibril formation by Plasmodium falciparum merozoite surface protein 2. *Biochemistry* **49**, 5899-5908 (2010).

127. Francioso, A., Mastromarino, P., Masci, A., d'Erme, M. & Mosca, L. Chemistry, stability and bioavailability of resveratrol. *Med. Chem.* **10**, 237-245 (2014).

128. Baell, J. & Walters, M. A. Chemistry: Chemical con artists foil drug discovery. *Nature* **513**, 481-483 (2014).

129. Wang, Q., Yu, X., Li, L. & Zheng, J. Inhibition of amyloid-beta aggregation in Alzheimer's disease. *Curr. Pharm. Des.* **20**, 1223-1243 (2014).

130. Patel, V. *et al.* Small molecules and Alzheimer's disease: misfolding, metabolism and imaging. *Curr. Alzheimer Res.* **12**, 445-461 (2015).

131. Wolman, M. & Bubis, J. J. The cause of the green polarization color of amyloid stained with Congo red. *Histochemie* **4**, 351-356 (1965).

132. Puchtler, H. & Sweat, F. Congo red as a stain for fluorescence microscopy of amyloid. *J. Histochem. Cytochem.* **13**, 693-694 (1965).

133. Hewlett, B. R. Studies on the staining of amyloid with Congo red. *Can. J. Med. Technol.* **28**, 248-261 (1966).

134. Lorenzo, A. & Yankner, B. A. Beta-amyloid neurotoxicity requires fibril formation and is inhibited by congo red. *Proc. Natl. Acad. Sci. U.S.A.* **91**, 12243-12247 (1994).

135. Abe, K., Kato, M. & Saito, H. Congo red reverses amyloid beta protein-induced cellular stress in astrocytes. *Neurosci. Res.* **29**, 129-134 (1997).

136. Podlisny, M. B. *et al.* Oligomerization of endogenous and synthetic amyloid beta-protein at nanomolar levels in cell culture and stabilization of monomer by Congo red. *Biochemistry* **37**, 3602-3611 (1998).

137. Pedersen, M. O. *et al.* NMR reveals two-step association of Congo Red to amyloid beta in low-molecular-weight aggregates. *J. Phys. Chem. B* **114**, 16003-16010 (2010).

138. Sinha, S. *et al.* Lysine-specific molecular tweezers are broad-spectrum inhibitors of assembly and toxicity of amyloid proteins. *J. Am. Chem. Soc.* **133**, 16958-16969 (2011).

139. Mihatsch, M. J. & Bremer, J. Acid fuchsin orange G-stain (AFOG) for glomerular protein deposits. *Clin. Nephrol.* **9**, 259 (1978).

140. Pollack, S. J., Sadler, II, Hawtin, S. R., Tailor, V. J. & Shearman, M. S. Sulfonated dyes attenuate the toxic effects of beta-amyloid in a structure-specific fashion. *Neurosci. Lett.* **197**, 211-214 (1995).

141. Landau, M. *et al.* Towards a pharmacophore for amyloid. *PLoS Biol.* **9**, e1001080 (2011).

142. Wainwright, M. & Crossley, K. B. Methylene Blue--a therapeutic dye for all seasons? *J. Chemother.* **14**, 431-443 (2002).

143. Necula, M. *et al.* Methylene blue inhibits amyloid Abeta oligomerization by promoting fibrillization. *Biochemistry* **46**, 8850-8860 (2007).

144. Irwin, J. A., Wong, H. E. & Kwon, I. Different fates of Alzheimer's disease amyloid-beta fibrils remodeled by biocompatible small molecules. *Biomacromolecules* **14**, 264-274 (2013).

145. Paban, V. *et al.* Therapeutic and preventive effects of methylene blue on Alzheimer's disease pathology in a transgenic mouse model. *Neuropharmacology* **76 Pt A**, 68-79 (2014).

146. Williams, A. D. *et al.* Structural properties of Abeta protofibrils stabilized by a small molecule. *Proc. Natl. Acad. Sci. U.S.A.* **102**, 7115-7120 (2005).

147. Guido, R. V., Oliva, G. & Andricopulo, A. D. Modern drug discovery technologies: opportunities and challenges in lead discovery. *Comb. Chem. High. Throughput. Screen.* **14**, 830-839 (2011).

148. Meiler, J. & Baker, D. ROSETTALIGAND: protein-small molecule docking with full side-chain flexibility. *Proteins* **65**, 538-548 (2006).

149. Davis, I. W. & Baker, D. RosettaLigand docking with full ligand and receptor flexibility. *J. Mol. Biol.* **385**, 381-392 (2009).

150. Jiang, L. *et al.* Structure-based discovery of fiber-binding compounds that reduce the cytotoxicity of amyloid beta. *Elife* **2**, e00857 (2013).

151. Fokkens, M., Schrader, T. & Klarner, F. G. A molecular tweezer for lysine and arginine. *J. Am. Chem. Soc.* **127**, 14415-14421 (2005).

152. Zheng, X. *et al.* Amyloid beta-protein assembly: The effect of molecular tweezers CLR01 and CLR03. *J. Phys. Chem. B* **119**, 4831-4841 (2015).

153. Malishev, R. *et al.* Toxicity inhibitors protect lipid membranes from disruption by Abeta42. *ACS Chem. Neurosci.* **6**, 1860-1869 (2015).

154. Attar, A., Chan, W. T., Klarner, F. G., Schrader, T. & Bitan, G. Safety and pharmacological characterization of the molecular tweezer CLR01 - a broad-spectrum inhibitor of amyloid proteins' toxicity. *BMC Pharmacol. Toxicol.* **15**, 23 (2014).

155. Pithadia, A. S. *et al.* Reactivity of diphenylpropynone derivatives toward metal-associated amyloid-beta species. *Inorg. Chem.* **51**, 12959-12967 (2012).

156. Dedeoglu, A. *et al.* Preliminary studies of a novel bifunctional metal chelator targeting Alzheimer's amyloidogenesis. *Exp. Gerontol.* **39**, 1641-1649 (2004).

157. Wu, W. H. *et al.* Sequestration of copper from beta-amyloid promotes selective lysis by cyclen-hybrid cleavage agents. *J. Biol. Chem.* **283**, 31657-31664 (2008).

158. Choi, J. S., Braymer, J. J., Nanga, R. P., Ramamoorthy, A. & Lim, M. H. Design of small molecules that target metal-A{beta} species and regulate metal-induced A{beta} aggregation and neurotoxicity. *Proc. Natl. Acad. Sci. U.S.A.* **107**, 21990-21995 (2010).

159. Cherny, R. A. *et al.* Treatment with a copper-zinc chelator markedly and rapidly inhibits beta-amyloid accumulation in Alzheimer's disease transgenic mice. *Neuron* **30**, 665-676 (2001).

160. Zhang, W. *et al.* F-18 stilbenes as PET imaging agents for detecting beta-amyloid plaques in the brain. *J. Med. Chem.* **48**, 5980-5988 (2005).

161. Ono, M. *et al.* Diphenylpropynone derivatives as probes for imaging beta-amyloid plaques in Alzheimer's brains. *Bioorg. Med. Chem. Lett.* **21**, 117-120 (2011).

162. Beck, M. W. *et al.* A rationally designed small molecule for identifying an in vivo link between metal–amyloid-β complexes and the pathogenesis of Alzheimer's disease. *Chem. Sci.*, **6**, 1879-1886 (2015).

163. Lee, S. *et al.* Rational design of a structural framework with potential use to develop chemical reagents that target and modulate multiple facets of Alzheimer's disease. *J. Am. Chem. Soc.* **136**, 299-310 (2014).

164. Kochi, A. *et al.* A novel hybrid of 6-chlorotacrine and metal–amyloid-β modulator for inhibition of acetylcholinesterase and metal-induced amyloid-β aggregation. *Chem. Sci.* **4**, 4137-4145 (2013).

165. Ames, D. J., Bhathal, P. S., Davies, B. M. & Fraser, J. R. E. Hepatotoxicity of Tetrahydroacridine. *The Lancet* **1**, 887 (1988).

166. Biancalana, M. & Koide, S. Molecular mechanism of Thioflavin-T binding to amyloid fibrils. *Biochim. Biophys. Acta.* **1804**, 1405-1412 (2010).

167. Batzli, K. M. & Love, B. J. Agitation of amyloid proteins to speed aggregation measured by ThT fluorescence: a call for standardization. *Mater. Sci. Eng. C. Mater. Biol. Appl.* **48**, 359-364 (2015).

168. Meisl, G. *et al.* Molecular mechanisms of protein aggregation from global fitting of kinetic models. *Nat. Protoc.* **11**, 252-272 (2016).

169. Arosio, P. *et al.* Kinetic analysis reveals the diversity of microscopic mechanisms through which molecular chaperones suppress amyloid formation. *Nat. Commun.* **7**, 10948 (2016).

170. Arosio, P., Meisl, G., Andreasen, M. & Knowles, T. P. Preventing peptide and protein misbehavior. *Proc. Natl. Acad. Sci. U.S.A.* **112**, 5267-5268 (2015).

171. Jha, S. *et al.* pH dependence of amylin fibrillization. *Biochemistry* **53**, 300-310 (2014).

172. Hudson, S. A., Ecroyd, H., Kee, T. W. & Carver, J. A. The thioflavin T fluorescence assay for amyloid fibril detection can be biased by the presence of exogenous compounds. *FEBS J.* **276**, 5960-5972 (2009).

173. Meng, F., Marek, P., Potter, K. J., Verchere, C. B. & Raleigh, D. P. Rifampicin does not prevent amyloid fibril formation by human islet amyloid polypeptide but does inhibit fibril thioflavin-T interactions: implications for mechanistic studies of beta-cell death. *Biochemistry* **47**, 6016-6024 (2008).

174. Suzuki, Y., Brender, J. R., Hartman, K., Ramamoorthy, A. & Marsh, E. N. Alternative pathways of human islet amyloid polypeptide aggregation distinguished by (19)f nuclear magnetic resonance-detected kinetics of monomer consumption. *Biochemistry* **51**, 8154-8162 (2012).

175. Wong, A. G. *et al.* Analysis of the Amyloidogenic Potential of Pufferfish (Takifugu rubripes) Islet Amyloid Polypeptide Highlights the Limitations of Thioflavin-T Assays and the Difficulties in Defining Amyloidogenicity. *Biochemistry* **55**, 510-518 (2016).

176. Easterhoff, D. *et al.* Fluorescence detection of cationic amyloid fibrils in human semen. *Bioorg. Med. Chem. Lett.* **23**, 5199-5202 (2013).

177. Arosio, P., Knowles, T. P. & Linse, S. On the lag phase in amyloid fibril formation. *Phys. Chem. Chem. Phys.* **17**, 7606-7618 (2015).

178. Wong, P. T. *et al.* Amyloid-beta membrane binding and permeabilization are distinct processes influenced separately by membrane charge and fluidity. *J. Mol. Biol.* **386**, 81-96 (2009).

179.   Pithadia, A. S. *et al.* Influence of a curcumin derivative on hIAPP aggregation in the absence and presence of lipid membranes. *Chem. Commun.* **52**, 942-945 (2016).

180.   Lee, J., Culyba, E. K., Powers, E. T. & Kelly, J. W. Amyloid-beta forms fibrils by nucleated conformational conversion of oligomers. *Nat. Chem. Biol.* **7**, 602-609 (2011).

181.   Lomakin, A., Teplow, D. B., Kirschner, D. A. & Benedek, G. B. Kinetic theory of fibrillogenesis of amyloid beta-protein. *Proc. Natl. Acad. Sci. U.S.A.* **94**, 7942-7947 (1997).

182.   Fu, Z., Aucoin, D., Davis, J., Van Nostrand, W. E. & Smith, S. O. Mechanism of Nucleated Conformational Conversion of Abeta42. *Biochemistry* **54**, 4197-4207 (2015).

183.   Mok, Y. F., Howlett, G. J. & Griffin, M. D. Sedimentation Velocity Analysis of the Size Distribution of Amyloid Oligomers and Fibrils. *Methods Enzymol.* **562**, 241-256 (2015).

184.   Engel, M. F. *et al.* Membrane damage by human islet amyloid polypeptide through fibril growth at the membrane. *Proc. Natl. Acad. Sci. U.S.A.* **105**, 6033-6038 (2008).

185.   Paravastu, A. K., Leapman, R. D., Yau, W. M. & Tycko, R. Molecular structural basis for polymorphism in Alzheimer's beta-amyloid fibrils. *Proc. Natl. Acad. Sci. U.S.A.* **105**, 18349-18354 (2008).

186.   Sachse, C., Grigorieff, N. & Fandrich, M. Nanoscale flexibility parameters of Alzheimer amyloid fibrils determined by electron cryo-microscopy. *Angew. Chem. Int. Ed. Engl.* **49**, 1321-1323 (2010).

187.   Schmidt, M. *et al.* Peptide dimer structure in an Abeta(1-42) fibril visualized with cryo-EM. *Proc. Natl. Acad. Sci. U.S.A.* **112**, 11858-11863 (2015).

188.   Yates, E. A. & Legleiter, J. Preparation protocols of abeta(1-40) promote the formation of polymorphic aggregates and altered interactions with lipid bilayers. *Biochemistry* **53**, 7038-7050 (2014).

189.   Gosal, W. S., Myers, S. L., Radford, S. E. & Thomson, N. H. Amyloid under the atomic force microscope. *Protein Pept. Lett.* **13**, 261-270 (2006).

190.   Von Helden, G., Wyttenbach, T. & Bowers, M. T. Conformation of Macromolecules in the Gas-Phase - Use of Matrix-Assisted Laser-Desorption Methods in Ion Chromatography. *Science* **267**, 1483-1485 (1995).

191.   Ruotolo, B. T. & Robinson, C. V. Aspects of native proteins are retained in vacuum. *Curr. Opin. Chem. Biol.* **10**, 402-408 (2006).

192. Ruotolo, B. T., Benesch, J. L. P., Sandercock, A. M., Hyung, S. J. & Robinson, C. V. Ion mobility-mass spectrometry analysis of large protein complexes. *Nat. Protoc.* **3**, 1139-1152 (2008).

193. Zhong, Y., Hyung, S. J. & Ruotolo, B. T. Ion mobility-mass spectrometry for structural proteomics. *Expert Rev. Proteomics* **9**, 47-58 (2012).

194. Saunders, J. C. *et al.* An in vivo platform for identifying inhibitors of protein aggregation. *Nat. Chem. Biol.* **12**, 94-101 (2016).

195. Hyung, S. J. *et al.* Insights into antiamyloidogenic properties of the green tea extract (-)-epigallocatechin-3-gallate toward metal-associated amyloid-beta species. *Proc. Natl. Acad. Sci. U.S.A.* **110**, 3743-3748 (2013).

196. Bernstein, S. L. *et al.* Amyloid-beta protein oligomerization and the importance of tetramers and dodecamers in the aetiology of Alzheimer's disease. *Nat. Chem.* **1**, 326-331 (2009).

197. Bleiholder, C., Dupuis, N. F., Wyttenbach, T. & Bowers, M. T. Ion mobility-mass spectrometry reveals a conformational conversion from random assembly to b-sheet in amyloid fibril formation. *Nat. Chem.* **3**, 172-177 (2011).

198. Young, L. M., Cao, P., Raleigh, D. P., Ashcroft, A. E. & Radford, S. E. Ion Mobility Spectrometry-Mass Spectrometry Defines the Oligomeric Intermediates in Amylin Amyloid Formation and the Mode of Action of Inhibitors. *J. Am. Chem. Soc.* **136**, 660-670 (2014).

199. Spencer, R. K., Li, H. & Nowick, J. S. X-ray Crystallographic Structures of Trimers and Higher-Order Oligomeric Assemblies of a Peptide Derived from A beta(17-36). *J. Am. Chem. Soc.* **136**, 5595-5598 (2014).

200. Truex, N. L. & Nowick, J. S. Coassembly of Peptides Derived from beta-Sheet Regions of beta-Amyloid. *J. Am. Chem. Soc.* **138**, 13891-13900 (2016).

201. Truex, N. L., Wang, Y. L. & Nowick, J. S. Assembly of Peptides Derived from beta-Sheet Regions of beta-Amyloid. J. Am. Chem. Soc. **138**, 13882-13890 (2016).

202. Suzuki, Y. *et al.* Resolution of oligomeric species during the aggregation of Abeta1-40 using (19)F NMR. *Biochemistry* **52**, 1903-1912 (2013).

203. Schanda, P. & Brutscher, B. Very fast two-dimensional NMR spectroscopy for real-time investigation of dynamic events in proteins on the time scale of seconds. *J. Am. Chem. Soc.* **127**, 8014-8015 (2005).

204. DeToma, A. S. *et al.* Synthetic Flavonoids, Aminoisoflavones: Interaction and Reactivity with Metal-Free and Metal-Associated Amyloid-beta Species. *Chem. Sci.* **5**, 4851-4862 (2014).

205. Fawzi, N. L., Ying, J., Ghirlando, R., Torchia, D. A. & Clore, G. M. Atomic-resolution dynamics on the surface of amyloid-beta protofibrils probed by solution NMR. *Nature* **480**, 268-272 (2011).

206. Bodner, C. R., Dobson, C. M. & Bax, A. Multiple tight phospholipid-binding modes of alpha-synuclein revealed by solution NMR spectroscopy. *J. Mol. Biol.* **390**, 775-790 (2009).

207. Bodner, C. R., Maltsev, A. S., Dobson, C. M. & Bax, A. Differential phospholipid binding of alpha-synuclein variants implicated in Parkinson's disease revealed by solution NMR spectroscopy. *Biochemistry* **49**, 862-871 (2010).

208. Fusco, G. *et al.* Direct observation of the three regions in alpha-synuclein that determine its membrane-bound behaviour. *Nat. Commun.* **5**, 3827 (2014).

209. Goerke, S. *et al.* Aggregation-induced changes in the chemical exchange saturation transfer (CEST) signals of proteins. *NMR Biomed.* (2016).

210. Tang, M., Comellas, G. & Rienstra, C. M. Advanced solid-state NMR approaches for structure determination of membrane proteins and amyloid fibrils. *Acc. Chem. Res.* **46**, 2080-2088 (2013).

211. Muller, H., Etzkorn, M. & Heise, H. Solid-state NMR spectroscopy of proteins. *Top. Curr. Chem.* **335**, 121-156 (2013).

212. Qiang, W., Akinlolu, R. D., Nam, M. & Shu, N. Structural evolution and membrane interaction of the 40-residue beta amyloid peptides: differences in the initial proximity between peptides and the membrane bilayer studied by solid-state nuclear magnetic resonance spectroscopy. *Biochemistry* **53**, 7503-7514 (2014).

213. DeToma, A. S., Choi, J. S., Braymer, J. J. & Lim, M. H. Myricetin: a naturally occurring regulator of metal-induced amyloid-beta aggregation and neurotoxicity. *Chembiochem* **12**, 1198-1201 (2011).

214. He, X. *et al.* Exploring the reactivity of flavonoid compounds with metal-associated amyloid-beta species. *Dalton Trans.* **41**, 6558-6566 (2012).

215. Pratico, D. Oxidative stress hypothesis in Alzheimer's disease: a reappraisal. *Trends Pharmacol. Sci.* **29**, 609-615 (2008).

216. Beranova, L., Cwiklik, L., Jurkiewicz, P., Hof, M. & Jungwirth, P. Oxidation changes physical properties of phospholipid bilayers: fluorescence spectroscopy and molecular simulations. *Langmuir* **26**, 6140-6144 (2010).

217. Negre-Salvayre, A. *et al.* Pathological aspects of lipid peroxidation. *Free Radic. Res.* **44**, 1125-1171 (2010).

218. Sultana, R., Perluigi, M. & Allan Butterfield, D. Lipid peroxidation triggers neurodegeneration: a redox proteomics view into the Alzheimer disease brain. *Free Radic. Biol. Med.* **62**, 157-169 (2013).

Chapter 2

Reactivity of Metal-Free and Metal-Associated Amyloid-β with Glycosylated Polyphenols and Their Esterified Derivatives

This chapter was adapted from the following publication:

Korshavn, K. J., Jang, M., Kwak, Y. J., Kochi, A., Vertuani, S., Manfredini, S., Ramamoorthy, A. & Lim, M. H. Reactivity of Reactivity of Metal-Free and Metal-Associated Amyloid-β with Glycosylated Polyphenols and Their Esterified Derivatives. *Sci. Rep.* **5**, 17842 (2015).

2.1. Introduction

Alzheimer's disease (AD) is a growing concern for global public health, spurred on, in part, by a lack of effective treatments or cures.[1] While potential therapeutics have been developed for AD, their clinical success has been hindered by a limited molecular level understanding of the disease's etiology.[2-4] AD is commonly considered a protein misfolding disease characterized by the presence of proteinaceous aggregates, including senile plaques composed primarily of amyloid-β (two main Aβ forms, Aβ$_{40}$ and Aβ$_{42}$).[4-6] Aβ undergoes a progressive aggregation process, advancing from a small, intrinsically disordered peptide to intermediate oligomers of various sizes and structures, finally forming extended fibers; individual aggregates are believed to have varying degrees of toxicity and relevance in AD.[4,6,7]

The senile plaques in the AD-affected brain have been shown to contain elevated concentrations of transition metals, specifically Cu, Zn, and Fe, which suggests that these metal ions interact with and alter the aggregation of Aβ.[4,8-10] Understanding the interactions between metal ions and Aβ *in vitro* could help elucidate potentially toxic mechanisms of both factors in

AD.[10-12] These metal ions could accelerate the aggregation of Aβ while simultaneously generating a variety of aggregates which may have biological functions distinct from those formed in the absence of metals.[9,10] Additionally, the binding of Aβ to redox active metals such as Cu and Fe can facilitate redox cycling and lead to the production of reactive oxygen species (ROS) resulting in an environment of exacerbated oxidative stress, a known characteristic of the AD-afflicted brain.[12-14] The effects of these interactions *in vivo* remain unclear, however; in-depth understanding is hindered by the multifactorial nature of the disease which makes it difficult to identify and quantify the influence of any of the potentially causative agents.

The application of chemical probes which can modulate the various factors associated with AD (*e.g.*, Aβ, metal ions) may advance our understanding of the disease and uncover different toxic factors by isolating individual potential culprits. Unfortunately, there remains a lack of understanding about the relationship between small molecules and their subsequent biological functions with regards to the multiple aspects associated with AD. It is believed that hydrophobic interactions drive early stages of Aβ aggregation and that compounds with similarly hydrophobic regions may effectively disrupt these aggregation-promoting forces and act as modulators of amyloid formation; some compounds of this nature have been investigated previously.[6] It is unclear, though, which chemical moieties on these compounds may be the most potent at redirecting this process. To increase the specificity of anti-amyloidogenic compounds, multifunctional compounds have been designed to target and modulate additional aspects associated with AD (*i.e.*, metal-associated Aβ (metal–Aβ), ROS) along with metal-free Aβ simultaneously.[15-17] Compounds known to interact with Aβ have been appended with known metal binding moieties to generate molecules capable of targeting both metal-free Aβ and metal–Aβ, and these multifunctional compounds have demonstrated an ability to modulate both factors

to differing extents.[15,16] As was the case with Aβ interaction, however, rational design of these
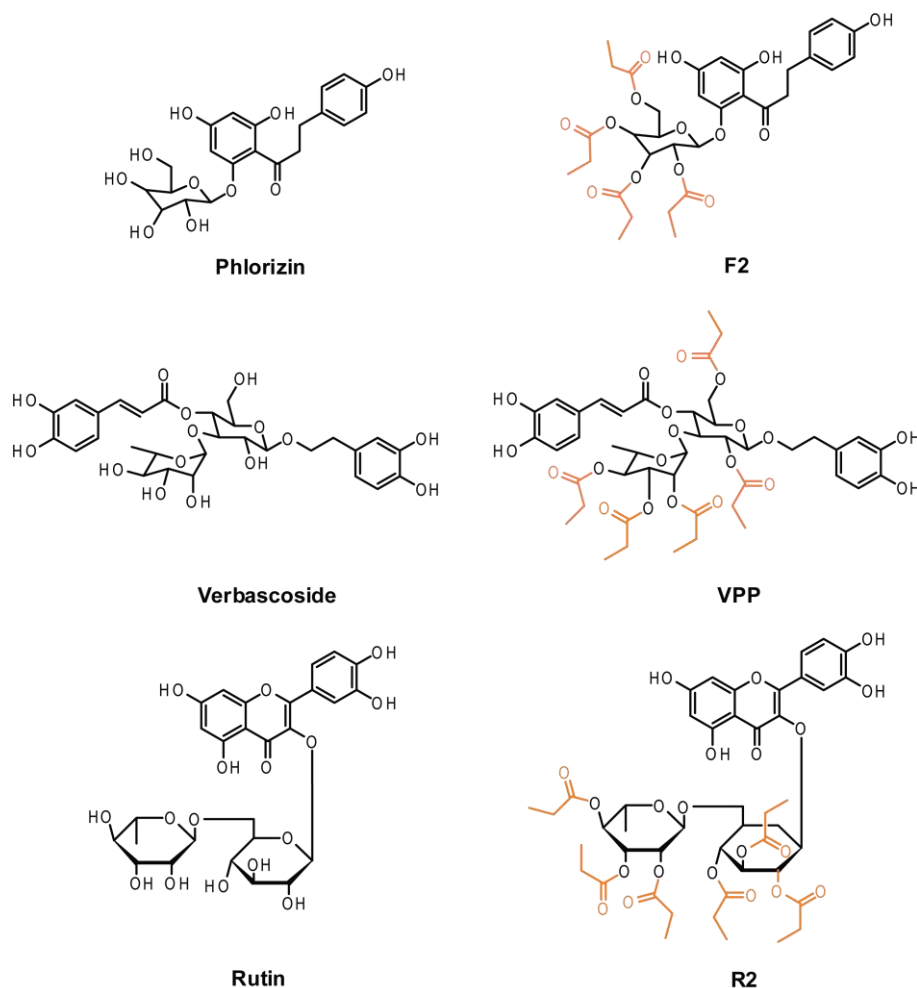
Figure 2.1. Chemical structures of glycosylated polyphenols and their derivatives. **Phlorizin**, 1-(2,4-dihydroxy-6-(((2S,3R,4R,6R)-3,4,5-trihydroxy-6-(hydroxymethyl)tetrahydro-2H-pyran -2-yl)oxy)phenyl)-3-(4-hydroxyphenyl)propan-1-one; **Verbascoside**, (2R,3R,4R,5R,6R)-6-(3,4-dihydroxyphenethoxy)-5-hydroxy-2-(hydroxymethyl)-4-(((2S,3R,4R,5R)-3,4,5-trihydroxy-6-methyltetrahydro-2H-pyran-2-yl)oxy)tetrahydro-2H-pyran-3-yl (E)-3-(3,4-dihydroxy phenyl)acrylate; **Rutin**, 2-(3,4-dihydroxyphenyl)-5,7-dihydroxy-3-(((2S,3R,4S,5S,6R)-3,4,5-trihydroxy-6-((((2S,3R,4R,5S)-3,4,5-trihydroxytetrahydro-2H-pyran-2-yl)oxy)methyl)tetra hydro-2H-pyran-2-yl)oxy)-4H-chromen-4-one; **F2**, (2S,3R,4R,6R)-2-(3,5-dihydroxy-2-(3-(4-hydroxyphenyl)propanoyl)phenoxy)-6-((propionyloxy)methyl)tetrahydro-2H-pyran-3,4,5-triyl tripropionate; **VPP**, (2S,3R,4R,5S)-2-(((2R,3R,4S,5R,6R)-2-(3,4-dihydroxyphenethoxy)-5-(((E)-3-(3,4-dihydroxyphenyl)acryloyl)oxy)-3-(propionyloxy)-6-((propionyloxy)methyl)tetrahydro-2H-pyran-4-yl)oxy)-6-methyltetrahydro-2H-pyran-3,4,5-triyl tripropionate; **R2**, (2R,3R,4R,5S,6S)-2-(((2R,3R,4S,5R,6S)-6-((2-(3,4-dihydroxyphenyl)-5,7-dihydroxy-4-oxo-4H-chromen-3-yl)oxy)-3,4,5-tris(propionyloxy)tetrahydro-2H-pyran-2-yl)methoxy)-6-methyl tetrahydro-2H-pyran-3,4,5-triyl tripropionate.

metal binding moieties is hindered by a limited understanding of how these chelating agents function in the complex AD environment. Additionally, while it is desirable for compounds to also mediate oxidative stress, both through the modulation of ROS and free radicals, this function is similarly difficult to rationally incorporate into a structural entity. Efforts have previously been made to design multifunctional compounds for investigating the role of metal-free Aβ, metal−Aβ, and pro-oxidants in AD,[18] but the advancements in the field are generally slowed by limited information on the structure-function relationships between small molecules and their ability to regulate these disease related features.

In order to gain better insight to this complex disease and to broaden current understanding of the connection between chemical structure and its function in the presence of factors associated with AD, three naturally occurring polyphenolic glycosides (**Phlorizin**, **Verbascoside**, and **Rutin**; Fig. 2.1) were chosen for a selective reactivity study towards both metal-free Aβ and metal−Aβ. The investigation of naturally occurring compounds gives the substantial advantage of a minimal toxicity profile and a significant amount of background information from traditional medicine. Natural polyphenolic products have been previously shown to possess potential anti-amyloidogenic activity.[19,20] Both **Verbascoside** and **Rutin** have demonstrated the capacity to redirect metal-free Aβ aggregation towards nontoxic species,[21-24] and phloretin, the non-glycosidic version of **Phlorizin**, has exhibited an ability to prevent membrane-associated aggregation of Aβ.[25] While these preliminary studies examined aggregation in the absence of metal ions, the presence of known metal interaction moieties, phenol and catechol groups in **Phlorizin** and **Verbascoside**/**Rutin**, respectively, suggests that these compounds may be capable of simultaneously interacting with both Aβ and metal ions.[26-29] Furthermore, all three compounds are known antioxidants, indicating that they could also help

mitigate oxidative stress associated with the AD-affected brain.[30-32] Finally, these compounds are naturally glycosylated, a modification which has been proposed to improve bioavailability and distribution in the brain,[33-35] as well as redirect the folding of metal-free Aβ species.[36,37] Combined, these structural and chemical features suggest that **Phlorizin**, **Verbascoside**, and **Rutin** possess unique chemical features desirable for a probe to target multiple factors (*i.e.*, metal-free and metal-bound Aβ) and mitigate their toxicity leading to AD.

To provide further insight into structure-activity relationships, selectively esterified derivatives, **F2**, **VPP**, and **R2** (Fig. 2.1), were prepared and investigated alongside their parent compounds.[30-32] Esterification could provide multiple benefits in the quest for an effective multifunctional probe while also acting as a general proof of concept that a prodrug approach is a viable method in the search for molecular tools in AD research. Ester formation may improve trafficking across lipid bilayers and facilitate targeted delivery of unprotected compounds within cells following cleavage by esterases; for these reasons, it is a commonly used modification in prodrug design.[38] The ester groups may also improve the ability of the compounds to passively diffuse across the blood brain barrier (BBB) due to greater lipophilicity.[16,39] Finally, the increased hydrophobicity could promote interactions between the compounds and the more aggregation prone regions of the Aβ sequence, which are similarly hydrophobic.[4,40] Overall, we believe that esterification may tune the ability of these three compounds to interact with both metal-free Aβ and metal–Aβ species while simultaneously improving the bioavailability, making them more suitable for future *in vivo* applications than their non-esterified counterparts. Using these six compounds, we aim to further expand the understanding of structure-function relationships between multifunctional probes towards both metal-free Aβ and metal–Aβ through a detailed, molecular level characterization.

2.2. Results

2.2.1. Influence of polyphenols on metal-free and metal-induced aggregation *in vitro*

To initially investigate the effects of the six polyphenols (Fig. 21) on the structure and formation of both metal-free and metal–Aβ aggregation pathways disaggregation (Fig. 2.2, 2.3, and A.1) and inhibition (Fig. A.2) experiments were performed. Both the more prevalent Aβ$_{40}$ and the more aggregation-prone Aβ$_{42}$ isoforms were employed in both inhibition and disaggregation studies.[4] For disaggregation experiments, Aβ was allowed to aggregate in either the absence or presence of either $CuCl_2$ or $ZnCl_2$ for 24 h to form aggregated species. The compounds were then added to these aggregates and incubated for either 4 or 24 h to determine their ability to redirect the size and structure of pre-aggregated Aβ species. In inhibition experiments, Aβ (for metal–Aβ samples, Aβ samples were treated with $CuCl_2$ or $ZnCl_2$) and the compounds were incubated for either 4 or 24 h to identify how they are capable of modulating the early steps in aggregation of both metal-free Aβ and metal–Aβ. Gel electrophoresis with Western blot (gel/Western blot) using an anti-Aβ antibody (6E10) and TEM were utilized to visualize the size distribution and morphology, respectively, of the resultant Aβ species upon treatment with polyphenols in the absence and presence of metal ions for both disaggregation and inhibition experiments.[18,41]

Neither **Phlorizin** nor **F2** demonstrated a significant ability to interact with Aβ or metal–Aβ species in either a disaggregatory or inhibitory manner. In disaggregation experiments, gel/Western blot revealed that neither of these compounds was able to transform preformed Aβ aggregates regardless of Aβ isoform or metal presence (Fig. 2.2a and 2.3a, lanes 2 and 3). **Phlorizin** did appear to slightly change the morphology of species to marginally more disordered than untreated fibrils based on TEM results; however, large and extended Aβ aggregates were
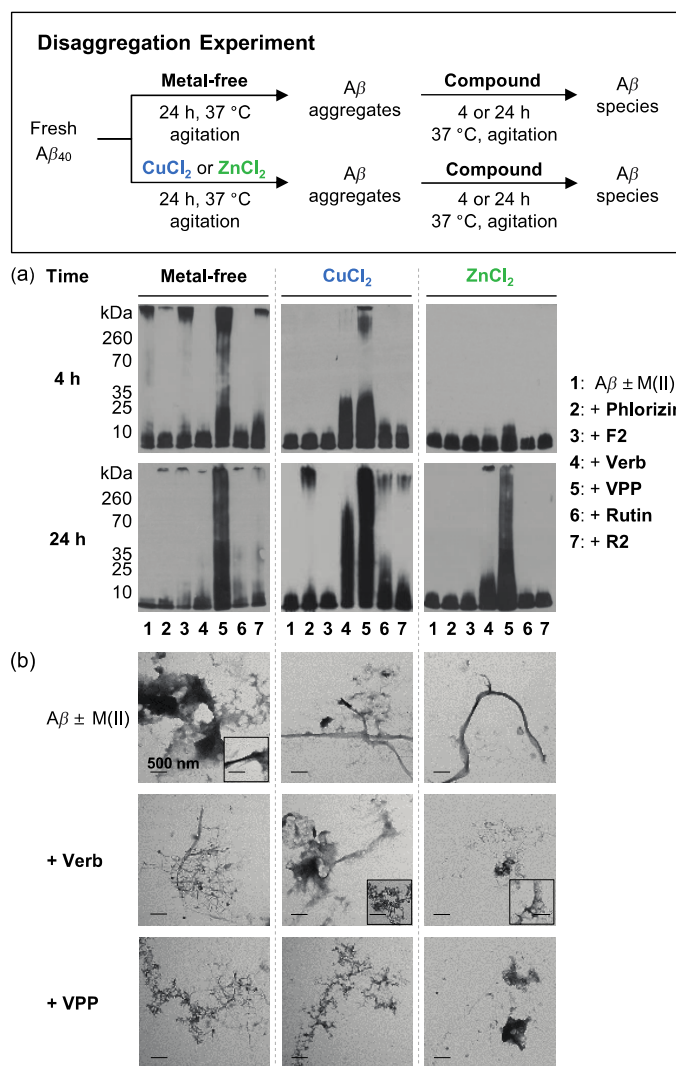
Figure 2.2. Modulation of preformed, metal-free and metal-induced Aβ$_{40}$ aggregates by **Phlorizin**, **F2**, **Verbascoside**, **VPP**, **Rutin**, or **R2**. A scheme of sample preparation for disaggregation experiments with Aβ$_{40}$ (top). (a) Analysis of the resultant Aβ$_{40}$ species by gel electrophoresis using Western blotting with an anti-Aβ antibody (6E10). (b) TEM images of the morphologies of the resultant Aβ species from the samples that were incubated for 24 h. Experimental conditions: [Aβ$_{40}$] = 25 μM; [CuCl$_2$ or ZnCl$_2$] = 25 μM; [compound] = 50 μM; 4 or 24 h incubation; pH 6.6 (for Cu(II) samples) or pH 7.4 (for metal-free and Zn(II) samples); 37 °C; constant agitation.

observed with and without metal ions (Fig. A.1). A similar lack of reactivity was observed in inhibition experiments (Fig. A.2, lanes 2 and 3). These two compounds appear unable to influence Aβ$_{40}$ and Aβ$_{42}$ aggregation behaviors regardless of the presence or absence of metal ions.

54

Both **Rutin** and **R2** showed mild reactivity with Aβ and/or metal–Aβ. Under disaggregation conditions, **R2** produced low MW aggregates of Aβ$_{40}$ (< 15 kDa) after 4 h in the absence of metal ions; after 24 h in the absence of metal ions, both **Rutin** and **R2** triggered relatively low MW aggregates (< 35 kDa) (Fig. 2.2a, lanes 6 and 7). The morphology of these species was slightly more compact that that of untreated Aβ$_{40}$ aggregates (Fig. A.1). A similarly sized range of Aβ$_{40}$ aggregates was generated by both **Rutin** and **R2** when CuCl$_2$ was present, after 24 h (Fig. 2.2a), and their morphology was even more compact than in the absence of metal ions (Fig. A.1). Neither **Rutin** nor **R2** appeared to have any impact on preformed Zn(II)−Aβ$_{40}$ aggregates. The two compounds displayed a minimal or no effect upon preformed Aβ$_{42}$ aggregates, regardless of the presence or absence of metal ions (Fig. 2.3a, lanes 6 and 7). **Rutin** and **R2** presented a modest ability to redirect Cu(II)-induced aggregation of Aβ$_{40}$ or Aβ$_{42}$ after 24 h incubation in inhibition studies (Fig. A.2, lanes 6 and 7). This suggests that both compounds have mild reactivity towards preformed Aβ aggregates, favoring those formed in the presence of CuCl$_2$.

Unlike the other four compounds, both **Verbascoside** and **VPP** were able to control Aβ$_{40}$ and Aβ$_{42}$ aggregation, though to different extents. When preformed, metal-free Aβ$_{40}$ aggregates were treated with **VPP** for 4 h, a wide MW range (10-260 kDa) of species was formed (Fig. 2.2a, lane 5). These species were still observed after 24 h incubation. **Verbascoside**, the non-esterified parent compound of **VPP**, did not indicate any reactivity against preformed metal-free Aβ$_{40}$ aggregates. Both compounds did demonstrate an ability to disaggregate Cu(II)−Aβ$_{40}$ aggregates, however (Fig. 2.2, lanes 4 and 5). After 4 h incubations the two compounds mainly generated low MW (< 35 kDa) aggregates, evident by gel/Western blot. Following 24 h incubation, both compounds were capable of producing much wider MW ranges of Cu(II)−Aβ$_{40}$ species (Fig.

2.2a, lanes 4 and 5). In the case of Zn(II)-containing aggregates; the initial disaggregation by **Verbascosde** and **VPP** was slower still. The $A\beta_{40}$ sample treated with **Verbascoside** for 24 h exhibited smaller-sized species while **VPP** triggered a wider range of aggregates, similar to that observed in both the absence of metals and the presence of Cu(II) (Fig. 2.2a). For all aggregates,
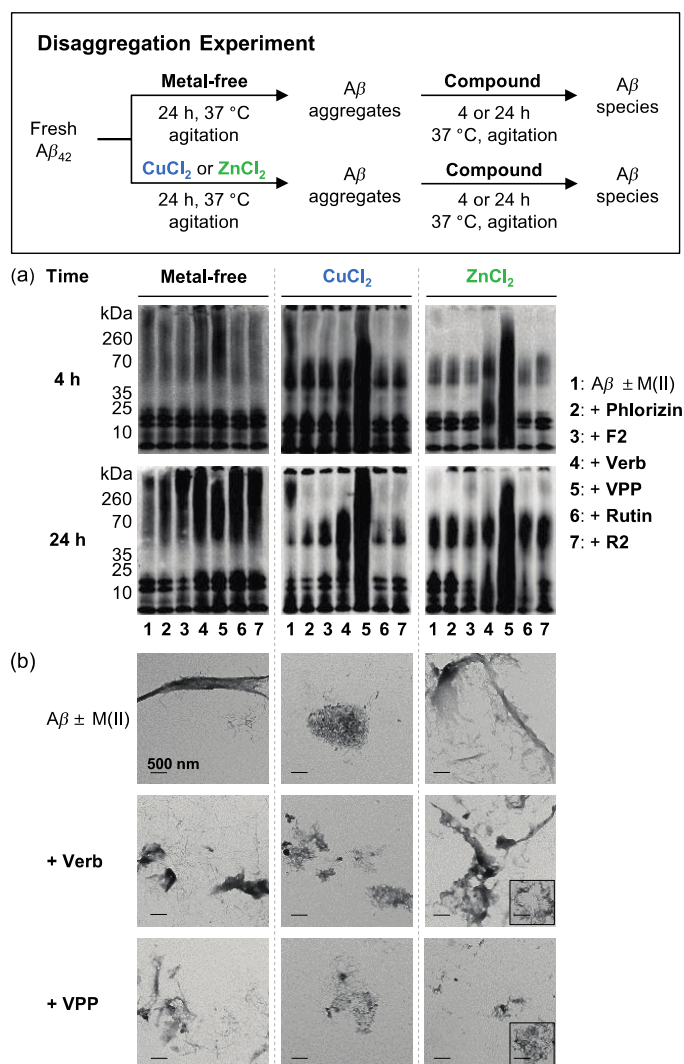
Figure 2.3. Influence of **Phlorizin**, **F2**, **Verbascoside**, **VPP**, **Rutin**, or **R2** on pre-generated metal-free and metal-induced $A\beta_{42}$ aggregates. A scheme of sample preparation for disaggregation experiments with $A\beta_{42}$ (top). (a) Analysis of the resultant $A\beta_{42}$ species by gel electrophoresis using Western blot with an anti-$A\beta$ antibody (6E10). (b) TEM images of the morphologies of the resultant $A\beta$ species from the samples that were incubated for 24 h. Experimental conditions: $[A\beta_{42}] = 25\ \mu M$; $[CuCl_2\ or\ ZnCl_2] = 25\ \mu M$; [compound] = 50 μM; 4 or 24 h incubation; pH 6.6 (for Cu(II) samples) or pH 7.4 (for metal-free and Zn(II) samples); 37 °C; constant agitation.

56

both **Verbascoside** and **VPP** were able to convert large extended fibrils into smaller, generally

amorphous structures (Fig. 2.2b). This same reactivity trend was observed when **Verbascoside**

and **VPP** were added to metal-free and metal-associated, preformed $A\beta_{42}$ aggregates (Fig. 2.3).

These compounds were capable of slightly altering $A\beta_{42}$ aggregates in the absence of metal ions.

Additionally, **VPP** generated various-sized aggregates of $Zn(II)-A\beta_{42}$ after 4 h only, a process

which required 24 h with $A\beta_{40}$ (Fig. 2.3a). Similar to $A\beta_{40}$, unstructured $A\beta_{42}$ aggregates induced

by treatment with the two compounds were shown by TEM (Fig. 2.3b).

 Verbascoside and **VPP** also displayed reactivity towards $A\beta_{40}$ and $A\beta_{42}$ in inhibition

experiments (Fig. A.2, lanes 4 and 5). Only **VPP** altered the aggregation of metal-free

$A\beta_{40}/A\beta_{42}$, an effect which was evident after just 4 h with both isoforms. Both **Verbascoside** and

VPP demonstrated inhibitory activity towards metal$-A\beta_{40}/A\beta_{42}$. In the presence of Cu(II), the

two compounds promoted a variety of aggregates to different extents after 4 h incubation;

Verbascoside generated a smaller MW range of aggregates than **VPP**, suggesting that their

activity may be size and/or conformation dependent. A similar trend in $A\beta$ aggregate size was

observed in the presence of Zn(II) when **Verbascoside** and **VPP** were introduced (Fig. A.2).

Verbascoside and **VPP** presented the similar time dependence in the presence of Zn(II) for the

inhibition of $A\beta_{40}$ aggregation as they did with $A\beta_{40}$ disaggregation; their reactivity towards

$Zn(II)-A\beta_{40}$ was noticeable only after 24 h (Fig. A.2a). This suggests that the timescale of

reactivity may be dependent upon solution conditions, specifically the presence or absence of

metal ions in solution and the morphology of aggregates, at a given time. Taken together, the

results from these disaggregation and inhibition experiments suggest that **Verbascoside** and

VPP have a distinct capacity to modulate the aggregation of metal$-A\beta$ (as well as metal-free $A\beta$

in the case of **VPP**) which is generally absent for the other four compounds analyzed in this

study. It is interesting to observe that among the selected polyphenols the reactive **Verbascoside** and **VPP** both feature two catechol moieties, bearing the two characteristic *ortho*-hydroxy groups. Meanwhile, **Rutin** and **R2** which only show mild reactivity have a single catechol moiety. **Phloririzin** and **F2** have no catechol moieties while also presenting no noticeable reactivity with Aβ species. This points to a potential role for the catechol moiety in the activity of these compounds. Additionally, from this set of compounds, it appears that structural modification of the sugar moiety (*i.e.*, selective esterification) can drastically alter the function of the parent compound, as was seen for both **Verbascoside/VPP** and **Rutin/R2**.

2.2.2. Metal binding properties of polyphenols

In order to elucidate the molecular level interactions responsible for the varied anti-amyloidogenic activity of the polyphenols towards metal–Aβ species it is necessary to understand the potential binding of each compound with the component parts of system: metal ions and Aβ monomers/aggregates. The potential interaction between the polyphenols and metal ions was investigated first. The OH groups found on the aromatic rings of all six compounds could potentially interact with transition metals; the catechol moieties of **Verbascoside**, **VPP**, **Rutin**, and **R2** are especially likely to bind metal ions in a manner similar to previously reported polyphenols.[20,28,42-44] It has already been suggested that both **Verbascoside** and **Rutin** could interact with Cu(II) in solution.[45-47] The Cu(II) binding properties of **Phlorizin/F2**, **Verbascoside/VPP**, and **Rutin/R2** were examined by UV−Vis while the Zn(II) binding of **Verbascoside** and **VPP** was monitored by ^{1}H NMR due to a lack of significant optical changes in the spectra when the ligand was treated with Zn(II) (Fig. 2.4, A.3, and A.4).

The UV−Vis spectra of the six polyphenols showed different levels of spectral changes following the titration of $CuCl_2$ in buffered aqueous solution (pH 7.4; Fig. 2.4a and A.3).

Addition of CuCl$_2$ to both **Verbascoside** and **VPP** in solution induced a slight change in the absorption bands at *ca*. 330 nm and 405 nm, implying potential interaction between the catechol moieties of both ligands and Cu(II) in solution (Fig. 2.4a).[48] The spectral change is more drastic in **VPP** than in **Verbascoside**, which suggests that esterification of the OH groups in the sugar ring could reduce their competitive interaction with Cu(II) and promote binding by the catechol moieties. Neither compound presented significantly noticeable spectral shifts indicative of
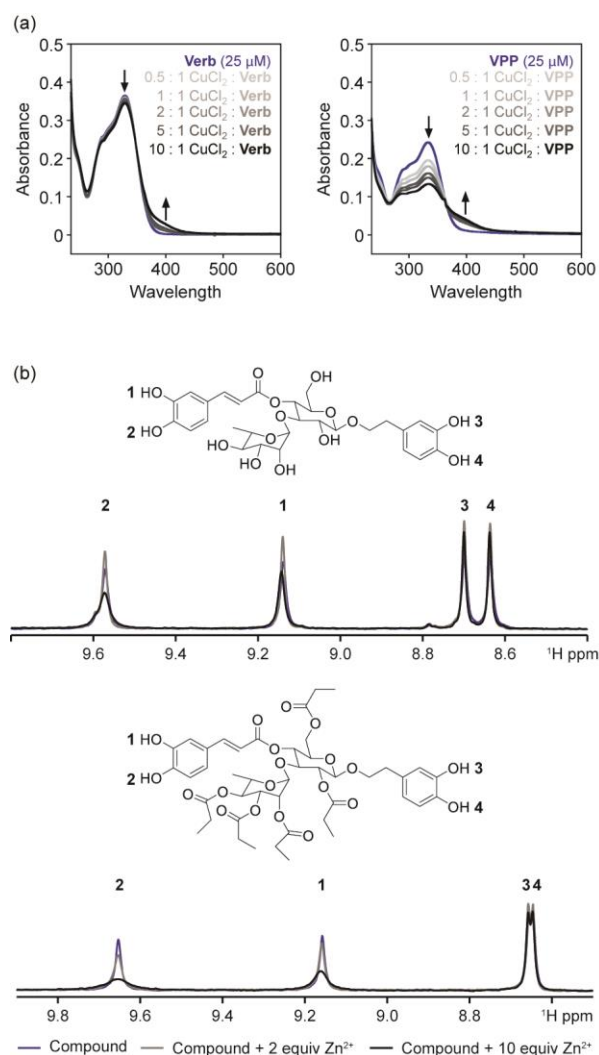
Figure 2.4. Metal binding studies of **Verbascoside** and **VPP**. (a) Cu(II) binding studies of **Verbascoside** (**Verb**) and **VPP** by UV−Vis. Samples were incubated for 2 h with or without Cu(II) (0.5 - 10 equiv) at pH 7.4 at room temperature. (b) Zn(II) binding studies of **Verbascoside** (top) and **VPP** (bottom) by ^{1}H NMR. The samples of compounds (2 mM) were titrated with ZnCl$_2$ (0, 2, and 10 equiv) in DMSO-d_6 at room temperature.

complex formation, however, suggesting that interaction of either **Verbascoside** or **VPP** with Cu(II) in solution could be weak. Previous studies on complex formation between **Verbascoside** and Cu(II) are unclear about the strength of the interaction which indicates that complexation could depend upon experimental conditions (*i.e.*, buffer, salt concentration, pH).[45,49] Addition of CuCl$_2$ to solutions of either **Phlorizin** or **F2** induced no significant shift in spectral features, likely due to the minimal interaction of the phenol moiety in the compounds for Cu(II) in solution (Fig. A.3). The presence of Cu(II) did induce modest changes in the spectrum of **Rutin**, including a decrease in the primary peak at *ca*. 330 nm and an increase in a shoulder at *ca.* 425 nm (Fig. A.3). This may be caused by the interaction between the catechol moiety and Cu(II). These shifts are similar, though of smaller magnitude, to those previously observed for **Rutin**−Cu(II) complexes.[50,51] Finally, **R2** exhibited slight spectral changes over the course of the titration, suggesting minimal interaction with Cu(II) in solution (Fig. A.3), suggesting that esterification of **Rutin** could change the interaction between the ligand and Cu(II). These results suggest that only **Verbascoside**, **VPP**, and **Rutin** have an observable ability to interact with Cu(II) under the conditions of this study.

The interaction of **Verbascoside** and **VPP** with Zn(II) was also investigated by ^{1}H NMR in DMSO-d_6 (Fig. 2.4b). When Zn(II) was titrated into **Verbascoside** up to 2 equiv, all phenolic protons exhibited some sharpening, likely the result of weak association with the metal in solution and subsequent decrease in the exchange rate of bound protons with the solvent. When additional Zn(II) was added to solution, however, the resonances associated with the caffeic acid moiety began to broaden. The hydroxytyrosine phenolic protons showed minimal change upon addition of more Zn(II). Selective broadening suggests that Zn(II) preferentially associates with the caffeic acid catechol moiety. A similar pattern was observed when Zn(II) was added to **VPP**.

During the titration, only caffeic acid associated protons broadened, suggesting interaction with the metal and subsequent proton exchange with the solvent. No other proton resonances demonstrate any shifts or broadening over the course of the titration for either compound (Fig. A.4). This would suggest that in both **Verbascoside** and **VPP**, Zn(II) selectively interacts with the phenolic protons of the caffeic acid moiety over all other portions of the compounds. Overall, both **Verbascoside** and **VPP** are shown to interact with both Cu(II) and Zn(II) under the conditions employed in this study, suggesting that this may be partially responsible for the ability of these compounds to redirect metal−Aβ aggregation (*vide supra*).

2.2.3. Interaction of polyphenols with multiple Aβ forms

Given the ability of both **Verbascoside** and **VPP** to redirect the morphology and aggregation of Aβ, the direct interaction of the two compounds, along with both **Phlorizin** and **R2**, with monomeric $Aβ_{40}$ was investigated (Fig. 2.5 and A.5). 2D band-Selective Optimized-Flip-Angle Short-Transient Heteronuclear Multiple Quantum Coherence (SOFAST-HMQC) NMR experiments were performed to identify potential residue-specific interactions between monomeric Aβ peptide and the compounds.[52] The chemical shift perturbation (CSP) for each resolvable residue was calculated by comparing the spectrum of ligand-free $Aβ_{40}$ with that of $Aβ_{40}$ in the presence of excess ligand (10 equiv) and these CSP values were compared to the average CSP values (Fig. 2.5a and b, and A.4) to identify potentially favored interactions.[20,28] All four compounds induced some mild to moderate (0.02−0.035 ppm) chemical shifts in varying regions of the peptide. **Verbascoside** (Fig. 2.5c) triggered a distinct shift in D23 and also weakly perturbed Q15 while **VPP** (Fig. 2.5d) caused some shift in Y10, E11, Q15, and F20. The interactions of **Verbascoside** seem to favor both polar and charged residues that are centrally located in the sequence, suggesting that both hydrophilic interactions and hydrogen bonding

61
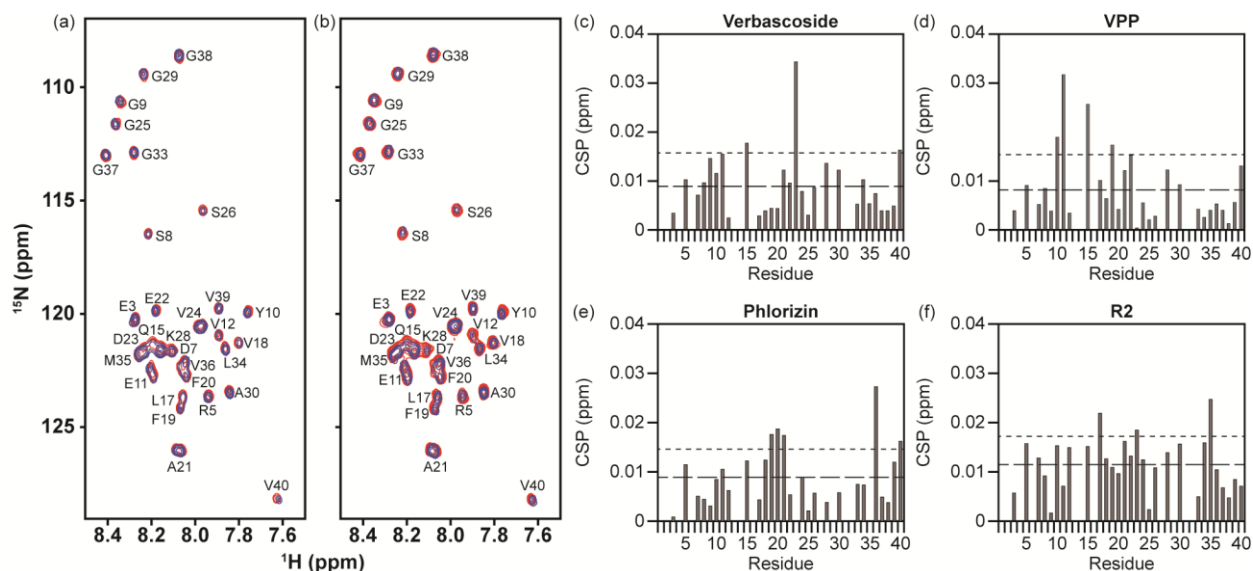
Figure 2.5. Ligand interaction with monomeric Aβ$_{40}$ by 2D ^{1}H/^{15}N SOFAST-HMQC NMR. **Verbascoside** (a) and **VPP** (b) were titrated into a solution of uniformly ^{15}N-labeled Aβ$_{40}$ (80 μM in 20 mM PO$_4$, 50 mM NaCl, pH 7.4, 7% D$_2$O (v/v), 10 °C). Blue color represents the spectrum obtained upon addition of 10 equiv of the ligand to Aβ$_{40}$ (red color: the spectrum of Aβ$_{40}$ only). All spectra were aligned at G29 due to non-uniform broadening of the water peak as a reference. Chemical shift perturbation (CSP) between the 0 and 10 equiv of all resolved residues was calculated and plotted as a function of the amino acid residue number in Aβ$_{40}$ for (c) **Verbascoside**, (d) **VPP**, (e) **Phlorizin**, and (f) **R2**. All CSP values are compared to the average (dashed line) and average + standard deviation (dotted line) for each titration. Values which exceed the average + standard deviation line are considered to be significant, suggesting potential interaction.

could direct potential ligand binding. **VPP**, however, perturbed a mixture of hydrophobic and hydrophilic residues, suggesting that the added acyl groups could encourage some nonpolar contacts during ligand interaction with Aβ. π–π stacking between **VPP** and the aromatic side chains of Y10 and/or F20 could also be responsible for the observed shifts. Despite causing shifts in unique residue resonances, both compounds alter residues near the purported metal binding site of Aβ (residues 1-16) suggesting that the compounds preferentially interact with the N-terminus and may be oriented in a manner which facilitates interaction with metal ions when present in solution or could alter the conformation of the N-terminus of the peptide, disrupting the peptide's ability to bind metal ions.[4,8-10] **Phlorizin** (Fig. 2.5e) caused minor chemical shifts in

both the hydrophobic core (F19-A21) and the C-terminus (V36); nonpolar forces may be responsible for any prospective **Phlorizin**−Aβ$_{40}$ interaction. **Rutin** (Fig. 2.5f) prompted small shifts in regions similar to those altered by **Phlorizin** (L17 and M35). These small and non-localized chemical shifts could be indicative of weak interaction and/or non-specific binding to the peptide by the two compounds. Both **Phlorizin** and **R2**, which show limited or no influence on amyloidogenesis, display potentially weak interactions with more C-terminal residues while the interaction of both **Verbascoside** and **VPP** with Aβ appear to be more centrally or N-terminally located. Due to the modest CSP values observed, these data may suggest a general preference for interaction rather than a conventional, structured binding site for all compounds examined. Our NMR studies, therefore, suggest a possible molecular mechanism responsible for their differing activities towards Aβ species *in vitro* (*vide supra*). Ligand association with the N-terminus (close to the metal binding site in Aβ) may be favorable in the development of multifunctional compounds to target metal-free and/or metal-associated Aβ species while interacting with the central hydrophobic residues of Aβ may also allow for general inhibition, as has been previously predicted.[4,6,9,10,15]

To gain further molecular level insight into the interactions between these polyphenols and different Aβ structures, saturation transfer difference (STD) NMR was employed to map the regions of both **Verbascoside** and **VPP** which bind to preformed Aβ$_{42}$ fibrils (Fig. 2.6).[18,28,53,54] The intensity of peaks within the STD spectra, relative to the reference spectra, is associated with the proximity of the ligand's protons to the fibril.[54] From these values, a group epitope map can be generated, determining which protons of **Verbascoside** and **VPP** are in proximity to and binding with the fibrils. **Verbascoside** (Fig. 2.6c) only showed STD signals for protons linked to the glucose and rhamose rings. While most of these protons presented modest to weak signals in

the STD spectrum, the protons on the C6 of the glucose ring indicated an extremely strong STD effect. For **VPP**, weak STD effect was observed around all methyl and ethyl protons of the esters appended to the sugar moieties. The stronger STD effect was observed around both the caffeic acid and hydroxytyrosol moieties, localized especially around the two aromatic protons of the catechol groups (Fig. 2.6d). This suggests that the esterification of the sugar rings of **Verbascoside** blocks the binding of the compound to the fibrils through the two sugar rings, redirecting their interaction to a different portion of the compound. It may be that the multiple hydroxyl groups of the sugars promote hydrogen bonds with some of the exposed side chains of the fibril; the esterification of the sugar rings could make these interactions sterically unfavorable and direct **VPP** to interact through hydrogen bonds and π–π interactions through the catechol moieties of the compound instead.

The different binding modes identified by STD experiments led us to explore the affinity of these two compounds for fibrillar Aβ. Using a fluorescence blue shift assay, the change in the fluorescence emission wavelength was monitored as fibril was titrated into solution (Fig. A.6a and b). **Verbascoside** and **VPP** were shown to have an affinity of 7.80 ± 0.75 μM and 6.98 ± 0.80 μM, respectively, under the condition employed in this study. Despite very different modes of binding to the fibril, the compounds have nearly identical affinities. It should be noted that the actual affinity for the fibril in solution is likely stronger than those measured; the concentration of fibrils was calculated based on the monomer equivalent concentration. It is not possible to measure the molar concentration of fibrils in solution given their heterogeneous length and subsequently heterogeneous molecular weight. The fibril concentration is likely much lower than the monomer equivalent which would affect the concentration values used in the fit. Because the exact fiber concentration cannot be measured, however, and because the same sample of fibril

was used for both titrations, we are confident that these results are internally consistent and suggest that the two compounds have very similar affinities.
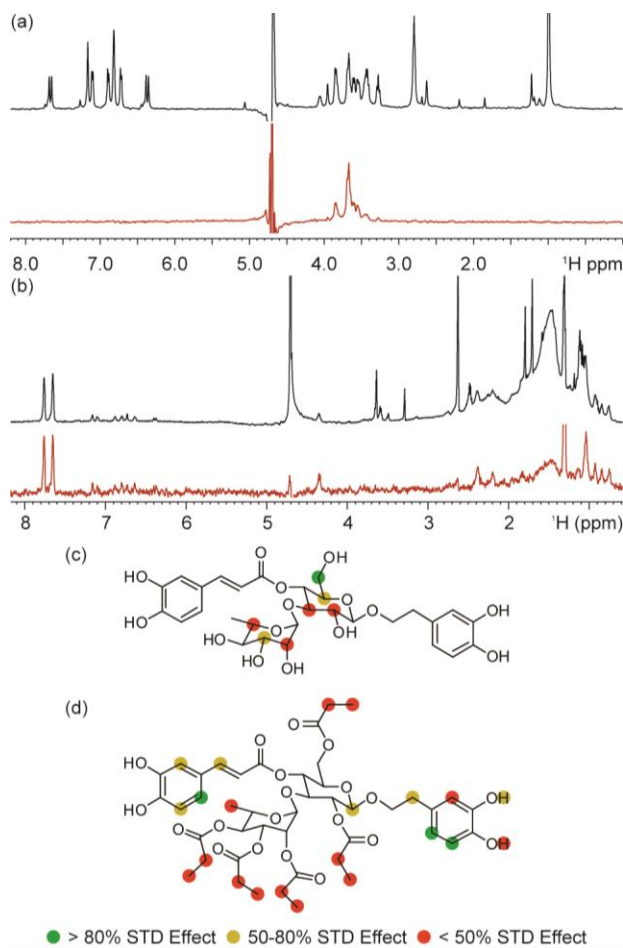
Figure 2.6. Ligand Interaction with fibrillar Aβ$_{42}$ by saturation transfer difference (STD) NMR. STD NMR spectra of (a) **Verbascoside** and (b) **VPP** at a 250:1 ligand to peptide ratio using pre-assembled Aβ$_{42}$ fibrils (1 μM). Comparison of the STD signal intensity (red) to the STD reference intensity (black) reflects the relative proximity of the corresponding proton to the Aβ$_{42}$ fibril. The STD effect calculated from relative intensities was correlated to the structure of **Verbascoside** (c) and **VPP** (d) to generate group epitope maps.

The distinct difference in group epitope but similar affinity led us to investigate the binding site on the fibril for these two compounds; it was expected that two compounds with similar affinities but unique binding moieties would likely bind to separate regions of the fibril structure and therefore not compete for binding. To probe this, we performed a competition titration

experiment in which fibrils were first treated with 1 equiv of a compound (either **Verbascoside** or **VPP**) and then titrated with the other compound. The intensity of an STD peak associated with each compound (relative to the intensity of the same peak in the reference spectrum) was then used to monitor the binding of each compound to the fibril. As the competing compound is titrated into solution, if the compounds bind in the same site, it is expected that the relative intensity of the first compound's peak will gradually decrease while the relative intensity of the titrant's peak will increase as it competes the first compound off of the binding site. Conversely, under non-competitive binding conditions, the initial compound would maintain a constant relative intensity while the relative intensity of the titrant would increase as it binds at higher and higher concentrations. When **Verbascoside** was titrated into a solution already containing **VPP** and fibrils (Fig. A.6c), it was observed that the relative intensity of the peak associated with **Verbascoside** increased during the titration while the relative intensity of the peak associated with **VPP** gradually decreased. This suggests that **Verbascoside** competes with **VPP** for a similar binding site on the fibril. The reverse of this experiment was performed (**VPP** titrated into a solution already containing **Verbascoside** and fibrils; Fig. A.6d) and the same trend was observed. The relative intensity of the **VPP** peak increased while the relative intensity of the **Verbascoside** peak decreased slightly. This implies that, while the two compounds bind to the fibril using unique portions of their related structure, they are targeting a similar location on the fibril. Additionally, the blue shift assay suggests that they do so with a nearly identical affinity. This is unexpected and suggests that the esterification changes how the two compounds are able to disaggregate fibrillar species (*vide supra*) but they bind to the fibril in a relatively similar manner though using unique parts of their structure. It could be that the differing orientation of the sugar and catechol moieties of the two compounds is at least partly responsible for this

66

difference in reactivity as STD group epitope maps reveal that the orientation is unique between compounds.

2.2.4. Antioxidant properties

Because oxidative stress is believed to play a role in AD, it would be valuable for multifunctional probes to possess antioxidant activity, on top of the ability to interact simultaneously with Aβ species and various transition metal ions.[9,13,14] The ability of these six compounds to scavenge an organic radical cation (*i.e.*, ABTS$^{\bullet+}$) was determined by the Trolox equivalence antioxidant capacity (TEAC) assay using cell lysates (Fig. 2.7a).[55,56] Both **Verbascoside** and **Rutin**, two known antioxidants,[31,32,57] scavenged ABTS$^{\bullet+}$ slightly better than Trolox (by a factor of *ca*. 1.4 and 1.2, respectively). **VPP**, **Phlorizin**, and **F2** showed a lower ability to scavenge ABTS$^{\bullet+}$ relative to Trolox, suggesting limited function as antioxidants relative to the other compounds investigated herein. **R2** presented no ability to scavenge ABTS$^{\bullet+}$. This, again, indicates that esterification of the sugar moiety transforms the function of the polyphenols. In this case, the antioxidant capacity of the all compounds was reduced upon esterification. **Verbascoside**'s activity was reduced by *ca*. 65% while **Rutin** lost all activity. The activity of **Phlorizin** was reduced by *ca*. 40%. This reduction in antioxidant capacity is surprising given the conservation of the catechol structures between **Verbascoside**/**VPP** and **Rutin**/**R2** which is thought to be potentially responsible for ABTS$^{\bullet+}$ quenching through semi-quinone and quinone formation.[28,56]

2.2.5. Regulating cytotoxicity related to metal-free and metal-associated Aβ

Previous studies of **Verbascoside** and **Rutin** have suggested the two compounds may alleviate the toxicity of Aβ species in SH-SY5Y and APPswe cells, respectively.[22,24] We probed this relationship further to examine the effect of these two compounds, as well as **VPP**, on the
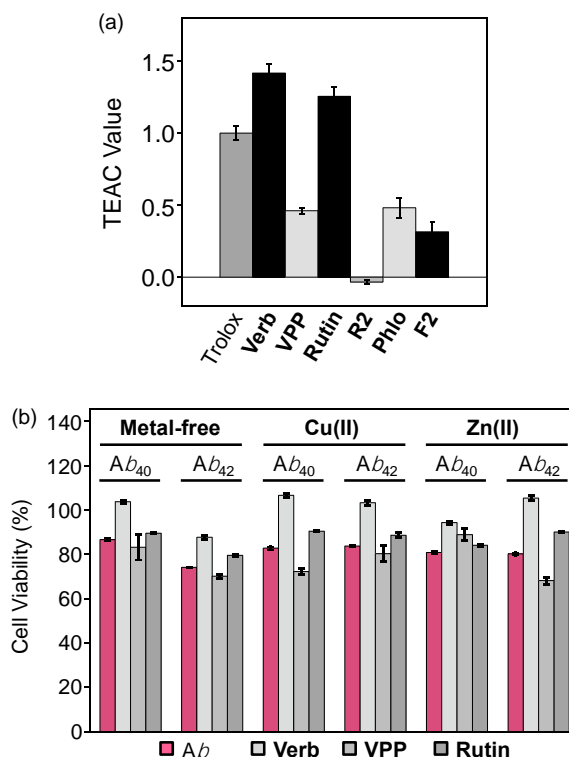
Figure 2.7. Biological activities of **Verbascoside (Verb)**, **VPP**, **Rutin**, **R2**, **Phlorizin (Phlo)**, and **F2**. (a) Free-radical scavenging activity of **Verbascoside**, **VPP**, **Rutin**, **R2**, **Phlorizin**, and **F2** evaluated by a cell lysate-based TEAC assay. The TEAC values are relative to a vitamin E analogue, Trolox (6-hydroxy-2,5,7,8-tetramethylchroman-2-carboxylic acid). (b) Influence of **Verbascoside**, **VPP**, and **Rutin** on cytotoxicity induced by metal-free Aβ and metal−Aβ species in N2a cells. Cells treated with Aβ$_{40}$ or Aβ$_{42}$ (20 μM), a metal chloride salt (CuCl$_2$ or ZnCl$_2$; 20 μM), and a compound [**Verbascoside**, **VPP**, and **Rutin** (20 μM)] were incubated for 24 h at 37 °C. Cell viability was determined by the MTT assay. Values of cell viability (%) were calculated compared to that of cells treated with DMSO only (0-1%, v/v). Error bars represent the standard errors from three independent experiments.

cytotoxicity of both metal-free Aβ and metal–Aβ in murine Neuro-2a neuroblastoma (N2a) cells.

In the absence of Aβ, **Verbascoside** was relatively nontoxic with and without metal ions (Fig. A.7). **VPP**, however, reduced cell viability (*ca.* 70%) at high concentrations in the presence of either Cu(II) or Zn(II), but showed minimal toxicity in the absence of metal ions. **Rutin** had no significant impact on cell viability under any conditions (Fig. A.6).

Cells incubated with Aβ (20 μM) in either the absence or presence of metal ions (Cu(II)

or Zn(II), 20 μM) indicated viability of *ca*. 70–80% under all conditions (Fig. 2.7b). The addition of **Verbascoside** (20 μM) improved cell survival (*ca.* 90–100%) regardless of both Aβ isoforms and the presence or absence of metal ions. **VPP** (20 μM), however, was generally unable to regulate Aβ-triggered cytotoxicity. Finally, treatment of cells with **Rutin** (20 μM) yielded slight improvements in cell survival under all conditions. Overall, **Verbascoside** was capable of attenuating the broad toxicity indicated in the presence of both metal-free Aβ and metal−Aβ. Furthermore, esterification of the compound is shown to limit these protective capabilities.

2.3. Discussion

Naturally occurring polyphenolic glycosides (**Phlorizin**, **Verbascoside**, and **Rutin**), along with their esterified derivatives (**F2**, **VPP**, and **R2**), were investigated for their potential to modulate the aggregation and toxicity of metal-free Aβ and metal−Aβ. Both **Verbascoside** and **VPP**, bearing multiple catechol moieties, were capable of distinctly redirecting the aggregation of metal-free Aβ (mainly, **VPP**) and/or metal−Aβ to different extents, as confirmed by both biochemical and TEM studies. The ability of these two compounds to interact with both metal ions and Aβ was confirmed through physical methods, including UV-Vis and 1D/2D/STD NMR. **Verbascoside** and **VPP** are able to interact with both Cu(II) and Zn(II) as well as with multiple forms of Aβ. The esterification of **Verbascoside** to **VPP** distinctly alters the interactions between the compounds and the components of the metal−Aβ system studied herein, suggesting that the properties (metal binding and Aβ interaction) can be tunable by synthetic modifications. In addition, **Verbascoside** is shown to have some promising chemical properties for a potential probe (antioxidant capacity, no toxicity, and cytoprotective against both metal-free Aβ and metal-Aβ). Overall, this study points to **Verbascoside** as a promising starting point for

constructing a new multifunctional probe to interrogate the etiology of AD.

This study also lends insight into the efficacy of unique chemical moieties in design of anti-amyloidogenic compounds. Comparing **Phlorizin**, **Verbascoside**, and **Rutin** to each other, there is a direct correlation between the number of catechol moieties and the efficacy of each compound against Aβ and metal−Aβ aggregation. This is further supported by the group epitope map generated from STD NMR for **VPP** which shows strong STD effect around both catechols. This suggests that the catechol moiety specifically, not just polyphenols as a general class of compounds, may be effective at redirecting the protein misfolding. Previous studies have also indicated that including a catechol-like moiety makes a small molecule more effective[28]; two of the most thoroughly investigated anti-amyloidogenic natural products, EGCG and curcumin, contain multiple variations of the catechol moiety (pyrogallol for EGCG, *o*-methyl-catechol for curcumin), further indicating that the catechol moiety is an effective component of an anti-amyloidogenic probe.[20,58] It should be noted, however, that catechol-containing compounds have been shown to be promiscuous in their action and functionality so their use and functionalization must be carefully considered in compound design for *in vivo* applications in order to avoid off-target effects.[59,60]

We have also highlighted the importance of carefully chosen synthetic alterations to efficacious reagents. In this suite of compounds, it is apparent that esterification of the sugar moieties affected the efficacy of the compounds in the various assays to differing extents; esterification increased the ability of **VPP** to alter the structure of metal-free Aβ aggregates while simultaneously maintaining its affinity for preformed fibrils relative to that of **Verbascoside**, its parent compound. Esterification also reduced the ability of all compounds to scavenge organic radicals despite not directly modifying the catechol moiety thought to be

responsible for the scavenging activity. Overall, this points to the unpredictability inherent in small molecule design for complex biological systems; with many variables all contributing to the disease phenotype, it is challenging, if not impossible, to accurately predict the effects of small structural changes on a compounds efficacy against the suite of potential targets. Thus, the performance of the compounds evaluated here may serve as a benchmark for which compounds are most worthwhile investigating further in more complex and biologically relevant systems. Furthermore, it indicates the care which must be taken when functionalizing known compounds. Even potentially reversible changes, such as esterification, may drastically alter the compound's function, in both beneficial and detrimental ways. Importantly, however, it appears from the data presented herein that **Verbascoside** possesses positive characteristics for a compound in the investigation of the role of Aβ in AD and, furthermore, is structurally amenable to a variety of future derivatization aimed at further improving its function.

2.4. Methods

2.4.1. Materials and procedures

All reagents were purchased from commercial suppliers and used as received unless otherwise noted. The natural products (**Phlorizin**, **Verbascoside**, and **Rutin**) and their previously synthesized, esterified derivatives (**F2**, **VPP**, and **R2**) were prepared following the previously reported methods.[30-32] Aβ$_{40}$ and Aβ$_{42}$ were purchased from Anaspec (Fremont, CA). Transmission electron microscopy (TEM) images were recorded on a Philips CM-100 transmission electron microscope (Microscopy and Image Analysis Laboratory, University of Michigan, Ann Arbor, MI, USA). Optical spectra for metal binding were recorded on an Agilent 8453 UV–Visible (UV–Vis) spectrophotometer. Nuclear magnetic resonance (NMR) spectra for the characterization of Zn(II) binding studies of **Verbascoside** and **VPP** were acquired on an

Agilent 400 MHz NMR spectrometer. NMR studies of ^{15}N-labeled Aβ_{40} with ligands were carried out on a Bruker 600 MHz NMR spectrometer equipped with a cryogenic probe. Absorbance values for biological assays, including the TEAC assay and cell viability assay, were measured on a SpectraMax M5 microplate reader (Molecular Devices, Sunnyvale, CA, USA).

2.4.2. Amyloid-β (Aβ) inhibition and disaggregation experiments

Aβ experiments were performed according to previously published methods.[28,41] Prior to the sample preparation, Aβ_{40} or Aβ_{42} was dissolved with ammonium hydroxide (NH$_4$OH, 1% v/v, aq), aliquoted, lyophilized, and stored at -80 °C. Stock solutions (ca. 200 μM) of Aβ_{40} and Aβ_{42} were prepared by dissolving the lyophilized peptide in 1% NH$_4$OH (10 μL) and diluting with doubly distilled (dd) H$_2$O. The peptide stock solution was diluted to a final concentration of 25 μM in buffered solution containing HEPES [4-(2-hydroxyethyl)-1-piperazineethanesulfonic acid; 20 μM, pH 6.6 for Cu(II) samples; pH 7.4 for metal-free and Zn(II) samples] and NaCl (150 μM). For the inhibition studies,[28,41] compound (50 μM final concentration, 1% v/v DMSO) was added to the sample of Aβ_{40} or Aβ_{42} in the absence and presence of a metal chloride salt (CuCl$_2$ or ZnCl$_2$, 25 μM) followed by incubation for 4 and 24 h at 37 °C with constant agitation. For the disaggregation studies,[28,41] Aβ_{40} or Aβ_{42} with and without metal ions was first incubated for 24 h at 37 °C with continuous agitation prior to the addition of compound (50 μM). The resulting samples were incubated for an additional 4 or 24 h at 37 °C with constant agitation.

2.4.3. Gel electrophoresis with Western blotting

The samples from the inhibition and disaggregation experiments were analyzed by gel electrophoresis with Western blot using an anti-Aβ antibody (6E10).[20,28] Each sample (10 μL) was separated on a 10-20% Tris-tricine gel (Invitrogen, Grand Island, NY, USA). Following separation, the gel was transferred onto nitrocellulose membrane which was blocked with bovine

serum albumin (BSA, 3% w/v, Sigma-Aldrich, St. Louis, MO, USA) in Tris-buffered saline (TBS) containing 0.1% Tween-20 (TBS-T) for 3 h at room temperature. The membrane was treated with antibody (6E10, Covance, Princeton, NJ, USA; 1:2000) in a solution of BSA (2% w/v) in TBS-T overnight at 4 °C. Following washing, the membrane was treated with horseradish peroxidase-conjugated goat antimouse secondary antibody (1:5000; Cayman Chemical, Ann Arbor, MI, USA) in 2% BSA in TBS-T solution for 1 h at room temperature. Protein bands were visualized using ThermoScientific Supersignal West Pico Chemiluminescent Substrate (Thermo Scientific, Rockford, IL, USA).

2.4.4. Transmission electron microscopy

The samples for TEM were prepared following a previously reported method.[28,41] Glow-discharged grids (Formar/Carbon 300-mesh, Electron Microscopy Sciences, Hatfield, PA, USA) were treated with the samples from the disaggregation experiments (5 μL, 25 μM Aβ) for 2 min at room temperature. Excess sample was removed with filter paper and washed with ddH$_2$O. Each grid was stained with uranyl acetate (1% w/v, ddH$_2$O, 5 μL, 1 min), blotted to remove excess stain, and dried for 15 min at room temperature. TEM images were taken by a Philips CM-100 transmission electron microscope (80 kV, 25,000x magnification).

2.4.5. Metal binding studies

The interaction of **Phlorizin**, **F2**, **Verbascoside**, **VPP**, **Rutin**, and **R2** with Cu(II) and Zn(II) was determined by UV−Vis or ^{1}H NMR, respectively, based on previously reported procedures.[20,61] A solution of ligand (20 μM, pH 7.4) was prepared, treated with 0.5 to 10 equiv of CuCl$_2$, and incubated at room temperature for 2 h (for **Phlorizin**, **F2**, **Verbascoside**, **VPP**, **Rutin**, and **R2**). The optical spectra of the resulting solutions were measured by UV−Vis. The interaction of both **Verbascoside** and **VPP** with ZnCl$_2$ was observed by ^{1}H NMR (500 MHz).

ZnCl$_2$ was titrated into a solution of **Verbascoside** or **VPP** (2 mM) in DMSO-d$_6$ and the spectra were recorded.

2.4.6. 2D NMR spectroscopy

The interaction of Aβ$_{40}$ with **Phlorizin**, **Verbascoside**, **VPP**, and **R2** was monitored by 2D band-Selective Optimized Flip-Angle Short Transient Heteronuclear Multiple Quantum Coherence (SOFAST-HMQC) at 8 °C.[52] Uniformly-^{15}N-labeled Aβ$_{40}$ (rPeptide, Bogart, GA, USA) was first dissolved in 1% NH$_4$OH and lyophilized. The peptide was re-dissolved in 3 μL of DMSO-d$_6$ (Cambridge Isotope, Tewksbury, MA, USA) and diluted with phosphate buffer, NaCl, D$_2$O, and ddH$_2$O to a final peptide concentration of 80 μM (20 mM PO$_4$, pH 7.4, 50 mM NaCl, 7% v/v D$_2$O). Each spectrum was obtained using 64 complex t$_1$ points and a 0.1 sec recycle delay on a Bruker Avance 600 MHz spectrometer. The 2D data were processed using TOPSPIN 2.1 (from Bruker). Resonance assignment was performed with SPARKY 3.1134 using published assignments for Aβ$_{40}$ as a guide.[62-64] Chemical shift perturbation (CSP) was calculated using the following equation:

$$\Delta\delta_{NH} = \sqrt{\Delta\delta H^2 + \left(\frac{\Delta\delta N}{5}\right)^2}$$

2.4.7. Saturation transfer difference (STD) NMR spectroscopy

For the STD NMR[53] experiments, an 150 μM solution of fibrillar Aβ$_{42}$ was prepared by incubating Aβ$_{42}$ for 24 h at 37 °C with constant agitation in 10 mM deuterated Tris–DCl, 95% D$_2$O at pD 7.4 (corrected for the isotope effect). The samples for STD experiments were prepared by diluting fiber to 1 μM (effective monomer concentration) into 10 mM deuterated Tris–DCl to which was added 250 μM of ligand (0.5% DMSO-d$_6$). STD experiments were acquired with a train of 50 dB Gausian-shaped pulses of 0.049 sec with an interval of 0.001 sec

at either -1.0 ppm (on resonance) or 40 ppm (off resonance) with a total saturation time of 2 sec on a Bruker 600 MHz NMR spectrometer. A total of 1024 scans were recorded for the STD spectrum and 512 scans were recorded for the reference spectrum at 25 °C. An inter-scan delay of 1 sec was used for both the STD and the reference experiments.

For the competition experiments with **Verbascoside** and **VPP**, the above procedure was followed for sample preparation. STD experiments were acquired with a train of 50 dB Gausian-shaped pulses of 0.049 sec with an interval of 0.001 sec at either -1.0 ppm (on resonance) or 40 ppm (off resonance) with a total saturation time of 2 sec on a Bruker 500 MHz NMR spectrometer. A total of 2048 scans were recorded for the STD spectrum and 1024 scans were recorded for the reference spectrum at 25 °C. An inter-scan delay of 1 sec was used for both the STD and the reference experiments. To a solution already containing either **Verbascoside** or **VPP** (250 μM), the other compound was titrated to 0.5 equiv (125 μM), 1 equiv (250 μM), and 3 equiv (750 μM). The intensity of peaks unique to **Verbascoside** (3.85 ppm) and **VPP** (7.78 ppm) in the STD spectra relative to their intensity in the reference spectra were used to monitor the binding of the compounds to the fiber.

2.4.8. Blue shift fluorescence assay

The change in the fluorescence emission wavelength of **Verbascoside** or **VPP** was monitored upon treatment with $A\beta_{42}$ fibrils on a Fluoromax-4 Spectrofluorimeter (Horiba Scientific, Edison, NJ, USA). A 25 μM solution of either **Verbascoside** or **VPP** in buffer (20 mM PO_4, pH 7.4, 50 mM NaCl) was titrated with preformed $A\beta_{42}$ fibrils, prepared as described above for STD experiments. The fluorescence emission was monitored between 380 and 550 nm following excitation (350 nm for **Verbascoside** and 330 nm for **VPP**) with slits set for 5 nm bandwidths. The blue shift was calculated by the difference between the emission maximum

wavelength of the titration point and the emission maximum wavelength of the compound in absence of fibrils. The data was then fit to a hyperbolic curve to calculate the K_d value.

2.4.9. Trolox equivalent antioxidant capacity (TEAC) assay

The antioxidant activity of **Phlorizin**, **F2**, **Verbascoside**, **VPP**, **Rutin**, and **R2** was determined by the TEAC assay employing cell lysate following the protocol of the antioxidant assay kit purchased from Cayman Chemical Company (Ann Arbor, MI, USA) with modifications.[18] Murine Neuro-2a (N2a) cells were used for this assay. This cell line, purchased from the American Type Culture Collection (ATCC, Manassas, VA, USA), was maintained in media containing 50% Dulbecco's modified Eagle's medium (DMEM) and 50% OPTI-MEM (GIBCO), supplemented with 10% fetal bovine serum (FBS, Sigma), 1% Non-essential Amino Acids (NEAA, GIBCO), 2 mM glutamine, 100 U/mL penicillin, and 100 mg/mL streptomycin (GIBCO). The cells were grown and maintained at 37 °C in a humidified atmosphere with 5% CO_2. For the antioxidant assay using cell lysates, cells were seeded in a 6 well plate and grown to approximately 80-90% confluence. Cell lysates were prepared following the previously reported method with modifications.[65] N2a cells were washed once with cold PBS (pH 7.4, GIBCO) and harvested by gently pipetting off adherent cells with cold PBS. The cell pellet was generated by centrifugation (2,000 x g for 10 min at 4 °C). This cell pellet was sonicated on ice (5 sec pulses, 5 times with 20 sec intervals between each pulse) in 2 mL of cold Assay Buffer (5 mM potassium phosphate, pH 7.4, containing 0.9% NaCl and 0.1% glucose). The cell lysates were centrifuged at 5,000 x g for 10 min at 4 °C. The supernatant was removed and stored on ice until use. To standard and sample wells in a 96 well plate, cell lysates (10 µL) were delivered; they were followed by addition of compound, metmyoglobin, ABTS, and H_2O_2 in order. After 5 min incubation at room temperature on a shaker, absorbance values at 750 nm were recorded. The

final concentrations (0.045, 0.090, 0.135, 0.180, 0.225, and 0.330 mM) of Trolox (Sigma-Aldrich; Trolox = 6-hydroxy-2,5,7,8-tetramethylchroman-2-carboxylic acid; dissolved in DMSO) and all polyphenolic glycosides were used. The percent inhibition was calculated according to the measured absorbance [% Inhibition = $(A_0−A)/A_0$, where A_0 is absorbance of the supernatant of cell lysates] and was plotted as a function of compound concentration. The TEAC value of ligands was calculated as a ratio of the slope of the standard curve of the compound to that of Trolox.

2.4.10. Cell viability measurements

Cell viability upon treatment with compounds was determined using the MTT assay (Sigma). N2a cells were seeded in a 96 well plate (15,000 cells in 100 μL per well). The cells were treated with Aβ (20 μM) with or without either $CuCl_2$ or $ZnCl_2$ (20 μM), followed by the addition of compound (20 μM, 1% v/v final DMSO concentration for **Verbascoside**, **VPP**, and **Rutin**) and incubated for 24 h in the cells. After incubation, 25 μL MTT [5 mg/mL in phosphate buffered saline (PBS), pH 7.4, GIBCO, Grand Island, NY, USA] was added to each well and the plate was incubated for 4 h at 37 °C. Formazan produced by the cells was solubilized using an acidic solution of N,N-dimethylformamide (DMF, 50% v/v, aq) and sodium dodecyl sulfate (SDS, 20% w/v) overnight at room temperature in the dark. The absorbance was measured at 600 nm using a microplate reader. Cell viability was calculated relative to cells treated an equivalent volume of DMSO.

2.5. Acknowledgements

77

2.6. Author Contributions

M.H.L., S.M. and A.R. directed the overall research. S.V. prepared the compounds. K.J.K., M.J. and Y.J.K. performed the gel/Western blot analyses. A.K. performed TEM studies. K.J.K. and A.B. conducted 2D and STD NMR studies. M.J. and K.J.K. carried out metal binding investigations. M.J. performed the TEAC assay, and toxicity studies in living cells. K.J.K. and M.H.L. wrote the manuscript with collaboration with S.V., S.M. and A.R. All authors reviewed and approved the manuscript.

2.7. References

1.   Jakob-Roetne, R. & Jacobsen, H. Alzheimer's disease: from pathology to therapeutic approaches. *Angew. Chem. Int. Ed. Engl.* **48**, 3030-3059 (2009).

2.   Franco, R. & Cedazo-Minguez, A. Successful therapies for Alzheimer's disease: why so many in animal models and none in humans? *Front. Pharmacol.* **5**, 146 (2014).

3.   Gouras, G. K., Olsson, T. T. & Hansson, O. beta-amyloid Peptides and Amyloid Plaques in Alzheimer's Disease. *Neurotherapeutics* (2014).

4.   Savelieff, M. G., Lee, S., Liu, Y. & Lim, M. H. Untangling amyloid-beta, tau, and metals in Alzheimer's disease. *ACS Chem. Biol.* **8**, 856-865 (2013).

5.   Rauk, A. The chemistry of Alzheimer's disease. *Chem. Soc. Rev.* **38**, 2698-2715 (2009).

6.   Hamley, I. W. The amyloid beta peptide: a chemist's perspective. Role in Alzheimer's and fibrillization. *Chem. Rev,* **112**, 5147-5192 (2012).

7.   Benilova, I., Karran, E. & De Strooper, B. The toxic Abeta oligomer and Alzheimer's disease: an emperor in need of clothes. *Nat. Neurosci.* **15**, 349-357 (2012).

8.   Lovell, M. A., Robertson, J. D., Teesdale, W. J., Campbell, J. L. & Markesbery, W. R. Copper, iron and zinc in Alzheimer's disease senile plaques. *J. Neurol. Sci.* **158**, 47-52 (1998).

9.   Kepp, K. P. Bioinorganic chemistry of Alzheimer's disease. *Chem. Rev.* **112**, 5193-5239 (2012).

10.   Faller, P., Hureau, C. & Berthoumieu, O. Role of metal ions in the self-assembly of the Alzheimer's amyloid-beta peptide. *Inorg. Chem.* **52**, 12193-12206 (2013).

11.   Bush, A. I. The metal theory of Alzheimer's disease. *J. Alzheimers. Dis.* **33 Suppl 1**, S277-281 (2013).

12.   Parthasarathy, S., Yoo, B., McElheny, D., Tay, W. & Ishii, Y. Capturing a reactive state of amyloid aggregates: NMR-based characterization of copper-bound Alzheimer disease amyloid beta-fibrils in a redox cycle. *J. Biol. Chem.* **289**, 9998-10010 (2014).

13.   Faller, P. & Hureau, C. A bioinorganic view of Alzheimer's disease: when misplaced metal ions (re)direct the electrons to the wrong target. *Chemistry* **18**, 15910-15920 (2012).

14.   Eskici, G. & Axelsen, P. H. Copper and oxidative stress in the pathogenesis of Alzheimer's disease. *Biochemistry* **51**, 6289-6311 (2012).

15.   Savelieff, M. G., DeToma, A. S., Derrick, J. S. & Lim, M. H. The ongoing search for small molecules to study metal-associated amyloid-beta species in Alzheimer's disease. *Acc. Chem. Res.* **47**, 2475-2482 (2014).

16.   Michael W. Beck, A. S. P., Alaina S. DeToma, Kyle J. Korshavn, Mi Hee Lim. in *Ligand Design in Medicinal Inorganic Chemistry* (ed Tim Storr) Ch. 10, 257-286 (John Wiley & Sons, Ltd, 2014).

17.   Beck, M. W. O., S. B.; Kerr, R. A.; Lee, H. J.; Kim, S. H.; Kim, S.; Jang, M. Ruotolo, B. T.; Lee, J.-Y.; Lim, M. H. . A rationally designed small molecule for identifying an in vivo link between metal–amyloid-β complexes and the pathogenesis of Alzheimer's disease. *Chem. Sci.* 6, 1879-1886 (2015).

18.   Lee, S. *et al.* Rational design of a structural framework with potential use to develop chemical reagents that target and modulate multiple facets of Alzheimer's disease. *J. Am. Chem. Soc.* **136**, 299-310 (2014).

19.   Porat, Y., Abramowitz, A. & Gazit, E. Inhibition of amyloid fibril formation by polyphenols: structural similarity and aromatic interactions as a common inhibition mechanism. *Chem. Biol. Drug. Des.* **67**, 27-37 (2006).

20. Hyung, S. J. *et al.* Insights into antiamyloidogenic properties of the green tea extract (-)-epigallocatechin-3-gallate toward metal-associated amyloid-beta species. *Proc. Natl. Acad. Sci. U.S.A.* **110**, 3743-3748 (2013).

21. Kurisu, M. *et al.* Inhibition of amyloid beta aggregation by acteoside, a phenylethanoid glycoside. *Biosci. Biotechnol. Biochem.* **77**, 1329-1332 (2013).

22. Wang, H. *et al.* Acteoside protects human neuroblastoma SH-SY5Y cells against beta-amyloid-induced cell injury. *Brain. Res.* **1283**, 139-147 (2009).

23. Wang, S. W. *et al.* Rutin inhibits beta-amyloid aggregation and cytotoxicity, attenuates oxidative stress, and decreases the production of nitric oxide and proinflammatory cytokines. *Neurotoxicology* **33**, 482-490 (2012).

24. Jimenez-Aliaga, K., Bermejo-Bescos, P., Benedi, J. & Martin-Aragon, S. Quercetin and rutin exhibit antiamyloidogenic and fibril-disaggregating effects in vitro and potent antioxidant activity in APPswe cells. *Life Sci.* **89**, 939-945 (2011).

25. Hertel, C. *et al.* Inhibition of the electrostatic interaction between beta-amyloid peptide and membranes prevents beta-amyloid-induced toxicity. *Proc. Natl. Acad. Sci. U.S.A.* **94**, 9412-9416 (1997).

26. Schweigert, N., Zehnder, A. J. & Eggen, R. I. Chemical properties of catechols and their molecular modes of toxic action in cells, from microorganisms to mammals. *Environ. Microbiol.* **3**, 81-91 (2001).

27. Severino, J. F., Goodman, B. A., Reichenauer, T. G. & Pirker, K. F. Is there a redox reaction between Cu(II) and gallic acid? *Free Radic. Res.* **45**, 115-124 (2011).

28. DeToma, A. S. *et al.* Synthetic Flavonoids, Aminoisoflavones: Interaction and Reactivity with Metal-Free and Metal-Associated Amyloid-beta Species. *Chem. Sci.* **5**, 4851-4862 (2014).

29. Milko, P. *et al.* The phenoxy/phenol/copper cation: a minimalistic model of bonding relations in active centers of mononuclear copper enzymes. *Chemistry* **14**, 4318-4327 (2008).

30. Baldisserotto, A. *et al.* Synthesis, antioxidant and antimicrobial activity of a new phloridzin derivative for dermo-cosmetic applications. *Molecules* **17**, 13275-13289 (2012).

31. Vertuani, S. *et al.* Activity and stability studies of verbascoside, a novel antioxidant, in dermo-cosmetic and pharmaceutical topical formulations. *Molecules* **16**, 7068-7080 (2011).

32. Baldisserotto, A. *et al.* Design, synthesis and biological activity of a novel Rutin analogue with improved lipid soluble properties. *Bioorg. Med. Chem.* **23**, 264-271 (2015).

33. Lampronti, I., Borgatti, M., Vertuani, S., Manfredini, S. & Gambari, R. Modulation of the expression of the proinflammatory IL-8 gene in cystic fibrosis cells by extracts deriving from olive mill waste water. *Evid. Based. Complement. Alternat. Med.* **2013**, 960603 (2013).

34. Egleton, R. D. & Davis, T. P. Development of neuropeptide drugs that cross the blood-brain barrier. *NeuroRx* **2**, 44-53 (2005).

35. Egleton, R. D. *et al.* Improved blood-brain barrier penetration and enhanced analgesia of an opioid peptide by glycosylation. *J. Pharmacol. Exp. Ther.* **299**, 967-972 (2001).

36. Yagi-Utsumi, M., Kameda, T., Yamaguchi, Y. & Kato, K. NMR characterization of the interactions between lyso-GM1 aqueous micelles and amyloid beta. *FEBS Lett.* **584**, 831-836 (2010).

37. McLaurin, J., Golomb, R., Jurewicz, A., Antel, J. P. & Fraser, P. E. Inositol stereoisomers stabilize an oligomeric aggregate of Alzheimer amyloid beta peptide and inhibit abeta -induced toxicity. *J. Biol. Chem.* **275**, 18495-18502 (2000).

38. Rautio, J. *et al.* Prodrugs: design and clinical applications. *Nat. Rev. Drug. Discov.* **7**, 255-270 (2008).

39. Pardridge, W. M. Drug transport across the blood-brain barrier. *J. Cereb. Blood Flow Metab.* **32**, 1959-1972 (2012).

40. Nguyen, P. & Derreumaux, P. Understanding amyloid fibril nucleation and abeta oligomer/drug interactions from computer simulations. *Acc. Chem. Res.* **47**, 603-611 (2014).

41. Hindo, S. S. *et al.* Small molecule modulators of copper-induced Abeta aggregation. *J. Am. Chem. Soc.* **131**, 16663-16665 (2009).

42. DeToma, A. S., Choi, J. S., Braymer, J. J. & Lim, M. H. Myricetin: a naturally occurring regulator of metal-induced amyloid-beta aggregation and neurotoxicity. *Chembiochem* **12**, 1198-1201 (2011).

43. Hider, R. C., Liu, Z. D. & Khodr, H. H. Metal chelation of polyphenols. *Methods Enzymol.* **335**, 190-203 (2001).

44. Satterfield, M. & Brodbelt, J. S. Enhanced detection of flavonoids by metal complexation and electrospray ionization mass spectrometry. *Anal. Chem.* **72**, 5898-5906 (2000).

45. Mmatli, E. E. *et al.* Identification of major metal complexing compounds in Blepharis aspera. *Anal. Chim. Acta.* **597**, 24-31 (2007).

46. Bai, Y. *et al.* Characterization of the rutin-metal complex by electrospray ionization tandem mass spectrometry. *Anal. Sci.* **20**, 1147-1151 (2004).

47.   Nkhili, E., Loonis, M., Mihai, S., El Hajji, H. & Dangles, O. Reactivity of food phenols with iron and copper ions: binding, dioxygen activation and oxidation mechanisms. *Food Funct.* **5**, 1186-1202 (2014).

48.   Sever, M. J. & Wilker, J. J. Visible absorption spectra of metal-catecholate and metal-tironate complexes. *Dalton Trans.*, 1061-1072 (2004).

49.   Seidel, V. *et al.* Phenylpropanoids from Ballota nigra L. inhibit in vitro LDL peroxidation. *Phytother. Res.* **14**, 93-98 (2000).

50.   Afanas'eva, I. B., Ostrakhovitch, E. A., Mikhal'chik, E. V., Ibragimova, G. A. & Korkina, L. G. Enhancement of antioxidant and anti-inflammatory activities of bioflavonoid rutin by complexation with transition metals. *Biochem. Pharmacol.* **61**, 677-684 (2001).

51.   Brown, J. E., Khodr, H., Hider, R. C. & Rice-Evans, C. A. Structural dependence of flavonoid interactions with Cu2+ ions: implications for their antioxidant properties. *Biochem. J.* **330 (Pt 3)**, 1173-1178 (1998).

52.   Schanda, P. & Brutscher, B. Very fast two-dimensional NMR spectroscopy for real-time investigation of dynamic events in proteins on the time scale of seconds. *J. Am. Chem. Soc.* **127**, 8014-8015 (2005).

53.   Mayer, M. & Meyer, B. Group epitope mapping by saturation transfer difference NMR to identify segments of a ligand in direct contact with a protein receptor. *J. Am. Chem. Soc.* **123**, 6108-6117 (2001).

54.   Meyer, B. & Peters, T. NMR spectroscopy techniques for screening and identifying ligand binding to protein receptors. *Angew. Chem. Int. Ed. Engl.* **42**, 864-890 (2003).

55.   Re, R. *et al.* Antioxidant activity applying an improved ABTS radical cation decolorization assay. *Free Radic. Biol. Med.* **26**, 1231-1237 (1999).

56.   Rice-Evans, C. A., Miller, N. J. & Paganga, G. Structure-antioxidant activity relationships of flavonoids and phenolic acids. *Free Radic. Biol. Med.* **20**, 933-956 (1996).

57.   Quirantes-Pine, R. *et al.* Phenylpropanoids and their metabolites are the major compounds responsible for blood-cell protection against oxidative stress after administration of Lippia citriodora in rats. *Phytomedicine* **20**, 1112-1118 (2013).

58.   Yang, F. *et al.* Curcumin inhibits formation of amyloid beta oligomers and fibrils, binds plaques, and reduces amyloid in vivo. *J. Biol. Chem.* **280**, 5892-5901 (2005).

59.   Priyadarsini, K. I. Chemical and structural features influencing the biological activity of curcumin. *Curr. Pharm. Des.* **19**, 2093-2100 (2013).

60.   Ingolfsson, H. I. *et al.* Phytochemicals perturb membranes and promiscuously alter protein function. *ACS Chem. Biol.* **9**, 1788-1798 (2014).

61. Pithadia, A. S. *et al.* Reactivity of diphenylpropynone derivatives toward metal-associated amyloid-beta species. *Inorg. Chem.* **51**, 12959-12967 (2012).

62. Vivekanandan, S., Brender, J. R., Lee, S. Y. & Ramamoorthy, A. A partially folded structure of amyloid-beta(1-40) in an aqueous environment. *Biochem. Biophys. Res. Commun.* **411**, 312-316 (2011).

63. Yoo, S. I. *et al.* Inhibition of amyloid peptide fibrillation by inorganic nanoparticles: functional similarities with proteins. *Angew. Chem. Int. Ed. Engl.* **50**, 5110-5115 (2011).

64. Fawzi, N. L., Ying, J., Torchia, D. A. & Clore, G. M. Kinetics of amyloid beta monomer-to-oligomer exchange by NMR relaxation. *J. Am. Chem. Soc.* **132**, 9948-9951 (2010).

65. Spencer, V. A., Sun, J. M., Li, L. & Davie, J. R. Chromatin immunoprecipitation: a tool for studying histone acetylation and transcription factor binding. *Methods* **31**, 67-75 (2003).

Chapter 3

Amyloid-β Adopts a Conserved, Partially Folded Structure upon Binding to Zwitterionic Lipid Bilayers Prior to Amyloid Formation

This chapter was adapted from the following publication:

> Korshavn, K. J., Bhunia, A., Lim, M. H., Ramamoorthy, A. Amyloid-β Adopts a Conserved, Partially Folded Structure upon Binding to Zwitterionic Lipid Bilayers Prior to Amyloid Formation. *Chem. Comm.*. **52**, 882-885 (2015).

3.1. Introduction

Alzheimer's disease (AD), one of the leading causes of death worldwide, is commonly considered a protein misfolding disease.[1] While identified by the deposition of insoluble aggregates of amyloid-β (Aβ) peptides as plaques in the brains of diseased patients,[1,2] it is presently thought that soluble, intermediate oligomers and the process of their interconversion are mostly responsible for neuronal death in AD.[3] The interaction of these soluble Aβ species with the lipid bilayer of neurons is believed to be responsible for toxicity, through both the formation of ion-selective channels as well as more dramatic membrane permeabilization and disruption *via* a two-step mechanism.[4] Preventing such toxic interactions and structural transitions could be an important strategy for blocking Aβ toxicity in AD. Unfortunately, high resolution mechanisms of peptide interaction with both itself and the cell membrane are unclear due, in large part, to the heterogeneous protein environments present during amyloid formation.[5] To date, most full length structural models of Aβ explore the structure of mature fibrils.[6-9] Monomeric and early soluble oligomers have also been investigated, though it is believed that

the monomer exists as a predominantly disordered backbone and most oligomers are too transient to garner significant structural data.[5,10,11] Most structured, low molecular weight structures are the result of stabilization of detergents and other micellular structures.[12-15] While these models provide insight about how Aβ prefers to partition between hydrophobic and hydrophilic environments, detergents are not a viable mimetic for biological membranes and the concentration and identity of the detergent can drastically impact the aggregate structure which raises questions of the physiological relevance of these structures. Greater understanding of *in vitro* intermediate structures adopted by Aβ, specifically within the biological context of intact lipid bilayers, is necessary to fully elucidate its *in vivo* aggregation pathways and toxic mechanisms.

High resolution structural insights into the membrane-associated Aβ species have been elusive to date. Recent developments in solid-state NMR have enabled some initial insights into some of the mechanisms and structures associated with late stages of membrane-associated Aβ aggregation.[16-18] The heterogeneity of early aggregation events makes them extremely difficult to investigate, however, and they remain poorly understood. It remains possible to apply solution NMR methodologies to interrogate early stages of membrane-Aβ$_{40}$ interaction. NMR, however, is hindered by both the large size of vesicle membrane models, which can broaden the lipid-bound protein signal beyond detection, and the ability of membranes to accelerate the aggregation of Aβ, reducing the free monomer concentration and limiting its intensity while simultaneously generating solution NMR invisible proteinaceous species.[19,20] It has been previously shown, however, that maintaining a static sample at lower temperature stabilizes the monomeric peptide[21] while using 100 nm large unilamellar vesicles (LUVs) composed solely of zwitterionic phosphatidylcholine (PC), containing lipids limits membrane-mediated catalysis of

amyloid formation while still allowing protein-membrane interactions.[20] Additionally, transfer- and relaxation-based solution NMR experiments are specifically designed to allow for the interrogation of lowly populated, transient states, traits which exemplify the early membrane-Aβ intermediates.[22] The use of zwitterionic lipids to considerably reduce the lipid bilayer binding affinity of the peptide enabled us to measure the secondary structure of the bilayer-bound peptide by promoting exchange between the free and bound populations of $Aβ_{40}$ and decreasing the membrane-associated aggregation of Ab which is promoted by the presence of net charge on model membranes. Herein, coupling non-aggregating $Aβ_{40}$ sample preparations with a suite of NMR experiments[22,23] and other biophysical approaches, we are able to successfully investigate the effect of early membrane interactions on the structure of $Aβ_{40}$ prior to its aggregation on the bilayer surface and identify a conserved, partially helical structure which is adopted upon binding to the lipid bilayer.
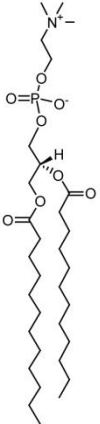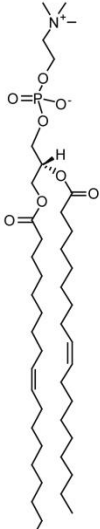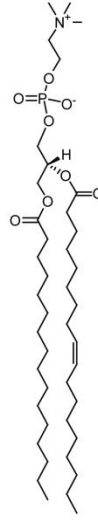
3.2. Results

3.2.1. Sample optimization

The interaction of $Aβ_{40}$ on the bilayer surface was probed with LUVs composed entirely of dilauroyl phosphatidylcholine (DLPC), dioleoyl phosphatidylcholine (DOPC), or 1-palmitoyl-2-oleoyl phosphatidylcholine (POPC) (Fig. 3.1). All three lipids form a liquid crystalline, zwitterionic bilayer above 0 °C while having variations in their hydrophobic thickness.[24,25] In so doing, we investigated the universality of binding events to fluid PC bilayers which have variations in degrees of unsaturation and hydrophobicity. Additionally, it has been suggested that lipid bilayers of diseased neurons in AD may be noticeably thinner than their non-diseased counterparts. The prevalence of oxidative stress in the AD brain is capable of generating short-chain lipids through peroxidation of unsaturated acyl chains.[26-28] Additionally, protein

aggregation on membranes, like that of Aβ, can induce local thinning *via* mechanical strain.[29-31] Thus, while exploring general mechanisms of peptide interactions at membrane surfaces, it may also be possible to glean a structural understanding of the role which pathogenic membrane thinning plays in AD.

Name	DLPC	DOPC	POPC
Structure			
T_m (°C)	-2	-17	-2
Hydrophobic Thickness (Å)	20.9	26.8	27.1
Acyl Chain Carbon Atoms	12	18	16; 18

Figure 3.1. Zwitterionic lipid structures. All lipids used in this study contain the zwitterionic phosphatidylcholine (PC) head group. They differ in their acyl chain length which determines the hydrophobic thickness (20.9-27.1 Å),[24,25] but does not dramatically impact their transition temperature (T_m), ensuring that all bilayers are in the liquid crystalline phase under our experimental conditions.

Upon the addition of substoichiometric concentrations of LUVs to Aβ40, circular dichroism (CD) suggests that the majority of the peptide is disordered in the presence of all three different bilayer systems, as has been previously suggested.[32] This predominantly unstructured state remains stable for at least 24 h under quiescent conditions suggesting the peptide remains

predominantly monomeric over the course of incubation (Fig. B.1). While the unchanged CD spectra show a bulk population which is unstructured and likely unbound from the bilayer, observing the same conditions by ^{1}H NMR reveals global broadening of the peptide's resonances following the addition of LUVs of each unique lipid composition to the peptide (Fig. B.2). Line broadening is suggestive of exchange between free, NMR-visible peptide and some form or forms of lipid-associated, NMR-invisible peptide on the NMR time scale. The existence of this invisible state solely in the presence of LUVs indicates the formation of an Aβ_{40}–bilayer complex and suggests that there is a sub-population of the peptide which exists in a structured or semi-structured, membrane-bound conformation which is overpowered by the bulk peptide's random coil conformation in CD measurements.

3.2.2. tr-NOESY provides structural insights

Due to the evident fast exchange of Aβ_{40} between the free and membrane-associated states, transferred ^{1}H–^{1}H nuclear Overhauser effect spectroscopy (tr-NOESY) was applied to probe the conformational changes induced by peptide-bilayer interactions while filtering out structural information from the unbound population of Aβ_{40}.[33-35] Traditionally, peptides and proteins associated with large lipid bilayer mimetics are difficult to investigate with traditional solution NMR spectroscopy due to their long correlation times and subsequent signal broadening. However, when the peptide of interest is in exchange between its bound and free forms, as it is in our Aβ_{40} system, tr-NOESY is able to provide NOEs between protons from the bound state *via* observation of the free Aβ_{40} population, thus overcoming the traditional signal broadening limits.

The obtained tr-NOESY spectra of Aβ_{40} in the presence of all three vesicles present a large number of NOEs which suggest the existence of an at least partially folded structure when

bound to each PC-containing LUV (Fig. 3.2). Furthermore, similar NOEs originating from the peptide were observed with all three different LUV types, implying that the partially folded conformation of $A\beta_{40}$ bound to the lipid bilayer is similar across DLPC, DOPC, and POPC bilayers (Fig. 3.3a). This demonstrates that initial interactions between $A\beta_{40}$ and the lipid
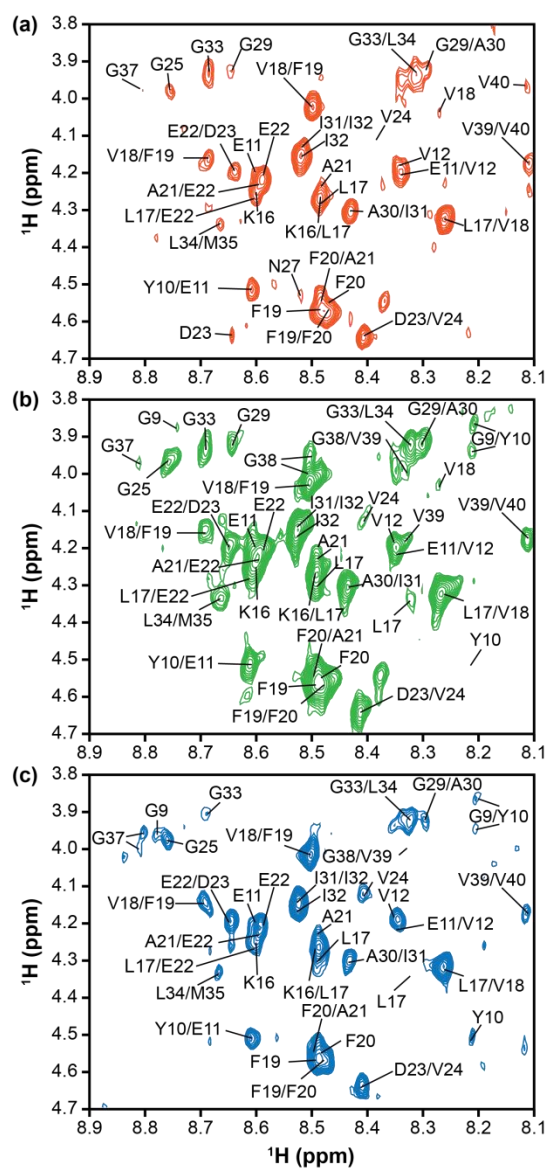
Figure 3.2. Select regions of tr-NOESY spectra of $A\beta_{40}$ (80 μM) in the presence of LUVs. The NH–H^{α} region of the tr-NOESY spectrum in the presence of LUVs (a) DLPC, (b) DOPC, or (c) POPC (16 μM lipid)(Bruker 900 MHz spectrometer using 80 ms mixing time, equipped with cryoprobe at 10 °C; 20 mM PO_4, pH 7.4, 50 mM NaCl). Moderate broadening of peaks hinders complete resonance assignment, but suggest a modest exchange rate between the lipid-bound and -free forms of the peptide.

membrane may, therefore, be predominantly controlled by the surface characteristics of the membrane (charge and head group) rather than hydrophobic characteristics (acyl chain saturation and thickness). The N-terminal residues (D1-Q15) show few NOEs, signifying a greater degree of flexibility relative to the rest of the peptide for which additional NOEs are observed. It is likely, therefore, that the N-terminus of $A\beta_{40}$ plays a minimal role in early adsorption to the bilayer surface and is not initially associated with the membrane. Sequential NH–NH and H^{α}–NH NOEs are prominent throughout the central region (K16-G25) of the $A\beta_{40}$ peptide, indicating
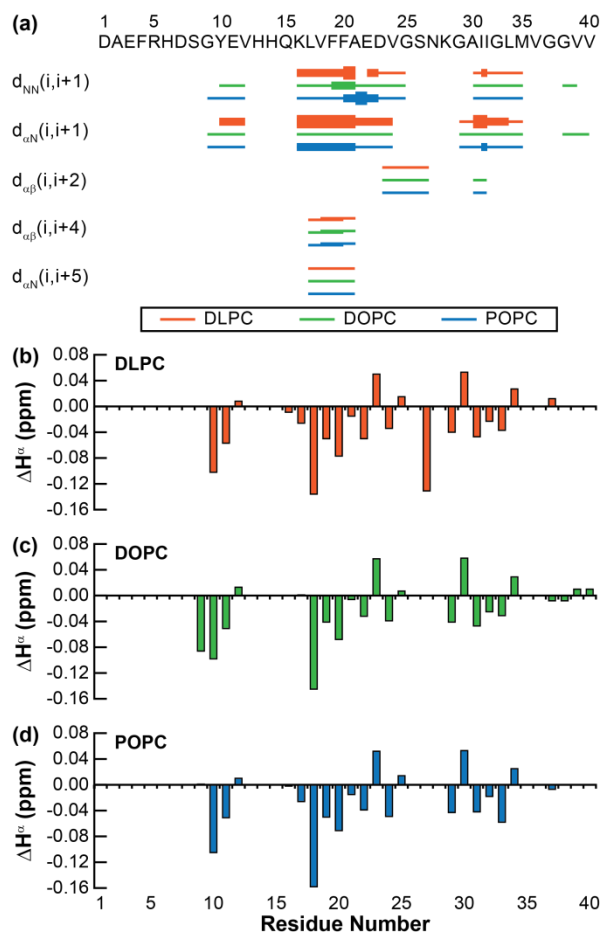
Figure 3.3. tr-NOE derived structural constraints for $A\beta_{40}$. (a) NOE connectivity plot shows a partially structured backbone conserved across all three different bilayers investigated. The strengths of NOEs are indicated by the height of the bars, graded as strong, medium, or weak. The H^{α} chemical shift for (b) DLPC, (c) DOPC, and (d) POPC was calculated for each resolved residue relative to the random coil chemical shift for each residue.

enhanced rigidity and a propensity for secondary structure. This region has previously been found to adopt a partially folded, 3_{10} helix in solution[10] while also being proposed to instigate the formation of amyloid fibrils as a self-recognition sequence.[1] A second string of sequential NH–NH and H^α–NH NOEs was seen for the more C-terminal hydrophobic region (G29-M35) which, similarly to the self-recognition sequence, has been implicated in fiber structure and formation.[1] Along with these sequential NOEs, multiple H^α–H^β i,i+4 NOEs were observed in the central sequence (L17-A21, V18-E22). These side chain NOEs are accompanied by an H^α–NH i,i+5 NOE between L17 and E22. This combination of i,i+4 and i,i+5 NOEs is suggestive of the peptide folding into a loosely packed π-helix in the central region.

In conjunction with these long distance NOEs, frequent negative ΔH^α values (Fig. 3.3) are predictive of a general helical propensity (Fig. 3.3b-d). Sequential helical propensity is most pronounced between K16 and E22 region, which, along with the NOE connectivity observed above, further supporting that the central portion of $A\beta_{40}$ adopts a helical conformation in the presence of all three PC bilayers upon binding. The presence of multiple, non-sequential negative ΔH^α values in the more C-terminal region may demonstrate a propensity toward a more random coil and rigid membrane associated conformation. Finally, the N-terminus displays few resonances in the presence of all three bilayers, indicating weak or no interaction with the lipid bilayer and a lack of defined structure or rigidity.

3.2.3. Probing membrane associated backbone topology

In order to better define the boundaries of membrane-bound and -unbound regions of the peptide, paramagnetic $MnCl_2$ was titrated into a solution of ^{15}N-$A\beta_{40}$ in the presence of the three different LUVs and SOFAST-HMQC spectra were recorded to observer the backbone amide signals. The paramagnetic Mn^{2+} ion is capable of selective quenching NMR signals from solvent

exposed residues not associated with the hydrophobic lipid bilayer (Fig. B.3). As was observed with tr-NOESY, $A\beta_{40}$ in the presence of each of the three lipid bilayers reacted similarly to the presence of $MnCl_2$. Substoichiometric concentrations of $MnCl_2$ (40 μM) reduced the signal intensity of the N-terminus (D1-Q15) to *ca.* 50% of their original value while stoichiometric concentrations (80 μM) decreased the same regions to *ca.* 30% of their original intensity. The same concentrations of $MnCl_2$ decreased the remainder of the peptide's resonances to *ca.* 90% and 85%, respectively. This suggests that the N-terminal residues, predicted to be flexible and unassociated with the membrane based on tr-NOESY spectra, are, in fact, not bound to the bilayer surface and instead free and unstructured in solution. The remainder of the peptide is associated with the bilayer surface, though only adopting defined structure in selective hydrophobic regions, according to the tr-NOESY results.

The relaxation and dynamics of the peptide in the presence of LUVs were measured to further interrogate the membrane-associated and membrane-unassociated regions of the peptide sequence. ^{15}NH-ΔR_2 values (the difference in ^{15}NH-R_2 in the presence of LUVs *versus* in the absence) measure the relative flexibility of the peptide backbone in the presence of PC bilayers. As a protein becomes more rigid or solid-like, its transverse relaxation rate (R_2) increases as spin-spin relaxation becomes more likely. It is expected that regions of the peptide which preferentially interact with the lipid bilayer will present an increase in their R_2 values relative to peptide free in solution. Interestingly, unlike what was observed in the tr-NOESY and PRE experiments above, the three lipids induced different dynamic changes to the peptide backbone suggesting a difference in the extent of lipid-peptide interaction that contributes to the rigidity of the residues in the structured region of the peptide, as discussed below (Fig. 3.4). Instead of each bilayer selectively increasing the relaxation rate (R_2) of the bound, structured region, there was

no sequence specificity for the relaxation increases observed; the increases were sporadic throughout the peptide sequence. Additionally, the average ΔR_2 differs for each of the three lipid systems. This suggests that the relaxation changes are not due to specific structural alterations and are instead the result of differential binding propensities and partitioning of free versus bound peptide to the three different bilayers. Fluorescence polarization was used to measure the binding affinity (K_d) of the peptide for the three distinct LUVs (Fig. B.4). There was an inverse correlation between bilayer thickness (Fig. 3.1) and the measured affinities (DLPC, 20.9 Å, $K_d = 1188 \pm 41$ μM; DOPC, 26.8 Å, $K_d = 801 \pm 45$ μM; DLPC, 27.1 Å, $K_d = 366 \pm 36$ μM). An
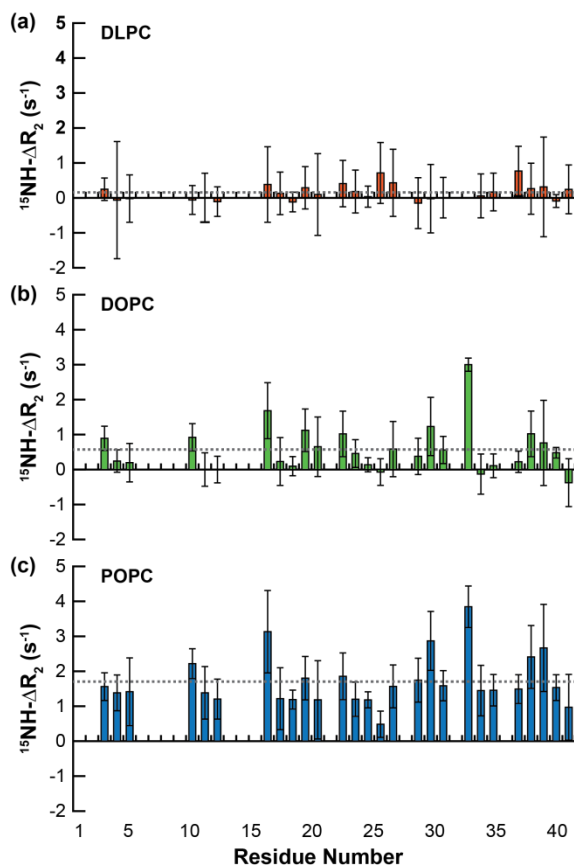


Figure 3.4. Peptide backbone dynamics in the presence of lipid bilayers. The ΔR_2 value for each resolvable residue was calculated as the difference between the relaxation of Aβ$_{40}$ in the presence LUVs containing either (a) DLPC, (b) DOPC, or (c) POPC and Aβ$_{40}$ free in solution. The average ΔR_2 of all residues of the peptide is represented by the dashed gray line.

additional inverse correlation exists between the ΔR_2 values and the binding affinity of $A\beta_{40}$ for each bilayer (Fig. B.5). Therefore, the increase in rigidity and subsequently accelerated relaxation rates observed for the peptide are the result of an increased population which binds to the bilayer surface rather than a result of the structural changes induced by peptide binding. It is likely that the bound peptide is adopting the relaxation rate of the LUV itself and the higher the population bound with LUV the more the R_2 value increases as the weighted average R_2 value for all species of peptide shifts to faster rates. It is also worth noting that this is the only parameter which correlates with the bilayer thickness. The thicker the membrane, the stronger the affinity and the more rigid the peptide population becomes. While the partially foldedstructure of $A\beta_{40}$ is conserved across bilayers, it may be that the increased hydrophobic thickness of the POPC membrane is more capable of stabilizing this transient species.

3.3. Discussion

It seems, therefore, that zwitterionic, liquid crystalline bilayers are capable of inducing a conserved fold in $A\beta_{40}$, tuneable by small alterations in the bilayer structure (*i.e.*, thickness and acyl chain saturation). In this common fold, the N-terminus is unstructured and unassociated with the membrane, while the more C-terminal region adopts a bound, more rigid coil structure and the central hydrophobic region become a more structured helix (Fig. 3.5.). This general topology is similar to both a previously proposed structure of partially folded $A\beta_{40}$ in solution[10] and a model of $A\beta_{40}$ bound to GM1 micelles.[12] It is, then, possible that this conserved helical fold may extend beyond PC bilayers and be a more universal early step in $A\beta_{40}$ folding and aggregation. General helical intermediates have previously been suggested, especially in the presence of heterogeneous bilayers, though the residue-specific topology is unclear in most cases.[12,32,36] We believe that this helical, membrane bound intermediate may represents the first
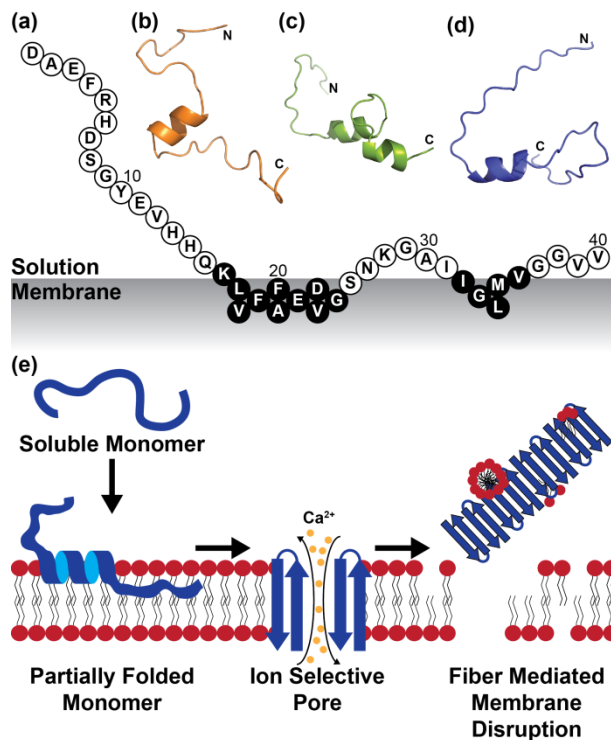
Figure 3.5. Structural modelling of membrane-bound Aβ$_{40}$. (a) Aβ$_{40}$ adopts a conserved binding mode with PC lipid bilayers. Those residues in black circles are believed to have an especially high propensity for structure based on observed tr-NOEs. 3D cartoon models were generated based on tr-NOE and paramagnetic quenching constraints for (b) DLPC, (c) DOPC, and (d) POPC lipid bilayers. (e) The folding of Aβ$_{40}$ on the bilayer into this conserved helix likely precedes the formation of other membrane-associated aggregate species related to membrane disruption. While monomer association happens almost instantaneously, pore formation occurs over the course of minutes, and fiber-mediated disruption occurs over the course of hours, it remains unclear whether one event proceeds from the previous or whether these events are decoupled.[4]

step in membrane-mediated Aβ aggregate formation, preceding both transmembrane pore formation and surface-catalyzed fiber formation and subsequent membrane disruption (Fig. 3.5e).[4] Our results suggest that the central region containing the self-recognition sequence of Aβ$_{40}$ (K16-E22) commonly associated with the cross β-strand amyloid structure may also be essential for the formation of early helical intermediates. In this model, we assume that membrane-associated oligomers form as the result of interactions between monomeric subunits on the bilayer, rather than forming in solution and subsequently inserting into the bilayer to enact

95

their function. It is necessary to further explore this possible mechanism further. It is likely that similar investigations to those performed here with bilayers that vary in their fluidity may be able to further clarify the role of membrane mediated aggregates versus aggregates which form in solution and subsequently associate with or insert into the membrane.

Additionally, it is interesting that, while it did not impact the surface-induced folded structure, bilayer hydrophobic thickness strongly influenced the affinity of the peptide for the bilayer and the population's rigidity. It is known that membrane hydrophobic thickness is capable of modulating the insertion and folding of conventional membrane proteins.[37,38] It is possible that our observed differences in binding affinity, which take into account the entire population of $A\beta_{40}$, rather than solely the partially folded structure, are the result of higher order intermediates which we have no observed here preferentially associating with the bilayer. If this is the case, it suggests that the peptide could interact with conventional bilayers and pathologically thinned bilayers differently.[27,28] While this study has only investigated the early monomer interactions with the bilayer, it will be advantageous to explore the effect of these altered affinities on the subsequent aggregation of $A\beta_{40}$ on membranes of varying thicknesses further. These studies may help explain relationships between two important physiological factors in AD.

3.4. Materials and methods

3.4.1. Materials

Unlabeled $A\beta_{40}$ (> 95% purity) was purchased from Genscript (Piscataway, NJ, USA). Uniformly ^{15}N-labeled $A\beta_{40}$ was purchased from rPeptide (Bogart, GA, USA). HiLyte Fluor 647-$A\beta_{40}$ was purchased from Anaspec (Fremont, CA, USA). All peptide was used as received without additional purification. 1,2-Dilauroy-*sn*-glycero-3-phosphocholine (DLPC), 1,2-

dioleoyl-*sn*-glycero-3-phosphocholine (DOPC), and 1-palmitoyl-2-oleoyl-*sn*-glycero-3-phosphocholine (POPC) were purchased from Avanti Polar Lipids *Inc*. (Alabaster, AL, USA). All other reagents were purchased from Sigma-Aldrich (St. Louis, MO, USA).

3.4.2. Vesicle preparation

Large unilamellar vesicles (LUVs) of pure DLPC, DOPC, and POPC were prepared from a chloroform solution. The resulting solution was dried under N_2 (g) and then placed under high vacuum overnight to remove the residual solvent. The resultant film was rehydrated with buffer solution (20 mM PO_4, pH 7.4, 50 mM NaCl) to yield a final lipid concentration of either 10 mg/mL (for fluorescence binding experiments) or 1 mM (for all other experiments). Lipid was resuspended by vigorous mixing and the resulting solution was extruded 23 times through a 100 nm polycarbonate Nucleopore membrane filter (Whatman) mounted on a mini-extruder (Avanti Polar Lipids *Inc*.) to obtain a homogenous solution of LUVs with an average diameter of 100 nm. The formation of vesicles was confirmed by dynamic light scattering to ensure solution homogeneity.

3.4.3. Peptide preparation

In order to break up preformed aggregates in the initial peptide aliquot, both unlabeled and uniformly ^{15}N-labeled peptide was dissolved in 1% NH_4OH and aliquoted to 0.1 mg/sample, and lyophilized. HiLyte Fluor 647-$A\beta_{40}$ was similarly dissolved in 1% NH_4OH and aliquoted to 0.01 mg/sample and lyophilized. All peptide was dried under vacuum for 48 h to remove excess moisture.

3.4.4. Circular dichroism studies

Circular dichroism (CD) measurements were carried out at a concentration of 20 μM Aβ$_{40}$ in the presence of 4 μM LUV in buffer (20 mM PO$_4$, 50 mM NaF, pH 7.4). Freshly lyophilized peptide was first dissolved in 5 μL of 1% NH$_4$OH prior to dilution into the buffer to prevent the formation of early aggregates. CD measurements were performed on a JASCO J-1500 CD Spectrometer using a 0.1 cm path length cell. The spectra were acquired at 10 °C at a scan rate of 100 nm/min and averaged over 10 scans. Measurements were taken immediately after mixing the sample (t = 0 h), after 4 h incubation at 4 °C, and after 24 h incubation at 4 °C.

3.4.5. Fluorescence anisotropy binding studies

To prepare the peptide for fluorescence experiments, HiLyte Fluor 647-Aβ$_{40}$ was dissolved in 5 μL 1% NH$_4$OH and diluted into buffer (20 mM PO$_4$, pH 7.4, 50 mM NaCl) to a final peptide concentration of 1 μM. Fluorescence measurements were performed on a Jasco FP-6500 fluorimeter equipped with excitation and emission polarizing filters. Fluorescence polarization was used to measure the binding affinity of Aβ$_{40}$ for 100 nm LUVs of the various lipids. 150 μL of a 1 μM solution of HiLyte Fluor 647-Aβ$_{40}$ was titrated with LUVs from a 10 mg/mL stock solution. Lipid was titrated into peptide solution to a maximum concentration of 7 mM. The fluorescence anisotropy was monitored with an excitation wavelength of 647 nm and emission wavelength of 660 nm using a 10 nm bandwidth for both excitation and emission at each titration point. Anisotropy (<r>) was calculated using equation 1 where G is defined by equation 2. I is the intensity observed with excitation (first subscript) and emission (second subscript) polarizers set to either vertical or horizontal, providing four measurements which contribute to the anisotropy calculation.

$$< r > = \frac{I_{VV} - G * I_{VH}}{I_{VV} + 2 * G * I_{VH}}$$

$$G = \frac{I_{HV}}{I_{HH}}$$

The anisotropy values measured were then plotted against their respective lipid concentrations and the data were fit using equation 3 to identify the binding affinity (K_d) of peptide for the LUVs.

$$< r > = \frac{<r>_{inf}*[lipid]}{K_d+[lipid]} + < r >_0$$

3.4.6. NMR spectroscopy

For all samples analyzed by NMR, 0.1 mg peptide (uniformly ^{15}N-labeled or unlabeled) was dissolved with 3 μL DMSO-d_6 (Cambridge Isotope, Tewksbury, MA, USA) and diluted with phosphate buffer, NaCl, D_2O, and ddH$_2$O to a final peptide concentration of 80 μM (20 mM PO$_4$, pH 7.4, 50 mM NaCl, 7% v/v D_2O). For those samples containing lipid, LUVs were also added from a 1 mM stock solution containing a single lipid for a final lipid concentration of 16 μM (0.2 equiv). For all experiments, spectral were processed using Topspin 2.1 (Bruker) while assignments and intensity fits were performed by SPARKY 3.113.

3.4.6.1. Transfer-NOESY (tr-NOESY)

Line broadening was first observed by 1D ^{1}H NMR upon the addition of 0.2 equiv (16 μM) lipid, suggesting exchange between unbound and bound species; this peptide:lipid ratio was

utilized throughout for lipid containing NMR samples and was observed to be stable over the course of the experiments. Therefore, transfer-NOESY (tr-NOESY) experiments were carried out on Bruker TCI 900 spectrometer, equipped with a cryo-probe to investigate the membrane bound state of unlabeled Aβ$_{40}$ to the three LUVs.[33-35] Two-dimensional (2D) ^{1}H-^{1}H TOCSY and ^{1}H-^{1}H tr-NOESY spectra were acquired at 80 and 150 ms mixing times, respectively at 10 °C. Tr-NOESY spectra were acquired using 2 K data points in t_2 and 512 data points in t_1 and a spectral width of 12 ppm in both dimensions. H$^\alpha$ chemical shifts were then calculated relative to the random coil shift values maintained by the Biological Magnetic Resource Bank (BMRB, University of Wisconsin).

3.4.6.2. Paramagnetic relaxation enhancement titration

A solution of MnCl$_2$ was titrated into a solution of uniformly ^{15}N-labeled Aβ$_{40}$ in the presence of LUVs described above and monitored by SOFAST-HMQC on a Bruker 600 MHz spectrometer equipped with a cryoprobe at 10 °C. Spectra of each sample in the presence of 0 equiv (0 μM), 0.5 equiv (40 μM), and 1 equiv (80 μM) MnCl$_2$ were obtained from 128 t_1 points and a 100 ms recycle delay. Relative intensities for all spectra were obtained by a comparison of spectra in the presence of spectra acquired in the presence of both 0.5 and 1.0 equiv MnCl$_2$ to spectra in the absence of the paramagnetic reagent. Peak assignments for the spectra were based on previously published spectra.[10]

3.4.6.3. Relaxation measurements

The ^{15}N transverse relaxation rate constants ($R_2 = 1/T_2$) for the residues of Aβ$_{40}$ were determined by collecting a series of ^{15}N-^{1}H HSQC spectra under a variety of relaxation delays on a Bruker 600 MHz spectrometer equipped with a cryoprobe at 17 °C using the uniformly ^{15}N-

labeled $A\beta_{40}$ samples described above; R_2 values were measured for samples in the presence of all three different bilayers, as well as in the absence of lipids. Relaxation delays of 8, 16, 32, 48, 64, 80, 96, 128, 160, 194, 240, and 320 ms were used for the measurement of R_2. ΔR_2 values were then calculated as the difference between the R_2 values of peptide in the presence of the three LUVs (DLPC, DOPC, and POPC) and the R_2 values of peptide in the absence of lipid. Positive ΔR_2 values are indicative of a protein population which is more rigid than the peptide population in the absence of lipid while negative ΔR_2 values are indicative or a less rigid population.

3.5. Acknowledgements

3.6. Author Contributions

A.R. and M.H.L. directed the overall research. K.J.K. performed all sample preparation and optical spectroscopies. K.J.K. and A.B. performed the NMR experiments and analyzed the data. All authors reviewed and approved the manuscript.

3.7. References

1   Savelieff, M. G., Lee, S., Liu, Y. & Lim, M. H. Untangling amyloid-beta, tau, and metals in Alzheimer's disease. *ACS Chem. Biol.* **8**, 856-865 (2013).

2   Selkoe, D. J. Alzheimer's disease. *Cold Spring Harb. Perspect. Biol.* **3** (2011).

3   Hardy, J. & Selkoe, D. J. The amyloid hypothesis of Alzheimer's disease: progress and problems on the road to therapeutics. *Science* **297**, 353-356 (2002).

4   Sciacca, M. F. *et al.* Two-step mechanism of membrane disruption by Abeta through membrane fragmentation and pore formation. *Biophys. J.* **103**, 702-710 (2012).

5   Kotler, S. A., Walsh, P., Brender, J. R. & Ramamoorthy, A. Differences between amyloid-beta aggregation in solution and on the membrane: insights into elucidation of the mechanistic details of Alzheimer's disease. *Chem. Soc. Rev.* **43**, 6692-6700 (2014).

6   Milojevic, J., Esposito, V., Das, R. & Melacini, G. Understanding the molecular basis for the inhibition of the Alzheimer's Abeta-peptide oligomerization by human serum albumin using saturation transfer difference and off-resonance relaxation NMR spectroscopy. *J. Am. Chem. Soc.* **129**, 4282-4290 (2007).

7   Narayanan, S. & Reif, B. Characterization of chemical exchange between soluble and aggregated states of beta-amyloid by solution-state NMR upon variation of salt conditions. *Biochemistry* **44**, 1444-1452 (2005).

8   Lu, J. X. *et al.* Molecular structure of beta-amyloid fibrils in Alzheimer's disease brain tissue. *Cell* **154**, 1257-1268 (2013).

9   Schutz, A. K. *et al.* Atomic-resolution three-dimensional structure of amyloid beta fibrils bearing the Osaka mutation. *Angew. Chem. Int. Ed. Engl.* **54**, 331-335 (2015).

10   Vivekanandan, S., Brender, J. R., Lee, S. Y. & Ramamoorthy, A. A partially folded structure of amyloid-beta(1-40) in an aqueous environment. *Biochem. Biophys. Res. Commun.* **411**, 312-316 (2011).

11   Roche, J., Shen, Y., Lee, J. H., Ying, J. & Bax, A. Monomeric Abeta(1-40) and Abeta(1-42) Peptides in Solution Adopt Very Similar Ramachandran Map Distributions That Closely Resemble Random Coil. *Biochemistry* **55**, 762-775 (2016).

12   Utsumi, M. *et al.* Up-and-down topological mode of amyloid beta-peptide lying on hydrophilic/hydrophobic interface of ganglioside clusters. *Glycoconj. J.* **26**, 999-1006 (2009).

13   Crescenzi, O. *et al.* Solution structure of the Alzheimer amyloid beta-peptide (1-42) in an apolar microenvironment. Similarity with a virus fusion domain. *Eur. J. Biochem.* **269**, 5642-5648 (2002).

14   Coles, M., Bicknell, W., Watson, A. A., Fairlie, D. P. & Craik, D. J. Solution structure of amyloid beta-peptide(1-40) in a water-micelle environment. Is the membrane-spanning domain where we think it is? *Biochemistry* **37**, 11064-11077 (1998).

15   Serra-Batiste, M. *et al.* Abeta42 assembles into specific beta-barrel pore-forming oligomers in membrane-mimicking environments. *Proc. Natl. Acad. Sci. U.S.A.* **113**, 10866-10871 (2016).

16   Qiang, W., Akinlolu, R. D., Nam, M. & Shu, N. Structural evolution and membrane interaction of the 40-residue beta amyloid peptides: differences in the initial proximity between peptides and the membrane bilayer studied by solid-state nuclear magnetic resonance spectroscopy. *Biochemistry* **53**, 7503-7514 (2014).

17   Qiang, W., Yau, W. M. & Schulte, J. Fibrillation of beta amyloid peptides in the presence of phospholipid bilayers and the consequent membrane disruption. *Biochim. Biophys. Acta.* **1848**, 266-276 (2015).

18   Delgado, D. A. *et al.* Distinct Membrane Disruption Pathways Are Induced by 40-Residue beta-Amyloid Peptides. *J. Biol. Chem,* **291**, 12233-12244 (2016).

19   Bodner, C. R., Dobson, C. M. & Bax, A. Multiple tight phospholipid-binding modes of alpha-synuclein revealed by solution NMR spectroscopy. *J. Mol. Biol.* **390**, 775-790 (2009).

20   Terakawa, M. S., Yagi, H., Adachi, M., Lee, Y. H. & Goto, Y. Small liposomes accelerate the fibrillation of amyloid beta (1-40). *J. Biol. Chem.* **290**, 815-826 (2015).

21   Suzuki, Y. *et al.* Resolution of oligomeric species during the aggregation of Abeta1-40 using (19)F NMR. *Biochemistry* **52**, 1903-1912 (2013).

22   Anthis, N. J. & Clore, G. M. Visualizing transient dark states by NMR spectroscopy. *Q. Rev. Biophys.* **48**, 35-116 (2015).

23   Karamanos, T. K., Kalverda, A. P., Thompson, G. S. & Radford, S. E. Mechanisms of amyloid formation revealed by solution NMR. *Prog. Nucl. Magn. Reson. Spectrosc.* **88-89**, 86-104 (2015).

24   Kucerka, N. *et al.* Structure of fully hydrated fluid phase DMPC and DLPC lipid bilayers using X-ray scattering from oriented multilamellar arrays and from unilamellar vesicles. *Biophys. J.* **88**, 2626-2637 (2005).

25   Kucerka, N., Tristram-Nagle, S. & Nagle, J. F. Structure of fully hydrated fluid phase lipid bilayers with monounsaturated chains. *J. Membr. Biol.* **208**, 193-202 (2005).

26   Pratico, D. Oxidative stress hypothesis in Alzheimer's disease: a reappraisal. *Trends Pharmacol. Sci.* **29**, 609-615 (2008).

27   Beranova, L., Cwiklik, L., Jurkiewicz, P., Hof, M. & Jungwirth, P. Oxidation changes physical properties of phospholipid bilayers: fluorescence spectroscopy and molecular simulations. *Langmuir* **26**, 6140-6144 (2010).

28   Negre-Salvayre, A. *et al.* Pathological aspects of lipid peroxidation. *Free Radic. Res.* **44**, 1125-1171 (2010).

29   Pannuzzo, M., Milardi, D., Raudino, A., Karttunen, M. & La Rosa, C. Analytical model and multiscale simulations of Abeta peptide aggregation in lipid membranes: towards a unifying description of conformational transitions, oligomerization and membrane damage. *Phys. Chem. Chem. Phys.* **15**, 8940-8951 (2013).

30   Last, N. B. & Miranker, A. D. Common mechanism unites membrane poration by amyloid and antimicrobial peptides. *Proc. Natl. Acad. Sci. U.S.A.* **110**, 6382-6387 (2013).

31   Lee, C. C., Sun, Y. & Huang, H. W. How type II diabetes-related islet amyloid polypeptide damages lipid bilayers. *Biophys. J.* **102**, 1059-1068 (2012).

32   Wong, P. T. *et al.* Amyloid-beta membrane binding and permeabilization are distinct processes influenced separately by membrane charge and fluidity. *J. Mol. Biol.* **386**, 81-96 (2009).

33   Clore, G. M. & Gronenborn, A. M. Theory and applications of the transferred nuclear overhauser effect to the study of the conformations of small ligands bound to proteins. *J. Magn. Reson* **48**, 402-417 (1982).

34   Bhunia, A., Mohanram, H. & Bhattacharjya, S. Lipopolysaccharide bound structures of the active fragments of fowlicidin-1, a cathelicidin family of antimicrobial and antiendotoxic peptide from chicken, determined by transferred nuclear Overhauser effect spectroscopy. *Biopolymers* **92**, 9-22 (2009).

35   Wang, Z., Jones, J. D., Rizo, J. & Gierasch, L. M. Membrane-bound conformation of a signal peptide: a transferred nuclear Overhauser effect analysis. *Biochemistry* **32**, 13991-13999 (1993).

36   Ikeda, K., Yamaguchi, T., Fukunaga, S., Hoshino, M. & Matsuzaki, K. Mechanism of amyloid beta-protein aggregation mediated by GM1 ganglioside clusters. *Biochemistry* **50**, 6433-6440 (2011).

37   Fattal, D. R. & Ben-Shaul, A. A molecular model for lipid-protein interaction in membranes: the role of hydrophobic mismatch. *Biophys. J.* **65**, 1795-1809 (1993).

38   Killian, J. A. Hydrophobic mismatch between proteins and lipids in membranes. *Biochim. Biophys. Acta.* **1376**, 401-415 (1998).

Chapter 4

Reduced Lipid Bilayer Thickness Regulates the Aggregation and Cytotoxicity of Alzheimer's Disease Related Amyloid-β

The content for this chapter will be included in the following reference:

> Korshavn, K. J., Satriano, C., Zhang, R., Lin, Y., Dulchavsky, M., Bhunia, A., Ivanova, M., Lee, Y. –H., La Rosa, C., Lim, M. H., Ramamoorthy, A. Reduced Lipid Bilayer Thickness Modulates the Aggregation of and Ablates the Cytotoxicity of Aβ. *Submitted.*

4.1. Introduction

The aggregation and fibrillation of amyloid-β (Aβ) in the brain has long been implicated in the neurotoxicity and pathogenesis of Alzheimer's disease (AD). Following its production via cleavage of the transmembrane amyloid precursor protein (APP), Aβ undergoes aggregation along a nucleated growth pathway towards its end state amyloid fibril.[1] It is believed that intermediate aggregates along this path are the primary culprit in AD-related cytotoxicity.[2,3] Early Aβ oligomers may perform their toxic function through interactions with the neuronal lipid bilayer.[4,5] Pore formation has been suggested to facilitate disruption of the ionic gradient across neuronal membranes.[6,7] Alternatively, elongation of the amyloid species on the bilayer may remove lipids from the membrane and create holes which allow for the uncontrolled transit of biomacromolecules across the membrane.[8,9] These two modes of membrane disruption have been proposed to coexist; it is thought that pore-like oligomers form first while the fibril-induced perturbations occur later.[8] Extensive work by Matsuzaki and colleagues has revealed that

incorporating glycolipids, such as the ganglioside GM1, can promote the formation of toxic, membrane-associated Aβ aggregates linked to membrane disruption.[5] Despite these insights, the overarching biological, chemical, and physical parameters that govern the interactions of Aβ with lipid bilayers and modulate the formation of toxic oligomers remain unclear.

Bilayer thickness, controlled by the acyl chain length, is one basic principle of membrane biophysics that has been shown to alter membrane protein folding and modulate energetic penalties caused by the hydrophobic mismatch.[10,11] It is therefore possible that alterations in the hydrophobic thickness can control amyloid aggregation and stabilize distinct intermediates. Short chain lipids may form within the AD-affected brain via lipid peroxidation promoted by the heightened oxidative stress found in the diseased state.[12-14] Incorporation of these shortened lipids can be toxic and result in localized bilayer thinning.[13,14] The interaction of amyloidogenic sequences with lipid membranes and their aggregation in bilayers can also reduce local bilayer thickness via mechanical strain.[15-17] Thus, characterizing the effects of thin bilayers on Aβ aggregation is of great importance for understanding the underlying physical parameters that drive misfolding and unveiling the roles of pathologically relevant Aβ-membrane interactions in AD. Herein we have used synthetic bilayers composed of dilauroyl phosphatidylcholine (DLPC; 20.9 nm thick), dioleoyl phosphatidylcholine (DOPC, 26.8 nm thick), or 1-palmitoyl-2-oleoyl phosphatidylcholine (POPC, 27.1 nm thick) to explore relationships between thin (DLPC) and thick (DOPC and POPC) bilayers, Aβ aggregation, and the stabilization of distinct Aβ oligomers.[18,19]

Using the thin DLPC can recapitulate the potential thin bilayers of the diseased cells within an *in vitro* setting while ensuring reproducibility. We have previously shown that monomeric Aβ

interacts with these three zwitterionic lipid bilayers through a conserved structure under non-aggregating conditions.[20] This initial binding is driven by surface interactions with the self-recognition sequence and is minimally affected by the hydrophobic thickness of the membrane. It is more likely that the hydrophobic thickness of lipid bilayers influences the generation and/or stabilization of higher order membrane-associated species because of the ability of these Aβ aggregates to insert themselves within the bilayer.[21] Both DOPC and POPC have been previously applied to examine the interactions between lipid bilayers and amyloidogenic proteins.[8,22-25] DLPC bilayers have been used in the study of a variety of membrane proteins and were observed to stabilize some membrane proteins *in vitro*, which are less tractable with other lipid bilayer systems, but they have not previously been used in the study of Aβ.[26,27]

Through a suite of biophysical techniques we have found that the thin, pathology-mimicking DLPC bilayers have a unique ability to stabilize prefibrillar oligomers within the bilayer while preventing the formation of mature fibrils. Surprisingly, it was observed that DLPC bilayers are also capable of remodeling mature Aβ fibrils into a semi-unfolded intermediate, a feat previously observed only after treatment with high concentrations of denaturants or exposure to high frequency sonication.[28] These results show that thin bilayers are able to dramatically alter Aβ aggregation compared to conventional lipid bilayers, and this redirected misfolding can stabilize distinct, membrane-associated species not previously observed.

4.2. Results

4.2.1. Unlike DOPC or POPC, DLPC Vesicles Inhibit Aβ Fibrillation

Lipid bilayers can modulate the rate of amyloid formation by Aβ, though the extent of modulation varies with the bilayer composition, incubation conditions, and detection method.[29-31]

Thioflavin-T (ThT), a dye which fluoresces in the presence of amyloid fibrils, can probe the formation of fibrillar aggregates and is useful in delineating mechanistic deviations in amyloid aggregation.[32-34] Thus, ThT was used to initially probe the aggregation propensity of Aβ in the presence of large unilamellar vesicles (LUVs) of either DOPC, POPC, or DLPC and characterize kinetic differences that result from different interactions caused by variation in hydrophobic thickness.

Aβ aggregation was accelerated by increasing concentrations of either DOPC or POPC (Fig. 4.1a-c), as previously reported.[29,30] As the lipid concentration increased from 0 to 200 μM, the lag phase became continually shorter, suggesting more rapid nucleation and earlier fibril formation. It is likely that the observed catalysis is the result of interactions between Aβ and membrane, which serve to reduce the dimensionality of the search by individual Aβ monomers for binding partners and increase the local Aβ concentration.[29] End state aggregates formed in the absence and presence of either DOPC or POPC were examined by circular dichroism (CD) spectroscopy and transmission electron microscopy (TEM) (Fig. C.1). As expected, all three samples exhibited a canonical peak at 220 nm in CD spectra, representative of a β-strand fold and amyloid formation. TEM further established the generation of fibrillar aggregates. Fibrils formed in the presence of DOPC or POPC are shorter than those formed in solution. This discrepancy in length may be due to the effects of increased local concentration on the bilayer surface, generating additional seeds for aggregation resulting in fewer free monomers available for the extension of the fibrils. These data support previous studies suggesting that both DOPC and POPC act as amyloid catalysts.[29,30]

Incubation of DLPC LUVs with Aβ elicited a dramatically different result compared to
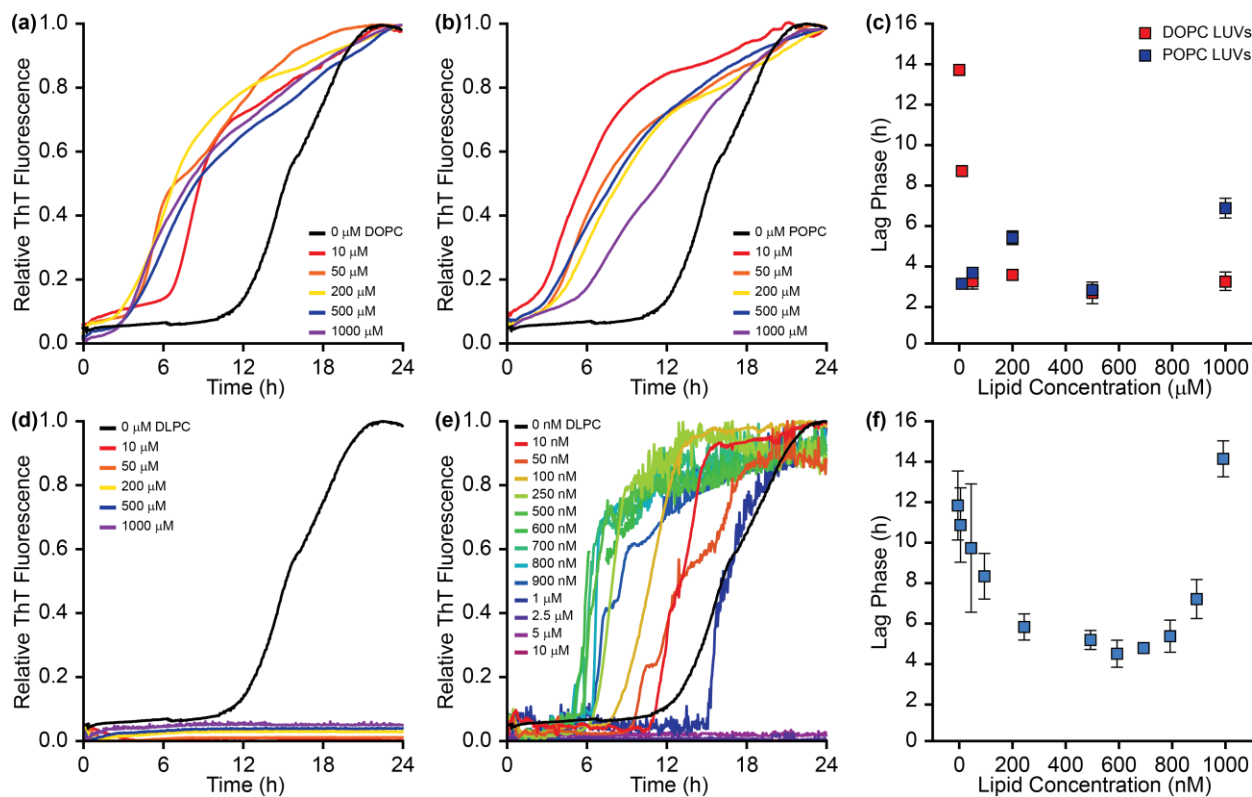
Figure 4.1. Effect of 100 nm phosphatidylcholine LUVs on Aβ aggregation kinetics. Both DOPC (a) and POPC (b) accelerate Aβ (10 μM) aggregation in a concentration dependent manner as determined by ThT (20 μM) fluorescence. (c) The lag phases suggest that kinetic acceleration is most potent at 500 μM lipid, though aggregation is rapidly accelerated at concentrations as low as 50 μM lipid. (d) DLPC LUVs inhibit Aβ aggregation at stoichiometric and super stoichiometric concentrations. (e) Low concentrations of DLPC (nM range) accelerate Aβ aggregation before reaching concentrations that eventually inhibit fibrillation. (f) The lag phase of Aβ aggregation in the presence of DLPC LUVs reaches a maximum acceleration at ~ 500-700 nM. Lag phases reported represent the average of three independent trials with error bars representing the standard deviation of these measurements.

DOPC or POPC (Fig. 4.1d). When Aβ aggregated in the presence of stoichiometric (10 μM; 1:1 lipid-peptide ratio) or higher DLPC concentrations, ThT fluorescence remained at baseline levels suggesting no fibril formation. ThT can provide false positives of inhibition resulting from dye displacement or the inability of unique amyloid sequences to bind ThT despite containing the canonical β-strand fold.[35,36] To rule out this possibility, CD and TEM were performed on endstage aggregates (Fig. C.1). CD results showed that the species formed in the presence of

109

DLPC maintained a random coil structure after 24 h incubation. The aggregates were also morphologically distinct from conventional amyloid fibrils. They were small, amorphous, and had no discrete fibril structure, as shown by TEM. Combined with ThT results, we confirmed that stoichiometric concentrations of DLPC LUVs halt amyloid fibril formation of Aβ.

To further characterize the potency of this inhibition, ThT was used to examine the kinetics of amyloid formation in the presence of substoichiometric concentrations of DLPC (Fig. 4.1 e and f). As DLPC concentration increased from 0 to 500 nM the lag phase of aggregation shortened, suggesting accelerated Aβ fibrillation. Increasing the concentration beyond 700 nM lengthened the lag phase. Aggregation was halted by DLPC concentrations above 1 μM. Similar kinetic profiles were observed in the presence of DLPC LUVs of different diameters, suggesting that the effect of DLPC on Aβ aggregation is independent of bilayer curvature (Fig. C.2), unlike the effect of other model membranes.[31] The profile by which DLPC initially accelerates and subsequently inhibits amyloid formation based on concentration is similar to the effect of detergents on amyloid formation.[37] This suggests that free DLPC, existing in equilibrium with DLPC encapsulated in LUVs, may play a role in modulating Aβ aggregation through a detergent-like mechanism. DLPC is able to act as a detergent with a very low critical micelle concentration (~100 nM).[38] However, free DLPC only inhibited Aβ aggregation at much higher concentrations than DLPC in LUVs (15 μM; Fig. C.3 a and b). These results suggest that DLPC micelles are insufficient to explain the observed modulation of Aβ aggregation.

4.2.2. Aβ Binding to DLPC Liposomes Induces Membrane Disruption and Unstructured Oligomers

To clarify the extent to which detergent-like activity of free DLPC is capable of modulating Aβ aggregation, it is essential to identify the source of free lipid. While there is an equilibrium between bilayer-inserted and free DLPC, this equilibrium is not capable of generating high concentrations of free DLPC in the absence of peptide.[39,40] It has been shown, however, that interactions between amyloidogenic peptides and lipid bilayers can extract lipids and generate micelle-like particles.[8,41,42] These species could exist as a result of Aβ-DLPC interactions and subsequently play a role in the observed modulation of Aβ aggregation.
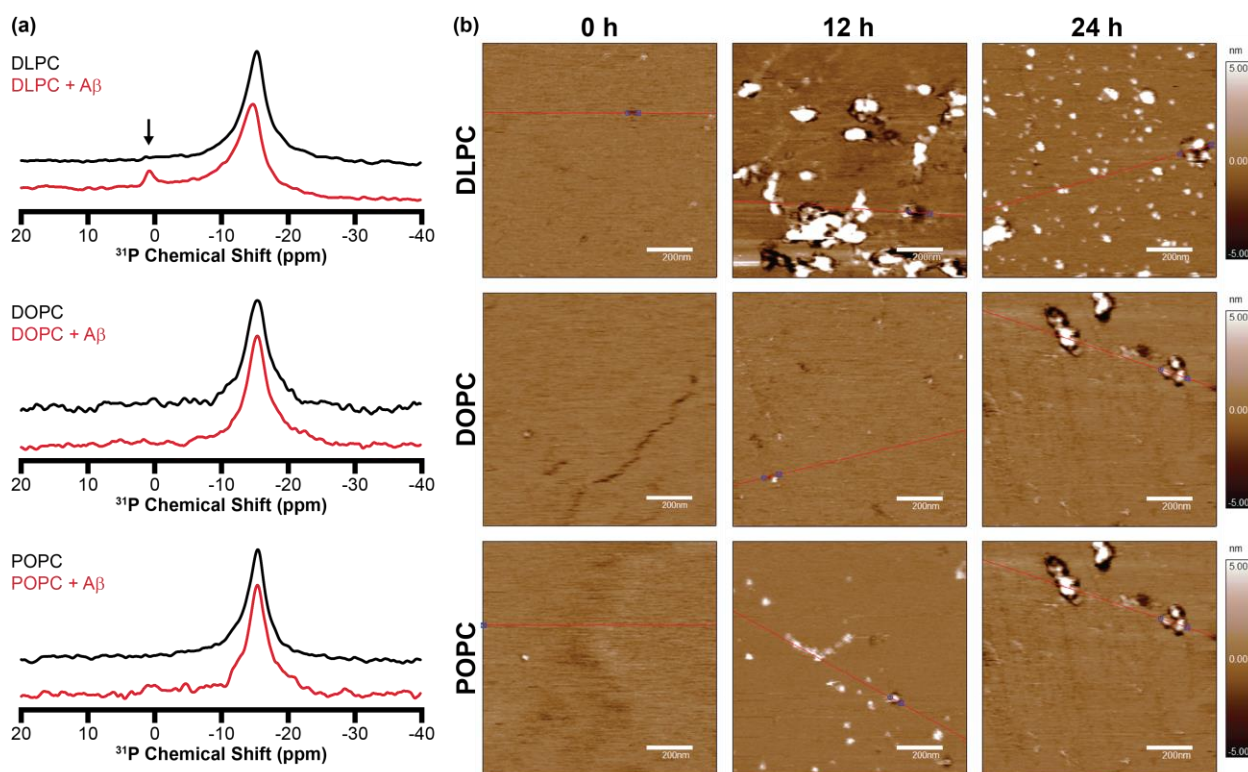
Figure 4.2. Membrane perturbations by Aβ. (a) ^{31}P solid-state NMR of 1000 nm LUVs (23 mM lipid) in the absence (black) and presence (red) of Aβ (230 μM). The anisotropic peak around -15 ppm represents the intact liposomes while the small peak near 0 ppm in the DLPC+Aβ spectrum (noted by an arrow) indicates the formation of small, rapidly tumbling lipid species suggestive of membrane fragmentation. (b) AFM was performed on SLBs of DLPC, DOPC, or POPC incubated in the presence of Aβ as a function of time in order to observe both the deposition of Aβ aggregates on the membrane and defects induced in the bilayer surface as a result of aggregation.

Differences between micelle-like lipid species and LUVs can be detected using ^{31}P solid-state NMR.[8,42,43] Due to their large size, intact vesicles of DLPC, DOPC, and POPC exhibit a powder pattern spectrum which spans from ~ -14 to ~ 25 ppm. Only the perpendicular edge (~ -14 ppm) of the spectrum is highly sensitive (Fig. 4.2a). Following incubation with Aβ under aggregating conditions for 24 h a new peak centered near 0 ppm was observed for LUVs composed of DLPC. This isotropic peak at 0 ppm suggests a new, small, lipid structure induced by Aβ (Fig. 4.2a). This provides a source for free DLPC; the interaction of Aβ with the surface of DLPC liposomes is capable of removing lipids from the bilayer, despite the lack of fibrillation. This is unique both in the lack of fiber formation which has previously been suspected as the causative agent in amyloid-based membrane disruption and in the absence of GM1 ganglioside in the bilayer, a lipid which is believed to be needed for the disruption of neuronal bilayers.[5,8,41,42]

While the disruption of DLPC LUVs by nonfibrillar Aβ species is novel, it is unlikely that the free DLPC generated is the sole cause of amyloid (Fig. C.3 a and b). A second mechanism of inhibition is necessary to explain the observed inhibition by DLPC LUVs. We initially hypothesized that changes in bilayer hydrophobic thickness may stabilize on and/or off pathway oligomers. To study intermediates formed on the surface of DLPC bilayers, we used atomic force microscopy (AFM) which is well suited for the interrogation and observation of bilayer-based aggregation of Aβ.[7,44-47] After incubating monomeric Aβ with supported lipid bilayers (SLBs) of DOPC or POPC, early globular and prefibrillar oligomers were observed by AFM after 24 h in a liquid cell (Fig. 4.2b). While ThT data suggested that mature fibrils exist by this point in aggregation, AFM was performed under quiescent conditions which delays fibrillation.[48] When DLPC SLBs were treated with Aβ, a large number of globular aggregates

were present on the bilayer after 12 h. Aggregates persisted after 24 h of incubation, though the size of individual particles shrank. Defects in the membrane were also evident around the aggregates after both 12 and 24 h, suggesting that these aggregates perturb the bilayer integrity, in agreement with the ^{31}P NMR results.

To quantify the membrane modification caused by Aβ, the root mean square roughness (R_q) and average roughness (R_a) of the samples with respect to time were calculated based on the AFM data (Table 1). While all three bilayers initially formed with a similar smoothness and without defects, DLPC bilayers demonstrated a large increase in their roughness after 12 and 24 h of incubation with Aβ relative to both the initial bilayer smoothness and the observed smoothness for DOPC and or POPC SLBs. The increase in both R_q and R_a is caused by both the formation of aggregates as well as bilayer disruption. While R_q and R_a of DLPC bilayers decrease between 12 and 24 h of incubation, this is likely caused by aggregates equilibrating, becoming smaller and more evenly dispersed across the bilayer surface. To better understand the

Sample	$R_q \pm$ S.D. (nm)	$R_a \pm$ S.D. (nm)
DLPC	0.36 ± 0.02	0.27 ± 0.01
+ Aβ (12 h)	3 ± 1	1.7 ± 0.8
+ Aβ (24 h)	1.5 ± 0.7	0.7 ± 0.2
DOPC	0.39 ± 0.04	0.29 ± 0.02
+ Aβ (12 h)	0.40 ± 0.03	0.29 ± 0.01
+ Aβ (24 h)	0.8 ± 0.1	0.51 ± 0.07
POPC	0.49 ± 0.03	0.39 ± 0.03
+ Aβ (12 h)	0.5 ± 0.1	0.27 ± 0.06
+ Aβ (24 h)	0.8 ± 0.5	0.4 ± 0.2

Table 4.1. Quantifying membrane perturbation. The root mean square roughness (R_q) and the average roughness (R_a) of SLBs incubated with Aβ at different time points are calculated from the AFM images.

kinetics of the observed aggregate formation on the bilayer surface, AFM images were taken at early time points following Aβ addition to DLPC SLBs (Fig. C.4). After just 5 minutes of incubation, holes were observed in the bilayer, indicative of dramatic disruption resulting from aggregation. Small, globular aggregates were also present. At later time points (15 and 20 min)the aggregates grew in size while the membrane defects shrank slightly due to lipid diffusion within the membrane.

The AFM results point to a unique characteristic of DLPC bilayers. DLPC SLBs facilitate the rapid formation of globular aggregates on the bilayer surface of, and possibly within, the membrane. In contrast, most reports of membrane-mediated Aβ aggregation using AFM demonstrate the formation of conventional fibrils.[45,49,50] This membrane-associated aggregation is likely responsible for the bilayer disruption, despite not occurring through the canonical amyloid formation pathway. Amorphous aggregation occurring selectively on DLPC SLBs suggests that it is at least partly the result of DLPC's uniquely small hydrophobic thickness. These globular species are stabilized by the short hydrophobic distance, which prevents their progression toward mature fibrils. There are, therefore, two mechanisms by which DLPC LUVs appear to inhibit the formation of Aβ fibers. Aβ-DLPC interactions generate micelle-like lipid species that can prevent aggregation; driving inhibition is the stabilization of globular, membrane-associated aggregates that are incapable of progressing toward fibrils.

4.2.3. DLPC remodels mature Aβ fibrils

While results to this point have illustrated how monomeric Aβ may interact with and aggregate on bilayers of varying thickness, it is equally important to investigate how preformed aggregates may interact with these bilayers. The addition of DLPC LUVs to premade fibrils

114

caused a rapid reduction in ThT fluorescence in a dose-dependent manner (Fig. 4.3a). Similar fluorescence reduction has previously been observed in small molecule-induced disaggregation of various amyloid fibrils, suggesting that DLPC LUVs may alter the structure of the traditionally stable fiber.[51-53] While ThT displacement is a possibility, the stabilization of the final fluorescence at ~40% of the original value, instead of returning to the baseline, suggests that ThT binding is maintained to some extent and that the changes are primarily structural.[35] Neither DOPC nor POPC LUVs caused a significant change in ThT fluorescence, suggesting that any structural changes to the fiber are specific to DLPC (Fig. 4.3b). The addition of free DLPC
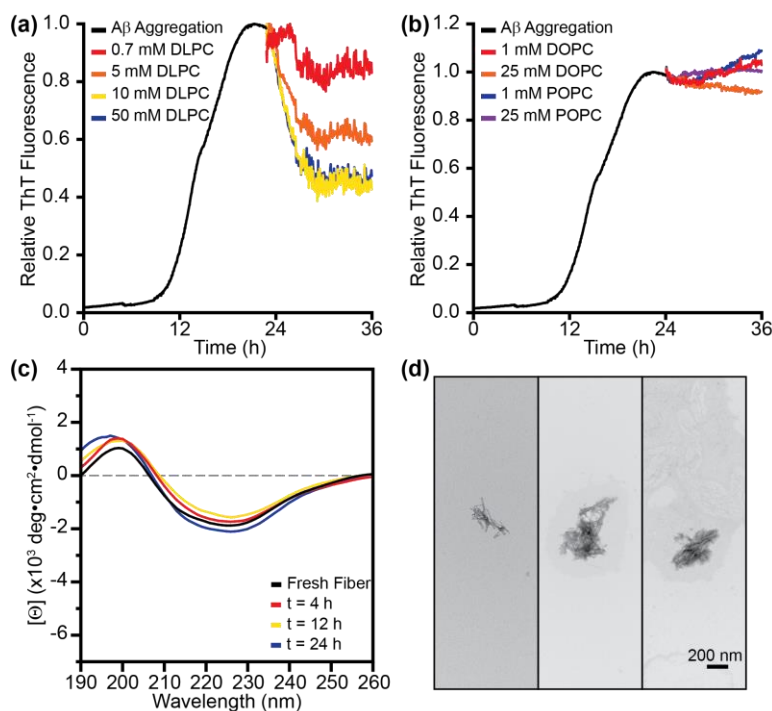
Figure 4.3. DLPC liposomes remodel preformed Aβ fibrils. (a) When 100 nm LUVs of DLPC were added to preformed Aβ fibrils (10 μM monomer concentration; preaggregated for 24 h), ThT (20 μM) fluorescence was decreased in a dose dependent manner. (b) The addition of 100 nm LUVs of DOPC or POPC at much higher concentrations did not impact ThT fluorescence. (c) The CD spectrum of fibrillar Aβ (30 μM) was monitored following the addition of 100 nm LUVs of DLPC (300 μM). (d) TEM images of the aggregates induced by incubating preformed Aβ fibrils (30 μM monomer concentration) with 100 nm DLPC LUVs (300 μM lipid).

to preformed aggregates also minimally altered the ThT fluorescence of the aggregates, suggesting that the mechanism of remodeling is not through detergent-like effects (Fig. C.3c)

Assuming that the DLPC-induced fluorescence reduction is a function of structural changes, CD was used to examine the extent of these changes. Surprisingly, the β-strand signal at 220 nm persists over the course of 24 h despite the observed reduction in ThT fluorescence stabilizing after 4 h (Fig. 4.3c). While seemingly contradictory, it has been previously demonstrated that amyloids can possess β-strand content and be unable to bind ThT.[36] Moreover, the TEM images of the preformed fibers treated with DLPC displayed a morphology distinct from mature fibers formed in solution (Figs. 3D and S1). The remodeled fibrils maintain some fiber-like characteristics, though they are much shorter and thinner than mature fibrils. These results confirm that DLPC LUVs are capable of remodeling mature Aβ aggregates, though not to the extent of some traditional studies of disaggregation.[51-53]

There are, then, three likely mechanisms by which DLPC LUVs may remodel preformed Aβ fibrils. (i) DLPC changes the monomer-fiber equilibrium and causes additional monomers of Aβ to enter solution via dissociation from the ends of fibers, resulting in shorter aggregates.[54] (ii) DLPC LUVs alter the hydrogen bonding network found within the fibril, generating distinct polymorphs of the aggregates which are less stable and can potentially become more similar to the immature protofibril structure.[54] (iii) DLPC LUVs rearrange the side chain packing of the mature fibrils and induce a partially unfolded state without significantly altering the hydrogen bonding of the fiber core.[28]

We first explored the monomer-fiber equilibrium with ^{1}H NMR. While monomeric Aβ is highly dynamic and yields strong signals in solution NMR, the fibrillar aggregates, due to their

large size and anisotropic tumbling, are essentially invisible (Fig. C.5a). This allows for the selective observation of monomeric and small, soluble intermediates over large species. It is also possible to correlate changes in signal intensity with the equilibrium between monomeric and aggregated Aβ.[54] DLPC LUVs were added to fibrillar Aβ and spectra were continually recorded for 23 h (Fig. C.5). While previous disaggregation studies using similar methods observed an increase in relative signal intensity over time during disaggregation, DLPC induced a minimal change in signal.[54] This suggests that the monomer-fiber equilibrium is minimally perturbed and thus insufficient to explain the remodeling of preformed fibrils. This observation does not, however, rule out a change in other possible exchange equilibria which are invisible to solution NMR. It is known that fiber fragmentation rates can depend upon changes in solution conditions and are capable of producing small, protofibirl-like oligomers.{Knowles, 2009} These new, small aggregates would remain too large for solution NMR and thus cannot be ruled out as a possible mechanism. Additionally, if the dissociation event involves larger oligomers that exist between the monomer and protofibril, these too would be invisible to solution NMR and remain an alternative mechanism.

We next explored the possibility of DLPC altering the β-strand topology of the fiber backbone and the stability which it imparts. It has been shown through extensive solid-state NMR studies that Aβ fibers can adopt distinct backbone folds and polymorphs while maintaining the requisite β-strand prominence and fiber core based on aggregation conditions.[55-58] It is possible that DLPC LUVs could exert a chaperone-like activity to convert one fiber polymorph into another. We explored the differences between the structures using thermal unfolding experiments. If fibers treated with DLPC LUVs result in altered β-strand folding and hydrogen bond networks their unfolding temperatures and enthalpy of unfolding will likely be different.[59-

[61] To this end, we studied the stability of Aβ fibers formed for 24 and 40 h, as well as fibers formed for 24 h and subsequently treated with either 5 or 20 equivalents of DLPC LUVs (Fig.
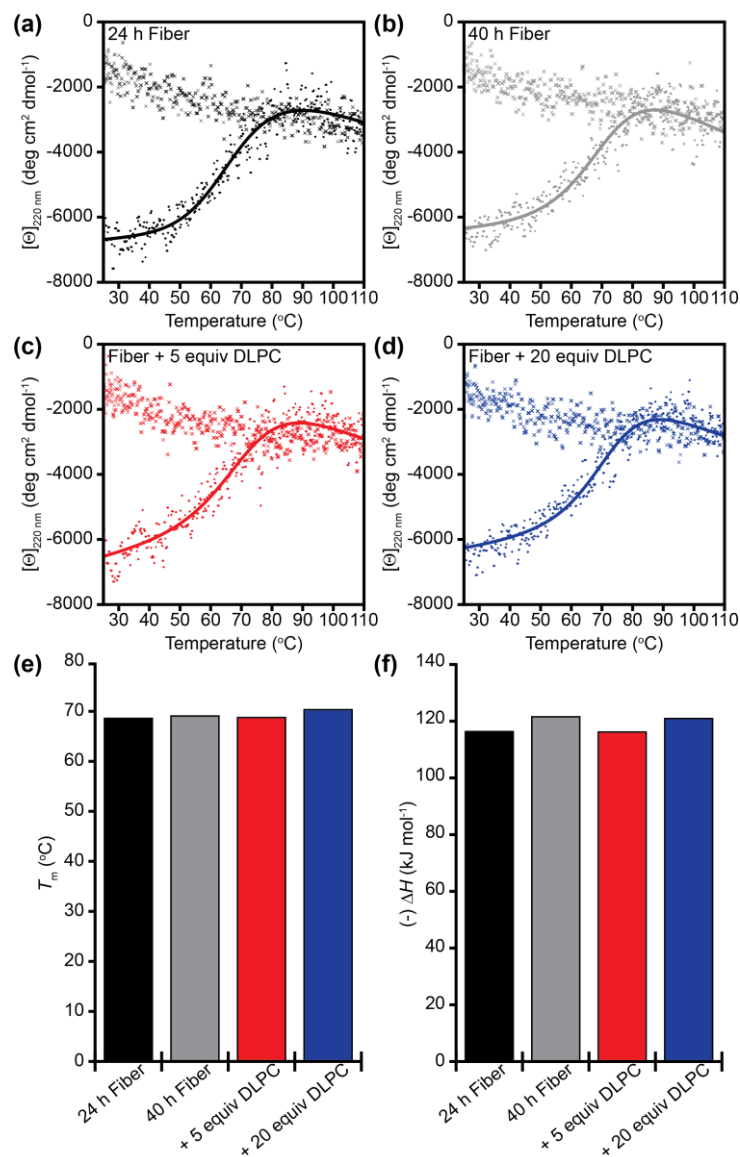
Figure 4.4. Thermodynamic stability of Aβ fibrils. Aβ fibrils (20 µM monomer concentration) formed after 24 h (a) and 40 h (b) were subjected to thermal denaturation and the β-strand signal at 220 nm was observed as function of time. Similar denaturation experiments were performed on Aβ fibrils formed by 24 h incubation and then treated with 5 equiv (c) or 20 equiv (d) of 100 nm DLPC LUVs. After the fiber was unfolded by heating, the sample was cooled from 110 °C down to 25 °C and the structural signal was again observed for all four samples (marked by an x). These denaturation curves were fit to extrapolate both the melting temperature (T_m) (e) and the enthalpy of denaturation (ΔH) (f) of the fibril under different conditions.

118

4.4). Samples were exposed to continuous shaking at 25 °C for the entirety of their aggregation and/or remodeling. All four samples exhibited similar melting temperatures (~ 68 °C) and enthalpies of denaturation (115-120 kJ mol^{-1}). This thermal unfolding was also found to be irreversible, in agreement with other studies.[59] The melting temperature is slightly lower than has previously been published for Aβ_{40}, likely due to different aggregation conditions, highlighting this method's ability to distinguish distinct fiber polymorphs.[59] The similarities in thermal denaturation suggest that, despite morphological differences based on TEM, the intermolecular forces responsible for aggregate stability are similar for all samples, and thus there is a low likelihood of distinct polymorphs being induced by the presence of DLPC.

It appears, then, that the DLPC-induced changes in ThT fluorescence and morphological differences observed by TEM are the result of more surface level disruptions. It has previously been shown that Aβ fibrils can adopt a pseudo transition state, termed the molten globule state, in which side chain packing at the fiber surface becomes perturbed.[28] The molten globule state was defined by a reduction in ThT fluorescence and truncation of the fibrillar structure while the β-strand signal was maintained in CD spectroscopy, similar to what we have observed in the presence of DLPC (28). This molten globule state has previously been observed only following treatment of mature aggregates with ultrasonication. Treatment of fibrils with conventional chemical denaturants such as detergents or guanidine hydrochloride has previously resulted in the generation of the unfolded, monomeric form of Aβ.[28] It is likely that DLPC is sufficiently mild in its perturbations so as not to fully denature and instead stabilize this unfolding transition state. While we observed that DLPC inhibits Aβ aggregation through a combination of detergent-like interactions and stabilization of membrane associated globulomers, it is likely that the fibrils are primarily altered through interactions with the surface of DLPC LUVs which

promote disorder in the traditionally ordered side chain packing of the fibril.[28,62] This increased disorder can facilitate a reduction in ThT binding and fluorescence. It may also increase the likelihood of Aβ fibrils to fragment in order to compensate for the increased sidechain flexibility, explaining the truncated fibril structures observed by TEM.[63,64] These two modes of disruption would be relatively independent of the main chain interactions and result in the maintenance of the conventional β-strand structure, resulting in an aggregate species which resembles a protofibrillar structure.[65,66]

4.2.4. Effect of lipid-Aβ aggregates on cell viability

Having shown that DLPC LUVs are capable of generating two distinct, non-fibrillar Aβ aggregates when the lipids are present, the biological function of these two different species becomes of interest. It has been proposed that oligomers act as the toxic agent in amyloid-related diseases, and different oligomers can enact various toxic functions.[2,3] Stabilizing and characterizing the formation of many of these oligomers has been difficult, however. We therefore examined the toxic effects of stable species induced by pre-incubating monomeric Aβ with DLPC LUVs as well as those species generated by treatment of mature fibrils with DLPC LUVs (Fig. 4.5 a and b). Aβ aggregates formed in the absence of DLPC were observed to reduce cellular viability by ~50%. Aggregates formed in the presence of DLPC, however, were found to be nontoxic (Fig. 4.5a). This further suggests that these Aβ oligomers formed in the presence of DLPC LUVs are off-pathway aggregates. Aβ fibrils remodeled by DLPC were found to induce cellular death to a similar extent as the untreated Aβ aggregate, suggesting that these molten globule aggregates resemble an on-pathway protofibrillar species, which has been suggested to be toxic.[66]

4.3. Discussion

While DLPC is not a lipid commonly found in eukaryotic membranes, it serves as a simplified model for membrane thinning associated with AD.[13,14,16,17] Our findings suggest that these thin bilayers serve to inhibit the formation of Aβ amyloid fibers instead by stabilizing disordered aggregates on the bilayer surface (Fig. 4.5c). This interaction, in turn, induces membrane disruption that causes lipids to shed from the bilayer and form micelle-like species above the CMC of DLPC. DLPC membranes are capable of reorganizing the surface and side
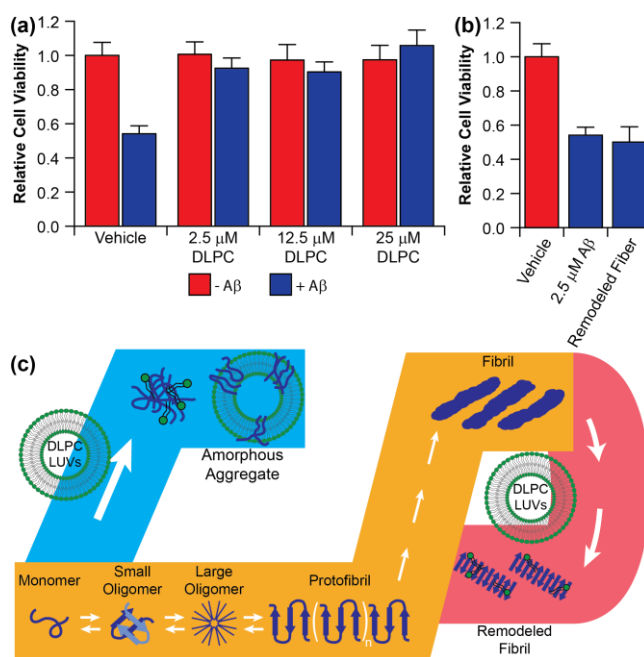
Figure 4.5. Function and identity of DLPC-induced Aβ aggregates. (a) Aβ (2.5 μM) aggregates were generated in the presence and absence of 100 nm DLPC LUVs and their toxicity against PC12 cells was compared by the MTT assay. (b) The toxicity of preformed Aβ aggregates subsequently incubated with 10 equiv (25 μM) DLPC. (c) The combined data from this study suggest that DLPC has two distinct modes of action against Aβ aggregation (orange pathway). When DLPC LUVs are added at the early stages of aggregation they promote the formation of unstructured, off pathway Aβ aggregates (blue pathway). When mature Aβ fibrils are treated with DLPC LUVs, the lipid induces a polymorphic change within the fibril without significantly altering the cross β-strand structure of the fibril, resulting in a more protofibrillar structure in the final aggregates (red pathway).

chain orientation of mature fibrils. Interestingly, a lipid bilayer composed of dilauroyl phosphatidylserine (DLPS), which shares the acyl chain length and hydrophobic thickness of DLPC, has been shown to promote the aggregation of α-synuclein, an amyloid implicated in Parkinson's disease.[67] This finding suggests that the inhibition of Aβ aggregation by DLPC may be dependent on peptide, lipid head group, or possibly both. It is essential that the functions of thin bilayers of more varied complexity are explored to clarify their functions within a biological context. Additionally, it will be valuable to further explore the universality of DLPC mediated inhibition of amyloid formation. If DLPC serves as a universal amyloid inhibitor, it may become a powerful tool in the examination of amyloid structure and function for its ability to remodel aggregates without dissociation by high concentrations of harsh chemicals or detergents (Fig. 4.5c).

4.4. Methods

4.4.1. Materials

All reagents were purchased from commercial suppliers and used as received unless noted otherwise. Aβ was purchased from BioBasic (Markham, ON, Canada) ($A\beta_{1-40}$= DAEFRHDSGYEVHHQKLVFFAEDVGSNKGAIIGLMVGGVV) at >95% purity and used without further purification. All lipids were purchased from Avanti Polar Lipids *Inc.* (Alabaster, AL, U.S.A.). All other reagents were purchased from Sigma-Aldrich (St. Louis, MO, U.S.A). Detailed experimental descriptions are included in SI Text.

4.4.2. Vesicle preparation

Large unilamellar vesicles (LUVs) of DLPC, DOPC, and POPC were prepared from stock chloroform solutions. The resulting solution was dried under a nitrogen stream and placed under vacuum overnight to remove residual solvent. The resultant lipid film was rehydrated in buffer (20 mM PO_4, pH 7.4, 50 mM NaCl) to yield a final lipid concentration of either 1 mM, 10 mM, or 24 mM (for solid-state NMR experiments). Dried lipid was resuspended by vortexing the solution and was subsequently extruded *via* 23 passes through a polycarbonate Nucleopore membrane filter (either 50, 100, 400 or 1000 nm, depending on experiment; Whatman) mounted to a mini-extruder (Avanti Polar Lipids *Inc.*) to obtain a homogeneous solution of LUVs. The formation of vesicles was subsequently confirmed by dynamic light scattering to ensure homogeneity.

4.4.3. Peptide preparation

Aβ was received having been treated with hexafluoroisopropanol intended to monomerize the peptide. To disrupt any remaining aggregates, Aβ was dissolved in 5% v/v NH_4OH at a concentration of 0.5 mg/mL. The peptide was aliquoted into 0.1 mg samples and lyopohilized overnight and stored at -20 C until they were needed for an experiment. To prepare monomeric Aβ for experimentation, peptide was dissolved in buffer (20 mM PO_4, pH 7.4, 50 mM NaCl) to a final concentration of 120 μM. The stock solution as sonicated for 10 s and then used immediately after preparation.

4.4.4. Thioflavin-T (ThT) assay

The kinetics of amyloid formation were monitored by the fluorescent, amyloid-specific dye ThT. Samples were prepared by diluting the 120 μM Aβ stock to a final concentration of 10 μM in the presence of 20 μM ThT. To this was also added lipid from the prepared stock at a

concentration ranging from 100 nM to 1 mM. Samples were plated in triplicate on Corning 96-well plates, maintained at 25 C, and subject to continuous, slow orbital shaking. Fluorescence readings were taken on a Biotek Synergy 2 microplate reader using Corning 96 well plates. Wells were read from the bottom with an excitation wavelength of 440 nm (30 nm bandwidth) and an emission wavelength of 485 nm (20 nm bandwidth) at three minute intervals.

After data acquisition, raw fluorescence values were background subtracted and then normalized. Normalized curves were then individually fit to Eq. 1 and Eq. 2 in order to calculate the individual lag phase (t_{lag}) for each curve.[48] These values were then averaged across three separate trials.

$$F(t) = F_{inf} + \frac{F_0 - F_{inf}}{(1 + e^{k(t - t_{50})})}$$

(1)

$$t_{lag} = t_{50} - \frac{2}{k}$$

(2)

For studies exploring fibril remodeling, fibrils were initially formed in the 96-well plate for 24 h. After mature fibrils were formed, lipid (either in LUVs or as free lipid) was added directly to wells at varying concentrations, diluting the volume by less than 1% to maintain signal intensity. The experiment was then restarted under identical conditions to those used to monitor fibril formation.

4.4.5. Circular dichroism (CD)

Single point CD measurements were carried out at a concentration of 30 μM Aβ in the absence or presence of 300 μM (10 equiv) 100 nm LUVs of either DLPC, DOPC, or POPC in buffer (20 mM PO$_4$, pH 7.4, 50 mM NaF). CD measurements were performed on a JASCO J-1500 CD Spectrometer using a 0.1 cm path length cell. Spectra were acquired at 25 °C using a bandwidth of 2nm, a scan rate of 200 nm/min, and averaging spectra over 20 scans. Measurements were taken immediately after mixing the sample (t = 0 h) and after 24 h incubation at 25 °C under slow orbital shaking (conditions mimicking those used in ThT kinetic assays).

For time course analysis of fibril remodeling, fibrils were initially formed at 30 μM in buffer by incubating for 24 h at 25 °C under slow orbital shaking. After formation of the mature fibrils, LUVs were added to the solution and the CD spectrum was monitored over time. In between reads, the sample was maintained at 25 °C under slow orbital shaking.

4.4.6. Transmission electron microscopy (TEM)

Samples used in TEM analysis were taken directly from the time course CD experiments after 24 h incubation (both for the modulation of fiber formation and the remodeling of preformed fibrils). Glow discharged grids (Formar/carbon 300 mesh, Electron Microscopy Sciences, Hatfield, PA, U.S.A.) were treated with samples (5 μL) for 2 min at room temperature. Excess buffer was removed *via* blotting and then washed three times with ddH$_2$O. Each grid was then incubated with uranyl acetate staining solution (1% w/v in ddH$_2$O, 5 μL) for 1 min, and excess stain was blotted away. Images from each sample were taken on a JEOL 1400-plus TEM (80 kV) at 50,000x magnification.

4.4.7. Atomic force microscopy (AFM)

Supported lipid bilayers (SLBs) of POPC, DOPC and DLPC were deposited on fleshly cleaved mica by immersion of the substrates in vials containing the lipid vesicle dispersions in phosphate buffer saline solution (PBS, 10 mM, pH=7.4 at 25°C), kept in a sonication bath for 1 h. AFM images were acquired with a Cypher S (Asylum Research, Oxford Instruments) microscope in liquid AC mode using rectangular-shaped Si_3N_4 cantilever tips (BL-RC-150VB, Olympus, Tokyo, Japan) with a nominal spring constant of 0.03 N/m.

4.4.8. ^{31}P solid-state NMR

Experiments were performed on a Varian 600 MHz solid-state NMR spectrometer. A Varian temperature control unit was used to maintain the sample temperature at 30 °C. All ^{31}P spectra were collected using a single pulse under 42 kHz two-pulse phase modulation decoupling of protons. A typical 90 pulse length of 6.0 μs was used with a recycle delay of 3 s. The ^{31}P chemical shift spectra are referenced with respect to 85% H_3PO_4 at 0 ppm. In each experiment, the ^{31}P spectrum of 200 μL of 1000 nm LUVs composed of 23 mM DLPC, DOPC, or POPC was first acquired in the absence of peptide in buffer (20 mM Hepes, pH 7.4, 50 mM NaCl). After acquisition of the control spectrum, Aβ was added to the lipid solution at a concentration of 230 μM (100:1 lipid-peptide ratio) and the sample was incubated at 25 °C under slow orbital shaking for 24 h to induce aggregation. Following aggregation, a ^{31}P spectrum was again acquired for each sample. Each spectrum is the result of 20,000 scans.

4.4.9. ^{1}H NMR

Experiments were performed on a Bruker 600 MHz NMR spectrometer equipped with a cryoprobe. A 1D ^{1}H spectrum of monomeric Aβ (50 mM) was initially acquired in buffer (20 mM PO_4, pH 7.4, 50 mM NaCl, 10% v/v D_2O). Peptide aggregation was then induced by

constant orbital shaking at 25 °C for 24 h. A spectrum was again taken of this aggregated sample. 100 nm DLPC LUVs were then added to the preformed aggregate sample (500 μM lipid) and acquisitions were taken continually for 23 h. Each spectrum was acquired at 25 °C and is the combination of 128 total scans. All spectra are normalized with respect to the initial monomer acquisition.

4.4.10. Thermal denaturation

Four types of amyloid fibrils of 20 μM Aβ in 20 mM sodium phosphate buffer (pH 7.4) containing 50 mM NaCl prepared with constant shaking (50-sec shaking – 10-sec quiescence) at 37 °C, were used for CD measurements. Aβ amyloid fibrils, which grew spontaneously from Aβ monomer solutions for 24 h without DLPC LUVs, were immediately used for CD measurements after confirming the stationary phase of fibrillation after the lag and exponential phase based on ThT fluorescence-based kinetics. The other three types of Aβ amyloid fibrils were obtained after a further 16 h incubation in the absence and presence of DLPC LUVs (100 μM and 400 μM DLPC) at 37 °C with the same shaking cycle above.

Heat scanning of all types of Aβ amyloid fibrils from 25 to 110 °C was performed by monitoring CD signals at 220 nm at a rate of 10 °C per minute. CD measurements were performed with a J-820 spectropolarimeter (Jasco, Japan) equipped with a water-circulating cell holder for temperature control. Temperature was regulated using a PTC-423L Peltier-unit (Jasco, Japan). A cell with a light path of 1 mm was sealed with a lid to prevent solvent evaporation during the heat treatment. CD signals were expressed as the mean residue ellipticity [θ] (deg cm^2 dmol^{-1}).

The melting temperature (T_m) and the enthalpy change (ΔH) of heat denaturation of Aβ amyloid fibrils were determined by a regression analysis using a nonlinear least squares fitting of data to the sigmoidal equation (3) under the assumption of a two-state transition between unfolded monomers and amyloid fibrils. It should be noted that we performed thermodynamic analyses although thermal denaturation of Aβ amyloid fibrils was irreversible.

$$\theta = \frac{(a - c) + (b - d)T}{1 + \exp\left(-\frac{\Delta H(T_m)}{R}\left(\frac{1}{T} - \frac{1}{T_m}\right) + \frac{\Delta C_p}{R}\left(\frac{T_m}{T} - 1 + \ln\frac{T}{T_m}\right)\right)} + (c + dT)$$

(3)

where θ is the signal intensity monitored by CD. The pre- and post-unfolding baselines are described by $a + bT$ and $c + dT$. T and R indicate temperature and gas constant, respectively. The change in heat capacity is shown by ΔC_p. Details of the derivation of the equation above are provided below. In our derivation, we assumed the two-state thermal denaturation model since the irreversible process in the Lumry-Eyring model can be neglected due to the high scan rate of 10 °C per minute used.[68,69]

4.4.11. Derivation of the fit equation for thermal denaturation

A model of the two-state thermal denaturation of Aβ amyloid fibrils is defined as:

$$F \leftrightarrow U$$

(4)

where F and U indicate the fibrillar and unfolded (i.e. denatured) states of Aβ, respectively.

128

The equilibrium constant of the unfolding reaction (K_U) is given by the ratio of the fraction of each conformational state:

$$K_U = \frac{f_U}{f_F}$$

(5)

where f_F and f_U represent the fraction of Aβ in the fibrillar and unfolded conformations, respectively.

The fraction is expressed as follows:

$$f_F + f_U = 1$$

(6)

Combining equations 4 and 5 gives:

$$f_F = \frac{1}{1 + K_U}$$

(7)

$$f_U = \frac{K_U}{1 + K_U}$$

(8)

The observed CD intensity (θ) of Aβ at a given temperature is expressed as:

$$\theta = f_F(T)\theta_F + f_U(T)\theta_U$$

where $f_F(T)$ and $f_U(T)$ are the fibrillar and unfolded fractions of Aβ at a given temperature (T), respectively. θ_F and θ_U indicate the CD signals of fibrillar and unfolded of Aβ, respectively.

Using equations 7 and 8, equation 9 becomes:

$$\theta = \frac{1}{1 + K_U}\theta_F + \frac{K_U}{1 + K_U}\theta_U$$

(10)

Rearranging equation 7 gives:

$$\theta = \frac{\theta_F - \theta_U}{1 + K_U} + \theta_U$$

(11)

θ_F and θ_U are CD signals of fibrillar and unfolded Aβ, respectively, over a certain temperature range and are expressed as follows:

$$\theta_F = a + bT$$

(12)

$$\theta_U = c + dT$$

(13)

where $a + bT$ and $c + dT$ are the baselines of pre- and post-unfolding. a and c are intercepts and b and d are slopes.

Substituting equations 12 and 13 into equation 11 gives the following equation:

$$\theta = \frac{(a + bT) - (c + dT)}{1 + K_U} + (c + dT)$$

<div align="right">(14)</div>

This is rearranged to the following equation:

$$\theta = \frac{(a - c) + (b - d)T}{1 + K_U} + (c + dT)$$

<div align="right">(15)</div>

The change in enthalpy, $\Delta H(T)$, and entropy, $\Delta S(T)$, for the thermal denaturation of Aβ amyloid fibrils at a certain temperature is expressed as follows:

$$\Delta H(T) = \Delta H(T_m) + \int_{T_m}^{T} \Delta C_p \, dT$$

<div align="right">(16)</div>

$$\Delta S(T) = \frac{\Delta H(T_m)}{T_m} + \int_{T_m}^{T} \Delta C_p \ln T \, dT$$

<div align="right">(17)</div>

where T_m is the midpoint temperature of the thermal denaturation of Aβ amyloid fibrils and ΔC_p is the heat capacity change between fibrillar and unfolded Aβ.

Equations 16 and 17 are solved as follows:

$$\Delta H(T) = \Delta H(T_m) + \Delta C_p(T - T_m)$$

$$\Delta S(T) \;=\; \frac{\Delta H(T_{\mathrm{m}})}{T_{\mathrm{m}}} \;+\; \Delta C_{\mathrm{p}}\ln\frac{T}{T_{\mathrm{m}}}$$

The temperature dependence of the change in Gibbs free energy, $\Delta G(T)$, at a certain temperature is defined by the following equations:

$$\Delta G(T) \;=\; -RT\ln K_{\mathrm{U}}$$

$$\Delta G(T) \;=\; \Delta H(T) \;-\; T\Delta S(T)$$

where R is the gas constant.

Equation 20 may be rearranged for K_{U}:

$$K_{\mathrm{U}} = \exp\left(-\frac{\Delta G(T)}{RT}\right)$$

where "exp" means an exponential function.

Substituting equation 22 into equation 15 gives:

$$\theta \;=\; \frac{(a-c)\;+\;(b-d)T}{1\;+\;\exp\left(-\dfrac{\Delta G(T)}{RT}\right)} \;+\; (c\;+\;dT)$$

Substituting equations 18 and 19 into equation 21 gives:

$$\Delta G(T) = (\Delta C_p (T - T_m)) - T\left(\frac{\Delta H(T_m)}{T_m} + \Delta C_p \ln\frac{T}{T_m}\right)$$

Equation 24 is rearranged to yield the following equation:

$$\Delta G(T) = \Delta H(T_m)\left(1 - \frac{T}{T_m}\right) - \Delta C_p\left(T_m - T + T\ln\frac{T}{T_m}\right)$$

Substituting equation 25 into equation 23 gives:

$$\theta = \frac{(a - c) + (b - d)T}{1 + \exp\left(-\dfrac{\Delta H(T_m)\left(1 - \frac{T}{T_m}\right) - \Delta C_p\left(T_m - T + T\ln\frac{T}{T_m}\right)}{RT}\right)} + (c + dT)$$

Equation 25 is rearranged to yield the final equation:

$$\theta = \frac{(a - c) + (b - d)T}{1 + \exp\left(-\frac{\Delta H(T_m)}{R}\left(\frac{1}{T} - \frac{1}{T_m}\right) + \frac{\Delta C_p}{R}\left(\frac{T_m}{T} - 1 + \ln\frac{T}{T_m}\right)\right)} + (c + dT)$$

4.4.12. Cellular culture and cytotoxicity analysis

PC12 cells were grown in RPMI-1640 media without L-glutamine supplemented with 5% fetal bovine serum, 10% horse serum, and 1% penicillin-streptomycin, in a humidified incubator at 37 °C with environment of 5% CO_2. Cells were kept between passage numbers 20-35. 10 cm cell culture dishes were used for culturing, and 96 flat bottom well trays for the MTT assays. Cells in a suspension of 90 μL (total of 10^4 cells) were dispensed in each well and allowed to adhere for 1 day before adding peptide aggregates.

Peptide aggregates were generated by incubating Aβ (25 μM) in the absence or presence of 100 nm DLPC LUVs (1-10 equiv) for 18 h at 25 °C in buffer (20 mM PO_4, pH 7.4, 50 mM NaCl). Aggregates were taken prior to complete fibrillation due to the purported toxicity of the intermediate aggregates.[3,70] 10 μL of aggregate solution was then added to the plated PC12 cells to a final volume of 100 μL (2.5 μM Aβ). After 24 h incubation of cells with aggregates, the MTT cell proliferation assay (Promega, G4000) was used to determine the toxicity of samples following the manufacturer protocol. 15 μL of the MTT dye solution was added to each well and set to incubate at 37 °C for 3-3.5 h. 100 μL of solubilization/stop buffer was added and set to incubate for 2-3 h. The absorbance of each well as then measured at both 570 nm and 700 nm (700 nm for background correction). All cellular viability values were normalized to cells treated with buffer. Values reported are the average of three independent trials and the error is reported as the standard deviation of these averages.

4.5. Acknowledgements

2014S1A2A2028270 (to M.H.L. and A.R.), and the University of Catania FIR 2014 (to C.L.).

4.6. Author Contributions

A.R. and M.H.L. directed the overall research. K.J.K. and A.B. performed all kinetic analyses and secondary structure analyses. K.J.K. and R.Z. performed all NMR experiments. C.S. and C.L. performed the AFM measurements. Y.L. and Y-H.L. performed the thermodynamic stability analysis. K.J.K., M.D., and M.I. performed the toxicity studies. K.J.K. and A.R. conceived the ideas for the project and wrote the paper. All authors reviewed the results and approved the manuscript.

4.7. References

1.   Savelieff, M. G., Lee, S., Liu, Y. & Lim, M. H. Untangling amyloid-beta, tau, and metals in Alzheimer's disease. *ACS Chem. Biol.* **8**, 856-865 (2013).

2.   Benilova, I., Karran, E. & De Strooper, B. The toxic Abeta oligomer and Alzheimer's disease: an emperor in need of clothes. *Nat. Neurosci.* **15**, 349-357 (2012).

3.   Hardy, J. & Selkoe, D. J. The amyloid hypothesis of Alzheimer's disease: progress and problems on the road to therapeutics. *Science* **297**, 353-356 (2002).

4.   Kotler, S. A., Walsh, P., Brender, J. R. & Ramamoorthy, A. Differences between amyloid-beta aggregation in solution and on the membrane: insights into elucidation of the mechanistic details of Alzheimer's disease. *Chem. Soc. Rev.* **43**, 6692-6700, (2014).

5.   Matsuzaki, K. How do membranes initiate Alzheimer's Disease? Formation of toxic amyloid fibrils by the amyloid beta-protein on ganglioside clusters. *Acc. Chem. Res.* **47**, 2397-2404 (2014).

6.   Jang, H. *et al.* beta-Barrel topology of Alzheimer's beta-amyloid ion channels. *J. Mol. Biol.* **404**, 917-934 (2010).

7.   Jang, H. *et al.* Disordered amyloidogenic peptides may insert into the membrane and assemble into common cyclic structural motifs. *Chem. Soc. Rev.* **43**, 6750-6764 (2014).

8.   Sciacca, M. F. *et al.* Two-step mechanism of membrane disruption by Abeta through membrane fragmentation and pore formation. *Biophys. J.* **103**, 702-710 (2012).

9.   Yip, C. M. & McLaurin, J. Amyloid-beta peptide assembly: a critical step in fibrillogenesis and membrane disruption. *Biophys. J.* **80**, 1359-1371 (2001).

10.   Fattal, D. R. & Ben-Shaul, A. A molecular model for lipid-protein interaction in membranes: the role of hydrophobic mismatch. *Biophys. J.* **65**, 1795-1809 (1993).

11.   Killian, J. A. Hydrophobic mismatch between proteins and lipids in membranes. *Biochim. Biophys. Acta.* **1376**, 401-415 (1998).

12.   Pratico, D. Oxidative stress hypothesis in Alzheimer's disease: a reappraisal. *Trends Pharmacol. Sci.* **29**, 609-615 (2008).

13.   Beranova, L., Cwiklik, L., Jurkiewicz, P., Hof, M. & Jungwirth, P. Oxidation changes physical properties of phospholipid bilayers: fluorescence spectroscopy and molecular simulations. *Langmuir* **26**, 6140-6144 (2010).

14.   Negre-Salvayre, A. *et al.* Pathological aspects of lipid peroxidation. *Free Radic. Res.* **44**, 1125-1171 (2010).

15.   Pannuzzo, M., Milardi, D., Raudino, A., Karttunen, M. & La Rosa, C. Analytical model and multiscale simulations of Abeta peptide aggregation in lipid membranes: towards a unifying description of conformational transitions, oligomerization and membrane damage. *Phys. Chem. Chem. Phys.* **15**, 8940-8951 (2013).

16.   Last, N. B. & Miranker, A. D. Common mechanism unites membrane poration by amyloid and antimicrobial peptides. *Proc. Natl. Acad. Sci. U.S.A.* **110**, 6382-6387 (2013).

17.   Lee, C. C., Sun, Y. & Huang, H. W. How type II diabetes-related islet amyloid polypeptide damages lipid bilayers. *Biophys. J.* **102**, 1059-1068 (2012).

18.   Kucerka, N. *et al.* Structure of fully hydrated fluid phase DMPC and DLPC lipid bilayers using X-ray scattering from oriented multilamellar arrays and from unilamellar vesicles. *Biophys. J.* **88**, 2626-2637 (2005).

19.   Kucerka, N., Tristram-Nagle, S. & Nagle, J. F. Structure of fully hydrated fluid phase lipid bilayers with monounsaturated chains. *J. Membr. Biol.* **208**, 193-202 (2005).

20.   Korshavn, K. J., Bhunia, A., Lim, M. H. & Ramamoorthy, A. Amyloid-beta adopts a conserved, partially folded structure upon binding to zwitterionic lipid bilayers prior to amyloid formation. *Chem. Commun.* **52**, 882-885 (2016).

21.   Arce, F. T. *et al.* Polymorphism of amyloid beta peptide in different environments: implications for membrane insertion and pore formation. *Soft Matter* **7**, 5267-5273 (2011).

22.   Kumar, S. & Miranker, A. D. A foldamer approach to targeting membrane bound helical states of islet amyloid polypeptide. *Chem. Commun.* **49**, 4749-4751 (2013).

23.   Jang, H. *et al.* Familial Alzheimer's disease Osaka mutant (DeltaE22) beta-barrels suggest an explanation for the different Abeta1-40/42 preferred conformational states observed by experiment. *J. Phys. Chem. B.* **117**, 11518-11529 (2013).

24. Sciacca, M. F. *et al.* The Role of Cholesterol in Driving IAPP-Membrane Interactions. *Biophys. J.* **111**, 140-151 (2016).

25. Stefanovic, A. N., Lindhoud, S., Semerdzhiev, S. A., Claessens, M. M. & Subramaniam, V. Oligomers of Parkinson's Disease-Related alpha-Synuclein Mutants Have Similar Structures but Distinctive Membrane Permeabilization Properties. *Biochemistry* **54**, 3142-3150 (2015).

26. Fleming, P. J., Freites, J. A., Moon, C. P., Tobias, D. J. & Fleming, K. G. Outer membrane phospholipase A in phospholipid bilayers: a model system for concerted computational and experimental investigations of amino acid side chain partitioning into lipid bilayers. *Biochim. Biophys. Acta.* **1818**, 126-134 (2012).

27. Rankenberg, J. M. *et al.* Proline kink angle distributions for GWALP23 in lipid bilayers of different thicknesses. *Biochemistry* **51**, 3554-3564 (2012).

28. Noda, S. *et al.* Thioflavin T-Silent Denaturation Intermediates Support the Main-Chain-Dominated Architecture of Amyloid Fibrils. *Biochemistry* **55**, 3937-3948 (2016).

29. Aisenbrey, C. *et al.* How is protein aggregation in amyloidogenic diseases modulated by biological membranes? *Eur. Biophys. J.* **37**, 247-255 (2008).

30. Gorbenko, G. P. & Kinnunen, P. K. The role of lipid-protein interactions in amyloid-type protein fibril formation. *Chem. Phys. Lipids* **141**, 72-82 (2006).

31. Terakawa, M. S., Yagi, H., Adachi, M., Lee, Y. H. & Goto, Y. Small liposomes accelerate the fibrillation of amyloid beta (1-40). *J. Biol. Chem.* **290**, 815-826 (2015).

32. Biancalana, M. & Koide, S. Molecular mechanism of Thioflavin-T binding to amyloid fibrils. *Biochim. Biophys. Acta.* **1804**, 1405-1412 (2010).

33. Arosio, P. *et al.* Kinetic analysis reveals the diversity of microscopic mechanisms through which molecular chaperones suppress amyloid formation. *Nat. Commun.* **7**, 10948 (2016).

34. Meisl, G. *et al.* Molecular mechanisms of protein aggregation from global fitting of kinetic models. *Nat. Protoc.* **11**, 252-272 (2016).

35. Suzuki, Y., Brender, J. R., Hartman, K., Ramamoorthy, A. & Marsh, E. N. Alternative pathways of human islet amyloid polypeptide aggregation distinguished by (19)f nuclear magnetic resonance-detected kinetics of monomer consumption. *Biochemistry* **51**, 8154-8162 (2012).

36. Wong, A. G. *et al.* Analysis of the Amyloidogenic Potential of Pufferfish (Takifugu rubripes) Islet Amyloid Polypeptide Highlights the Limitations of Thioflavin-T Assays and the Difficulties in Defining Amyloidogenicity. *Biochemistry* **55**, 510-518 (2016).

37. So, M. *et al.* Supersaturation-Limited and Unlimited Phase Spaces Compete to Produce Maximal Amyloid Fibrillation near the Critical Micelle Concentration of Sodium Dodecyl Sulfate. *Langmuir* **31**, 9973-9982 (2015).

137

38.   Marsh, D. *CRC Handbook of Lipid Bilayers*. (CRC Press, 1990).

39.   La Rosa, C., Scalisi, S., Lolicato, F., Pannuzzo, M. & Raudino, A. Lipid-assisted protein transport: A diffusion-reaction model supported by kinetic experiments and molecular dynamics simulations. *J. Chem. Phys.* **144**, 184901 (2016).

40.   Buboltz, J. T. & Feigenson, G. W. Phospholipid solubility determined by equilibrium distribution between surface and bulk phases. *Langmuir* **21**, 6296-6301 (2005).

41.   Sparr, E. *et al.* Islet amyloid polypeptide-induced membrane leakage involves uptake of lipids by forming amyloid fibers. *FEBS Lett.* **577**, 117-120 (2004).

42.   Brender, J. R., Durr, U. H., Heyl, D., Budarapu, M. B. & Ramamoorthy, A. Membrane fragmentation by an amyloidogenic fragment of human Islet Amyloid Polypeptide detected by solid-state NMR spectroscopy of membrane nanotubes. *Biochim. Biophys. Acta.* **1768**, 2026-2029 (2007).

43.   Nakazawa, Y., Suzuki, Y., Williamson, M. P., Saito, H. & Asakura, T. The interaction of amyloid Abeta(1-40) with lipid bilayers and ganglioside as studied by 31P solid-state NMR. *Chem. Phys. Lipids.* **158**, 54-60 (2009).

44.   Connelly, L. *et al.* Effects of point substitutions on the structure of toxic Alzheimer's beta-amyloid channels: atomic force microscopy and molecular dynamics simulations. *Biochemistry* **51**, 3031-3038 (2012).

45.   Yates, E. A. & Legleiter, J. Preparation protocols of abeta(1-40) promote the formation of polymorphic aggregates and altered interactions with lipid bilayers. *Biochemistry* **53**, 7038-7050 (2014).

46.   Yates, E. A. *et al.* Specific domains of Abeta facilitate aggregation on and association with lipid bilayers. *J. Mol. Biol.* **425**, 1915-1933 (2013).

47.   Scalisi, S. *et al.* Self-assembling pathway of hIAPP fibrils within lipid bilayers. *Chembiochem* **11**, 1856-1859 (2010).

48.   Batzli, K. M. & Love, B. J. Agitation of amyloid proteins to speed aggregation measured by ThT fluorescence: a call for standardization. *Mater. Sci. Eng. C. Mater. Biol. Appl.* **48**, 359-364 (2015).

49.   Yi, X. *et al.* Ca(2+) Interacts with Glu-22 of Abeta(1-42) and Phospholipid Bilayers to Accelerate the Abeta(1-42) Aggregation Below the Critical Micelle Concentration. *Biochemistry* **54**, 6323-6332 (2015).

50.   Canale, C. *et al.* Different effects of Alzheimer's peptide Abeta(1-40) oligomers and fibrils on supported lipid membranes. *Biophys. Chem.* **182**, 23-29 (2013).

51.   Pithadia, A. S. *et al.* Influence of a curcumin derivative on hIAPP aggregation in the absence and presence of lipid membranes. *Chem. Commun.* **52**, 942-945 (2016).

52. Ahsan, N., Mishra, S., Jain, M. K., Surolia, A. & Gupta, S. Curcumin Pyrazole and its derivative (N-(3-Nitrophenylpyrazole) Curcumin inhibit aggregation, disrupt fibrils and modulate toxicity of Wild type and Mutant alpha-Synuclein. *Sci. Rep.* **5**, 9862 (2015).

53. Cao, P. & Raleigh, D. P. Analysis of the inhibition and remodeling of islet amyloid polypeptide amyloid fibers by flavanols. *Biochemistry* **51**, 2670-2683 (2012).

54. Rezaei-Ghaleh, N., Amininasab, M., Kumar, S., Walter, J. & Zweckstetter, M. Phosphorylation modifies the molecular stability of beta-amyloid deposits. *Nat. Commun.* **7**, 11359 (2016).

55. Lu, J. X. *et al.* Molecular structure of beta-amyloid fibrils in Alzheimer's disease brain tissue. *Cell* **154**, 1257-1268 (2013).

56. Tycko, R. Physical and structural basis for polymorphism in amyloid fibrils. *Protein. Sci.* **23**, 1528-1539 (2014).

57. Schutz, A. K. *et al.* Atomic-resolution three-dimensional structure of amyloid beta fibrils bearing the Osaka mutation. *Angew. Chem. Int. Ed. Engl.* **54**, 331-335 (2015).

58. Elkins, M. R. *et al.* Structural Polymorphism of Alzheimer's beta-Amyloid Fibrils as Controlled by an E22 Switch: A Solid-State NMR Study. *J. Am. Chem. Soc.* **138**, 9840-9852 (2016).

59. Ikenoue, T. *et al.* Cold denaturation of alpha-synuclein amyloid fibrils. *Angew. Chem. Int. Ed. Engl.* **53**, 7799-7804 (2014).

60. Cobb, N. J., Apostol, M. I., Chen, S., Smirnovas, V. & Surewicz, W. K. Conformational stability of mammalian prion protein amyloid fibrils is dictated by a packing polymorphism within the core region. *J. Biol. Chem.* **289**, 2643-2650 (2014).

61. Nystrom, S. *et al.* Multiple substitutions of methionine 129 in human prion protein reveal its importance in the amyloid fibrillation pathway. *J. Biol. Chem.* **287**, 25975-25984 (2012).

62. Eisenberg, D. & Jucker, M. The amyloid state of proteins in human diseases. *Cell* **148**, 1188-1203 (2012).

63. Knowles, T. P. *et al.* An analytical solution to the kinetics of breakable filament assembly. *Science* **326**, 1533-1537 (2009).

64. Tanaka, M., Collins, S. R., Toyama, B. H. & Weissman, J. S. The physical basis of how prion conformations determine strain phenotypes. *Nature* **442**, 585-589 (2006).

65. Nichols, M. R. *et al.* Biophysical comparison of soluble amyloid-beta(1-42) protofibrils, oligomers, and protofilaments. *Biochemistry* **54**, 2193-2204 (2015).

66. O'Nuallain, B. *et al.* Amyloid beta-protein dimers rapidly form stable synaptotoxic protofibrils. *J. Neurosci.* **30**, 14411-14419 (2010).

67. Galvagnion, C. *et al.* Chemical properties of lipids strongly affect the kinetics of the membrane-induced aggregation of alpha-synuclein. *Proc. Natl. Acad. Sci. U.S.A.* **113**, 7065-7070 (2016).

68. Larosa, C., Milardi, D., Grasso, D., Guzzi, R. & Sportelli, L. Thermodynamics of the Thermal Unfolding of Azurin. *J. Phys. Chem.* **99**, 14864-14870 (1995).

69. Manetto, G. D., La Rosa, C., Grasso, D. M. & Milardi, D. Evaluation of thermodynamic properties of irreversible protein thermal unfolding measured by DSC. *J. Therm. Anal. Calorim.* **80**, 263-270 (2005).

70. Ono, K., Condron, M. M. & Teplow, D. B. Structure-neurotoxicity relationships of amyloid beta-protein oligomers. *Proc. Natl. Acad. Sci. U.S.A.* **106**, 14745-14750 (2009).

Chapter 5

Conclusions and Perspectives

5.1.   General Conclusions

The multivariate nature of AD makes it difficult to characterize the impact which individual molecular and cellular components have upon the disease's presentation and progression.[1-3] Previous research has suggested that metal ion dyshomeostasis, the resultant oxidative stress, and neuronal membranes are all capable of perturbing the aggregation of Aβ commonly associated with AD. The roles of metal-Aβ aggregation in AD remain clouded due to a lack of effective tools to interrogate individual aspects of the fibrillation pathway.[4,5] Meanwhile, investigations of membrane-associated aggregation have done little to investigate the role of disease relevant membrane parameters outside the role of GM1 ganglioside.[6,7] Through a combination of biochemical and biophysical approaches we have characterized the effects of new series of natural product small molecules and their synthetic derivatives on the aggregation of Aβ in both the absence and presence of metal ions in pursuit of new molecular tools. Additionally, we have characterized the effect of lipid membrane thinning, a phenomenon resulting of lipid peroxidation,[8-10] on Aβ aggregation. The results of these studies have provided new insights into multifunctional ligand design and suggest previously undiscovered pathways of peptide aggregation on lipid bilayers.

Results in Chapter 2 differentiate the modulation of metal-Aβ by a suite of three previously identified amyloid modulators (**Phlorizin**, **Verbascoside**, and **Rutin**) and the effect

of esterification on their function and stability. It was observed that only compounds with the conventional bidentate metal binding catechol moiety were capable of significantly modulating aggregation in the presence of metal ions. Additionally, esterification of the compounds altered the method of aggregation modulation but did not significantly impact their capacity to bind metal ions. Esterification also redirected the modes of interaction between the compounds and both monomeric and fibrillar Aβ, but minimally affected the affinity. Finally, by altering the modes of inhibition and peptide binding, esterification significantly altered the ability of the compounds to inhibit the toxicity of Aβ aggregation. The results suggest that, while these molecules, particularly **Verbascoside**, demonstrate extremely promising structures for the future study of Aβ aggregation, modifications of the framework must be performed selectively so as not to reduce the molecule's functionality. Additionally, due to the presence of the catechol moieties of **Verbascoside** which are responsible for driving the interaction with transition metal ions, care must be taken in any implementation of the compound in a more complex environment. These pharmacophores are known to promiscuously drive a range of non-specific interactions with proteins and are especially prone to oxidation in cells and *in vivo*.[11] Further optimization of the framework may generate a more stable and specific probe for further study, but **Verbascoside**, in its current state, is a viable tool for the continued *in vitro* characterization of metal-Aβ aggregation.

Chapter 3 represents a change of direction; instead of developing new tools for interrogation of metal-Aβ aggregation, we applied existing tools and methodologies to investigate the interaction of Aβ with lipid bilayers of varying thickness. It has been suggested previously that Aβ adopts a helical fold when bound to lipid bilayers, though all previous structural insight with residue specific resolution into these interactions were obtained in the

presence of micelles, a poor mimetic of a lipid bilayer.[12-14] Traditionally, when an amyloidogenic peptide binds to the membrane, its signal in solution NMR spectroscopy broadens due to the decreased tumbling rate of the peptide-lipid complex and the introduction of one or more new populations of peptide.[15,16] We took advantage of the exchange between the unbound and bound populations of Aβ to interrogate the structural constraints of the bound peptide without a significant reduction in signal intensity using solution NMR. Transfer-NOESY (tr-NOESY) has previously been applied to investigate the interaction of small molecule ligands with their protein partners and small peptide binding to larger species.[17-21] Here, we applied the same methodologie to examine the exchange between free peptide and peptide bound to three different model membranes. Our results represent the largest binding species characterized by tr-NOESY to date. Based on the observed NOEs and chemical shift results, we identified a partially folded helical intermediate adopted in the presence of all three lipid bilayers. This result suggests that the initial folding event when Aβ interacts with a lipid bilayer is driven predominantly by the surface environment and is independent of the hydrophobic thickness and acyl chain characteristics of the lipid bilayer. Additionally, the helical region which was identified (K16-G25) is also implicated in the early self-association events in amyloid formation and forms one of the β-strands observed in fibrillar structures.[1] This region has also been suggested to adopt a helical structure in a soluble, folded model of $A\beta_{40}$.[22] The prevalence of this sequence appearing in a variety of structural forms at different stages of aggregation strongly supports the hypothesis that it plays a driving role in many of the aggregation events. Interestingly, the hydrophobic thickness did modulate the affinity of the peptide for the lipid bilayer and the distribution between bound and unbound Aβ; the thicker the bilayer the tighter the affinity which was observed. This suggests that either bilayer thickness controls the distribution of free and bound peptide without

modulating the monomeric structure or bilayer thickness regulates the progression of Aβ from its monomeric form towards intermediate aggregates as those distinctions were not able to be made based on our fluorescence-based binding study.

The differences in the equilibrium between bound and unbound Aβ populations regulated by the membrane hydrophobic thickness made us begin to question how bilayer thinning may impact the progression of Aβ from its conserved, partially folded state towards mature amyloid fibrils (Chapter 4). It is known that Aβ is capable of forming membrane-inserted oligomeric species.[23-25] Additionally, it is known from the field of membrane proteins that hydrophobic match and mismatch between the bilayer and the inserted protein is able to regulate the stability distinct the inserted protein.[26,27] We expected, therefore, that the observed differences in membrane association result from the stabilization or destabilization of distinct membrane inserted oligomers which could be on or off pathway. While the membranes of traditional thickness, DOPC and POPC, promoted canonical Aβ fibrillation, as has been previously reported,[28,29] we found that substoichiometric concentrations of DLPC, a synthetic mimic of the membrane thinning associated with AD, were sufficient to completely inhibit the fibrillation of Aβ. Through a combination of ThT-fluorescence, CD spectroscopy, and microscopy, we discovered that DLPC bilayers stabilized globular, membrane associated oligomers which were not observed to progress towards fibrils. Additionally, oligomer formation on the membrane surface produced micelle-like lipid aggregates which have the potential to serve as a second sink for non-fibrillar Aβ aggregates. DLPC bilayers were also found to be capable of remodeling preformed Aβ fibrils by stabilizing a pseudo-unfolded intermediate state which resembles protofibrillar assemblies. These results indicate that alterations to membrane composition and structure resulting from metabolic alterations in AD are capable of redirecting the misfolding of

membrane-associated Aβ into unique oligomeric states. These sorts of stabilized intermediates have not been previously reported and may represent a new, disease relevant aspect of Aβ aggregation.

5.2.   Future Outlook

The work presented in this dissertation has characterized tools with the potential to inform our broader understanding of amyloid misfolding in both AD and other disease states. Metal ion-modulated aggregation is not unique to Aβ and AD. Zn(II) is known to modulate the aggregation of hIAPP associated with type II diabetes while α-synuclein, implicated in the pathogenesis of Parkinson's disease, is known to interact with Zn(II), Cu(I/II), and Fe(II/III).[30-32] It is possible that small molecules which are found to modulate metal-Aβ aggregation may have more wide ranging antiamyloidogenic activity against other metal-associated, amyloidogenic peptides and proteins. A lack of universal activity by a known modulator may also assist in distinguishing aspects of amyloid formation which are sequence specific. Protein aggregation into amyloid fibrils is often discussed as a single, common pathway,[33] yet the diversity of sequences which can aggregate into fibrils suggests that there exist intermediate states between monomer and fiber which are unique to individual proteins. If a small molecule is capable of modulating the metal-associated aggregation of some proteins and not others, this supports this idea. Characterizing which small molecules are capable of modulating which aggregation pathways can help identify aspects unique to each amyloidogenic sequence. By characterizing the unique aspects of amyloid formation it may be possible to begin to treat amyloid formation as a more diverse pathway than it currently is.

Despite the conclusions of Chapter 4 suggesting that DLPC remodels preformed $A\beta_{40}$ fibrils by stabilizing a molten-globule-like intermediate, there remains a lack of structural data to suggest just how such an intermediate may be stabilized for $A\beta_{40}$ or any other amyloid fibril.[34] While changes in stability have been attributed to side chain perturbations, which side chains are most affected (whether they form the steric zipper on the interior or the fiber are solvent exposed) and the ways in which they are affected remain unknown. As discussed in Chapter 4, structural analysis of amyloid aggregates is made difficult by the presence of sample heterogeneity. Immediately following DLPC-induced remodeling it is likely that a variety of aggregate states exist. However, it has been demonstrated that molten-globule-like remodeled fibrils are capable of seeding fiber formation.[34] Additionally, seeding is known to propagate seed structure.[35] Through a combination of these two methods, it may be possible to generate a homogeneous population of $A\beta_{40}$ aggregates which possess the DLPC-remodeled side chain arrangement. With a homogeneous population in hand, solid-state NMR methods could subsequently characterize these altered aggregates at atomic resolution. These data would further characterize the mechanism by which ThT functions, which remains uncertain, while also helping clarify which side chains are most integral for $A\beta$ fiber stability and which are most susceptible to perturbation by environmental changes.

While identifying oligomeric intermediates along the amyloid formation pathway is essential to solving the black box that exists between monomeric peptide and fibrillar aggregate, structurally characterizing them remains a daunting task. Oligomer identification has been possible, but the transient and unstable nature of their formation has limited their structural analysis.[36] In this respect, the use of lipid bilayers can become a powerful tool. While membranes are usually considered a complicating factor in $A\beta$ aggregation, the results of

Chapter 4 have revealed that the careful selection of membrane composition can stabilize non-fibrillar aggregates stabilized by the presence of the lipid bilayer. Additionally, the ongoing developments of lipid nanodisc technology, constrained lipid bilayer systems with a finite surface area and highly customizable composition, has expanded the techniques available for the study of membrane proteins and protein complexes formed in the lipid bilayer.[37-39] Nanodiscs facilitate structure determination of traditional membrane proteins by solution NMR.[37] More recently, the investigation of protein-protein complexes formed in native membrane environments has been facilitated by isotropic nanodiscs.[40] Additionally, nanodiscs have enabled FRET-based structural analysis of a dimer formed by the non-amyloidogenic rat variant of IAPP.[41] Despite the advantages of nanodiscs in the structural study of membrane-associated proteins and protein complexes, they remain relatively unexplored in the study of amyloid oligomer formation. Combining this technology with our current understanding of how pathological membrane compositions can modulate the formation of Aβ intermediates, it may be possible to not only identify unique aggregation intermediates but also to generate structural models of them. With structural insights in hand, the rational design of small molecule modulators, with an eye towards eventual therapeutic development, ought to be improved. By better understanding the misfolding pathways of Aβ in AD it may be possible to reduce the toll which the disease places on world economies, health care industries, caregivers, families, and those who suffer from the disease. 110 years after the first descriptions of AD, patients are ready for progress.

5.3. References

1.   Savelieff, M. G., Lee, S., Liu, Y. & Lim, M. H. Untangling amyloid-beta, tau, and metals in Alzheimer's disease. *ACS Chem. Biol.* **8**, 856-865 (2013).

2.   Kepp, K. P. Bioinorganic chemistry of Alzheimer's disease. *Chem. Rev.* **112**, 5193-5239 (2012).

3.   Benilova, I., Karran, E. & De Strooper, B. The toxic Abeta oligomer and Alzheimer's disease: an emperor in need of clothes. *Nat. Neurosci.* **15**, 349-357 (2012).

4.   Faller, P., Hureau, C. & Berthoumieu, O. Role of metal ions in the self-assembly of the Alzheimer's amyloid-beta peptide. *Inorg. Chem.* **52**, 12193-12206 (2013).

5.   Derrick, J. S. & Lim, M. H. Tools of the trade: investigations into design strategies of small molecules to target components in Alzheimer's disease. *Chembiochem* **16**, 887-898 (2015).

6.   Kotler, S. A., Walsh, P., Brender, J. R. & Ramamoorthy, A. Differences between amyloid-beta aggregation in solution and on the membrane: insights into elucidation of the mechanistic details of Alzheimer's disease. *Chem. Soc. Rev.* **43**, 6692-6700 (2014).

7.   Matsuzaki, K. How do membranes initiate Alzheimer's Disease? Formation of toxic amyloid fibrils by the amyloid beta-protein on ganglioside clusters. *Acc. Chem. Res.* **47**, 2397-2404 (2014).

8.   Montine, T. J. *et al.* Lipid peroxidation in aging brain and Alzheimer's disease. *Free Radic. Biol. Med.* **33**, 620-626 (2002).

9.   Negre-Salvayre, A. *et al.* Pathological aspects of lipid peroxidation. *Free Radic. Res.* **44**, 1125-1171 (2010).

10.   Sultana, R., Perluigi, M. & Allan Butterfield, D. Lipid peroxidation triggers neurodegeneration: a redox proteomics view into the Alzheimer disease brain. *Free Radic. Biol. Med.* **62**, 157-169 (2013).

11.   Baell, J. & Walters, M. A. Chemistry: Chemical con artists foil drug discovery. *Nature* **513**, 481-483 (2014).

12.   Wong, P. T. *et al.* Amyloid-beta membrane binding and permeabilization are distinct processes influenced separately by membrane charge and fluidity. *J. Mol. Biol.* **386**, 81-96 (2009).

13.   Coles, M., Bicknell, W., Watson, A. A., Fairlie, D. P. & Craik, D. J. Solution structure of amyloid beta-peptide(1-40) in a water-micelle environment. Is the membrane-spanning domain where we think it is? *Biochemistry* **37**, 11064-11077 (1998).

14.   Utsumi, M. *et al.* Up-and-down topological mode of amyloid beta-peptide lying on hydrophilic/hydrophobic interface of ganglioside clusters. *Glycoconj. J.* **26**, 999-1006 (2009).

15. Bodner, C. R., Dobson, C. M. & Bax, A. Multiple tight phospholipid-binding modes of alpha-synuclein revealed by solution NMR spectroscopy. *J. Mol. Biol.* **390**, 775-790 (2009).

16. Bodner, C. R., Maltsev, A. S., Dobson, C. M. & Bax, A. Differential phospholipid binding of alpha-synuclein variants implicated in Parkinson's disease revealed by solution NMR spectroscopy. *Biochemistry* **49**, 862-871 (2010).

17. Clore, G. M. & Gronenborn, A. M. Theory and applications of the transferred nuclear overhauser effect to the study of the conformations of small ligands bound to proteins. *J. Magn. Reson.* **48**, 402-417 (1982).

18. Bhunia, A., Mohanram, H. & Bhattacharjya, S. Lipopolysaccharide bound structures of the active fragments of fowlicidin-1, a cathelicidin family of antimicrobial and antiendotoxic peptide from chicken, determined by transferred nuclear Overhauser effect spectroscopy. *Biopolymers* **92**, 9-22 (2009).

19. Wang, Z., Jones, J. D., Rizo, J. & Gierasch, L. M. Membrane-bound conformation of a signal peptide: a transferred nuclear Overhauser effect analysis. *Biochemistry* **32**, 13991-13999 (1993).

20. Vogtherr, M. & Fiebig, K. NMR-based screening methods for lead discovery. *EXS*, 183-202 (2003).

21. Aguirre, C., Cala, O. & Krimm, I. Overview of Probing Protein-Ligand Interactions Using NMR. *Curr. Protoc. Protein. Sci.* **81**, 17 18 11-24 (2015).

22. Vivekanandan, S., Brender, J. R., Lee, S. Y. & Ramamoorthy, A. A partially folded structure of amyloid-beta(1-40) in an aqueous environment. *Biochem. Biophys. Res. Commun.* **411**, 312-316 (2011).

23. Arispe, N., Rojas, E. & Pollard, H. B. Alzheimer disease amyloid beta protein forms calcium channels in bilayer membranes: blockade by tromethamine and aluminum. *Proc. Natl. Acad. Sci. U.S.A.* **90**, 567-571 (1993).

24. Quist, A. *et al.* Amyloid ion channels: a common structural link for protein-misfolding disease. *Proc. Natl. Acad. Sci. U.S.A.* **102**, 10427-10432 (2005).

25. Serra-Batiste, M. *et al.* Abeta42 assembles into specific beta-barrel pore-forming oligomers in membrane-mimicking environments. *Proc. Natl. Acad. Sci. U.S.A.* **113**, 10866-10871 (2016).

26. Fattal, D. R. & Ben-Shaul, A. A molecular model for lipid-protein interaction in membranes: the role of hydrophobic mismatch. *Biophys. J.* **65**, 1795-1809 (1993).

27. Killian, J. A. Hydrophobic mismatch between proteins and lipids in membranes. *Biochim. Biophys. Acta.* **1376**, 401-415 (1998).

28. Aisenbrey, C. *et al.* How is protein aggregation in amyloidogenic diseases modulated by biological membranes? *Eur. Biophys. J* **37**, 247-255 (2008).

29. Gorbenko, G. P. & Kinnunen, P. K. The role of lipid-protein interactions in amyloid-type protein fibril formation. *Chem. Phys. Lipids* **141**, 72-82 (2006).

30. Brender, J. R. *et al.* Role of zinc in human islet amyloid polypeptide aggregation. *J. Am. Chem. Soc.* **132**, 8973-8983 (2010).

31. Salamekh, S. *et al.* A two-site mechanism for the inhibition of IAPP amyloidogenesis by zinc. *J. Mol. Biol.* **410**, 294-306 (2011).

32. Bush, A. I. Metals and neuroscience. *Curr. Opin. Chem. Biol.* **4**, 184-191 (2000).

33. Harrison, R. S., Sharpe, P. C., Singh, Y. & Fairlie, D. P. Amyloid peptides and proteins in review. *Rev. Physiol. Biochem. Pharmacol.* **159**, 1-77 (2007).

34. Noda, S. *et al.* Thioflavin T-Silent Denaturation Intermediates Support the Main-Chain-Dominated Architecture of Amyloid Fibrils. *Biochemistry* **55**, 3937-3948 (2016).

35. Petkova, A. T. *et al.* Self-propagating, molecular-level polymorphism in Alzheimer's beta-amyloid fibrils. *Science* **307**, 262-265 (2005).

36. Suzuki, Y., Brender, J. R., Hartman, K., Ramamoorthy, A. & Marsh, E. N. Alternative pathways of human islet amyloid polypeptide aggregation distinguished by (19)f nuclear magnetic resonance-detected kinetics of monomer consumption. *Biochemistry* **51**, 8154-8162 (2012).

37. Hagn, F., Etzkorn, M., Raschle, T. & Wagner, G. Optimized phospholipid bilayer nanodiscs facilitate high-resolution structure determination of membrane proteins. *J. Am. Chem. Soc.* **135**, 1919-1925 (2013).

38. Orwick, M. C. *et al.* Detergent-free formation and physicochemical characterization of nanosized lipid-polymer complexes: Lipodisq. *Angew. Chem. Int. Ed. Engl.* **51**, 4653-4657 (2012).

39. Anantharamaiah, G. M. *et al.* Studies of synthetic peptide analogs of the amphipathic helix. Structure of complexes with dimyristoyl phosphatidylcholine. *J. Biol. Chem.* **260**, 10248-10255 (1985).

40. Zhang, M. *et al.* Reconstitution of the Cytb5-CytP450 Complex in Nanodiscs for Structural Studies using NMR Spectroscopy. *Angew. Chem. Int. Ed. Engl.* **55**, 4497-4499 (2016).

41. Nath, A., Miranker, A. D. & Rhoades, E. A membrane-bound antiparallel dimer of rat islet amyloid polypeptide. *Angew. Chem. Int. Ed. Engl.* **50**, 10859-10862 (2011).

Appendix A

## Supporting Information for Chapter 2

A.1. Supplementary Figures
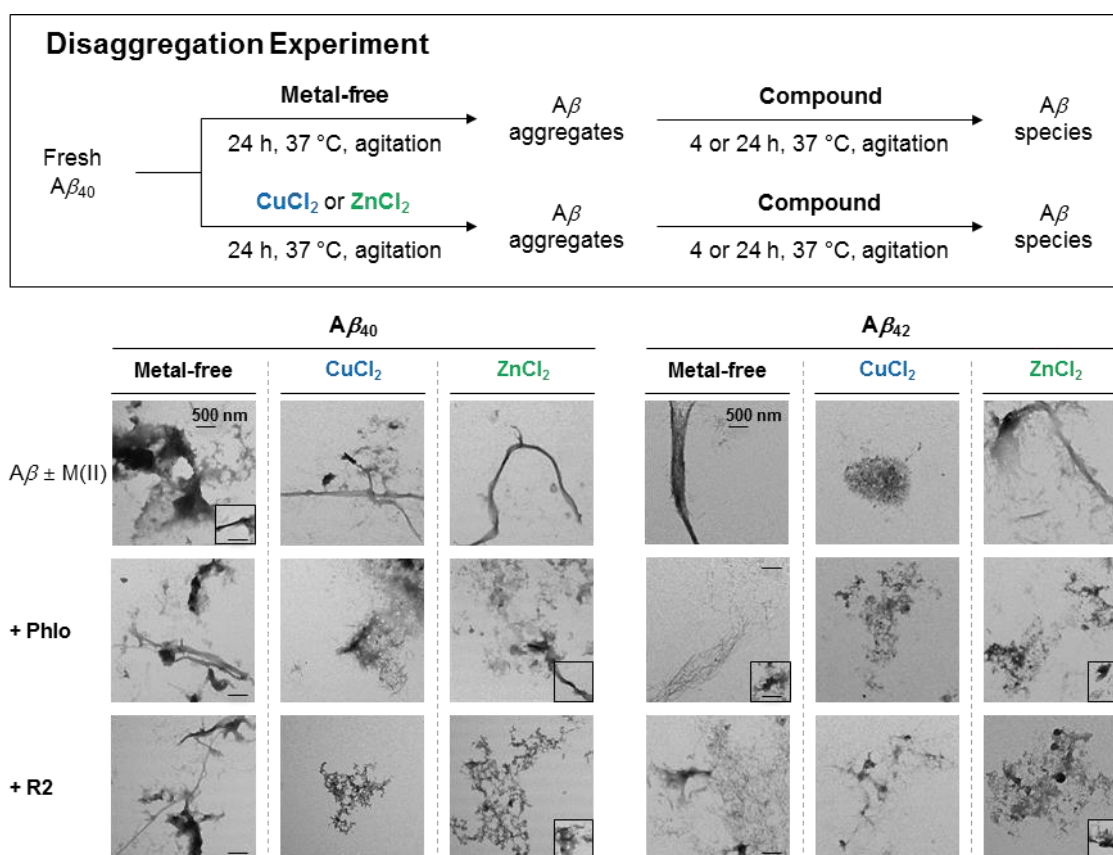
Figure A.1. Visualization of the morphologies of the resultant Aβ species from the disaggregation samples that were incubated with **Phlorizin** or **R2** for 24 h by TEM. Conditions: [Aβ] = 25 μM; [CuCl$_2$ or ZnCl$_2$] = 25 μM; [compound] = 50 μM; incubation for 4 or 24 h; pH 6.6 (for Cu(II) samples) or pH 7.4 (for metal-free and Zn(II) samples); 37 °C; constant agitation.
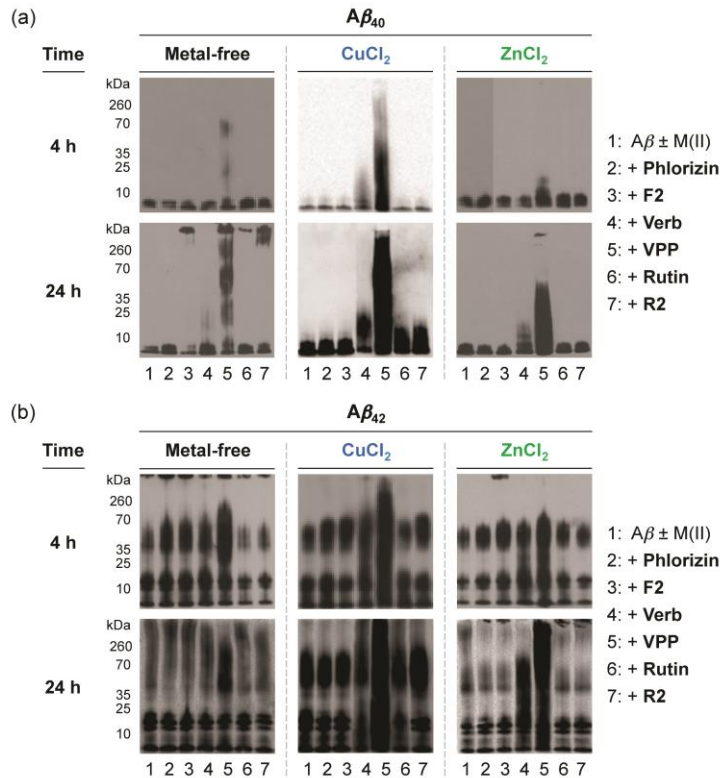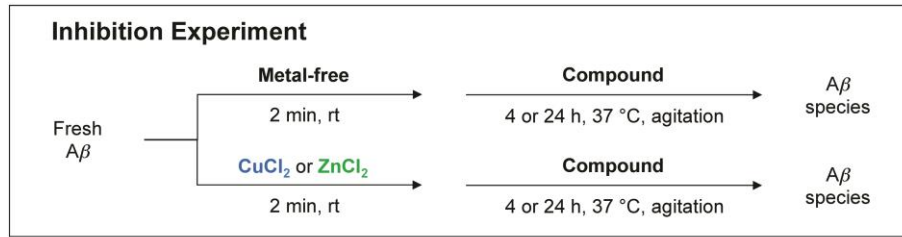
Figure A.2. Effect of **Phlorizin**, **F2**, **Verbascoside**, **VPP**, **Rutin**, or **R2** on the formation of metal-free and metal-induced $A\beta_{40}/A\beta_{42}$ aggregates. $A\beta_{40}$ (a) and $A\beta_{42}$ (b) were co-incubated with or without compound in both the absence and presence of either $CuCl_2$ or $ZnCl_2$ for either 4 or 24 h and visualized by gel/Western blot. Conditions: $[A\beta] = 25$ μM; $[CuCl_2$ or $ZnCl_2] = 25$ μM; [compound] = 50 μM; 4 or 24 h incubation; pH 6.6 (for Cu(II) samples) or pH 7.4 (for metal-free and Zn(II) samples); 37 °C; constant agitation.
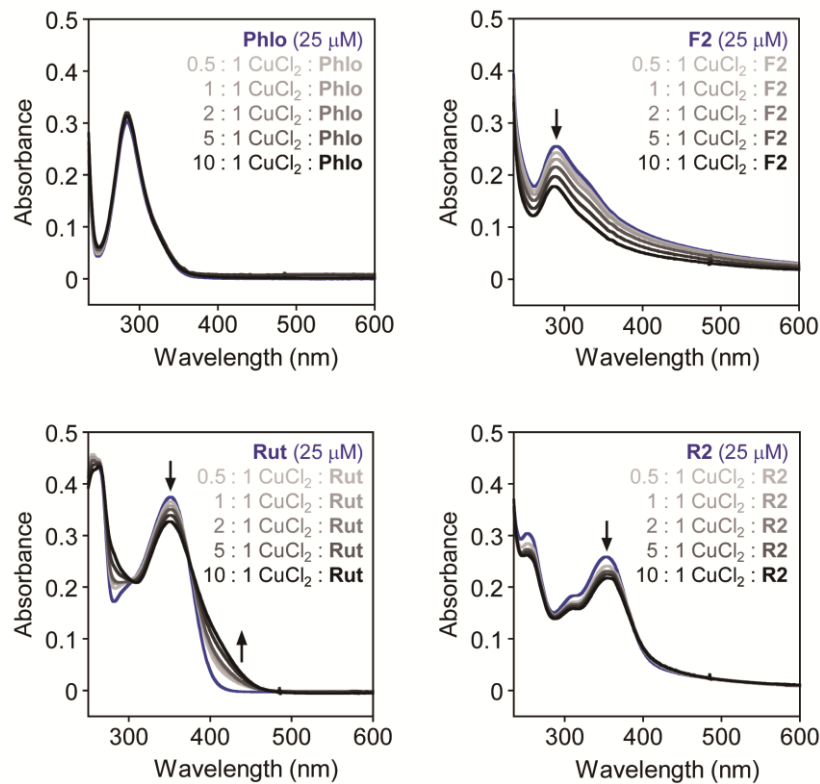
Figure A.3. Cu(II) binding studies of **Phlorizin** (**Phlo**), **F2**, **Rutin**, and **R2** by UV-Vis. Compounds were dissolved in buffer at pH 7.4 and titrated with Cu(II) and incubated for 2 h between reads. Experimental condition: [compound] = 25 µM; incubation for 2 h; room temperature.
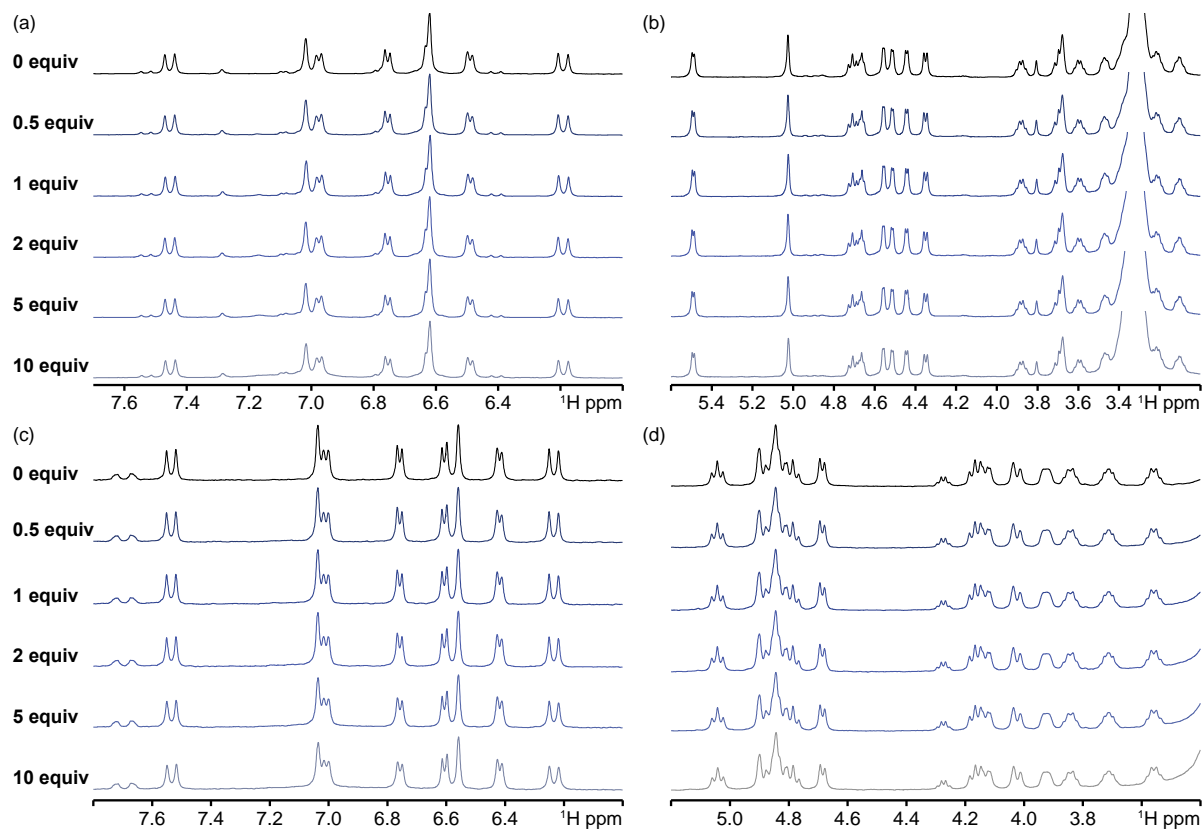
Figure A.4. Zn(II) binding of non-phenolic protons of **Verbascoside** and **VPP**. Samples of (a and b) **Verbascoside** and (c and d) **VPP** were dissolved in DMSO-d$_6$ (2 mM) and titrated with ZnCl$_2$ (0-10 equiv). Broadening or shifts of protons in the aromatic region (a and c) and the sugar ring region (b and d) of the ^{1}H spectra were not observed over the course of the titration.
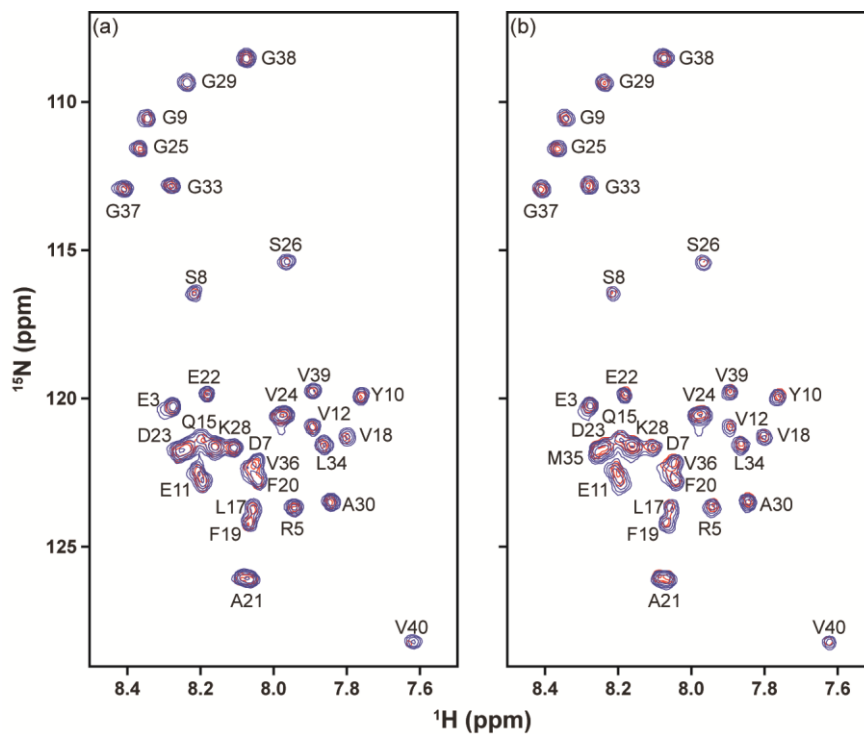
Figure A.5. Interaction of **Phlorizin** or **R2** with monomeric Aβ$_{40}$ by SOFAST-HMQC NMR. (a) **Phlorizin** or (b) **R2** was titrated into a solution of uniformly ^{15}N-labeled Aβ$_{40}$ (80 μM in 20 mM PO$_4$, pH 7.4, 50 mM NaCl, 7% v/v D$_2$O, 10 °C). The spectrum obtained upon incubation of Aβ$_{40}$ with 10 equiv of the ligand was indicated in blue; the spectrum of Aβ$_{40}$ only was depicted in red. All spectra were aligned at G29 due to non-uniform broadening of the water peak as a reference.
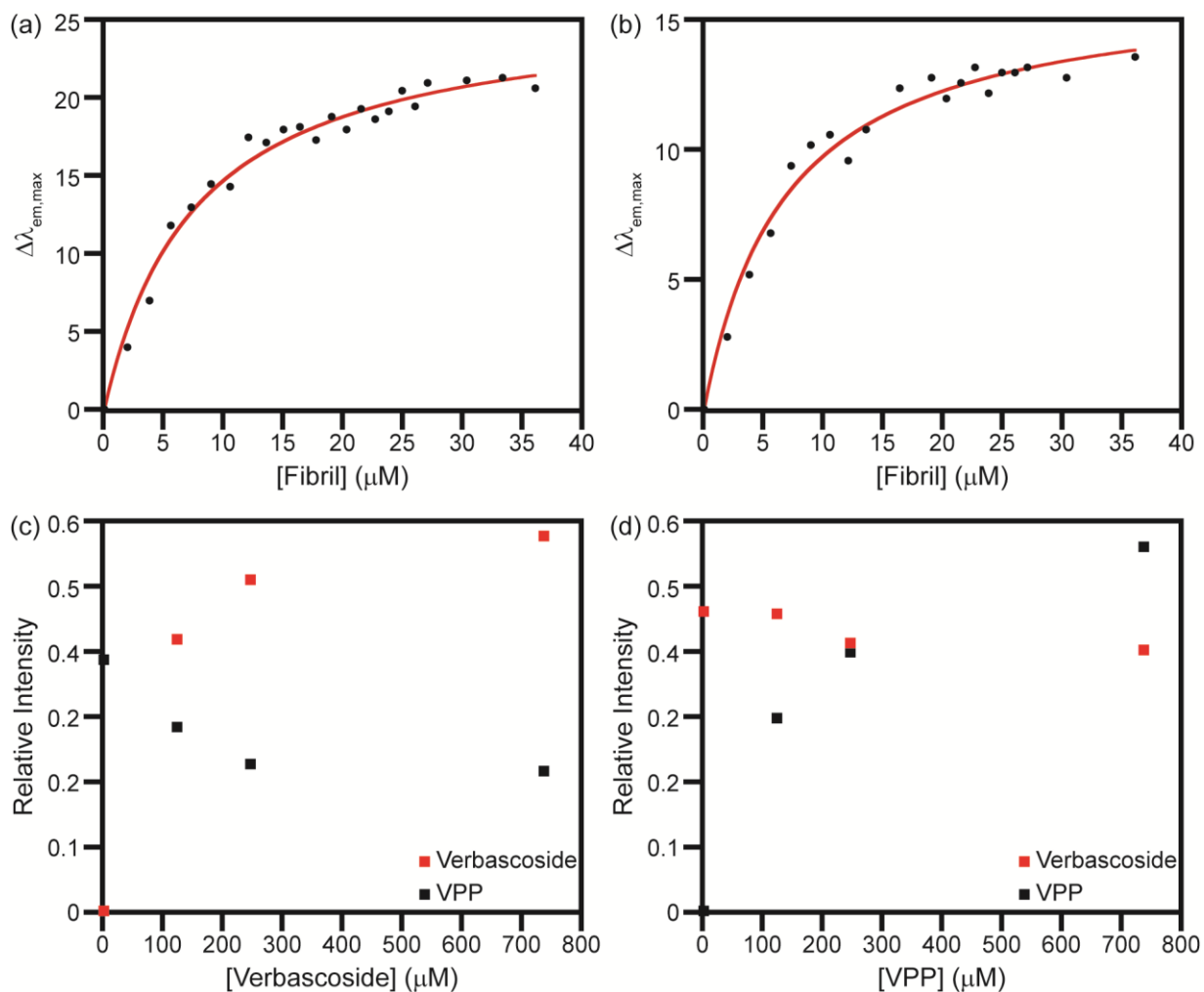
Figure A.6. Affinity and competition of **Verbascoside** and **VPP** for Aβ$_{42}$ fibrils. The affinity of (a) **Verbascoside** and (b) **VPP** for Aβ fibrils was measured by a blue shift fluorescence assay. The data were fit to a hyperbolic function to calculate the affinities (red line). The ligands were then tested for binding competition by STD. The relative intensity of the selected peaks in the STD spectra (relative to the reference spectra) were monitored over the course of a titration of (c) **Verbascoside** into the fibrils pretreated with **VPP**; (d) **VPP** into the fibrils pretreated with **Verbascoside**.
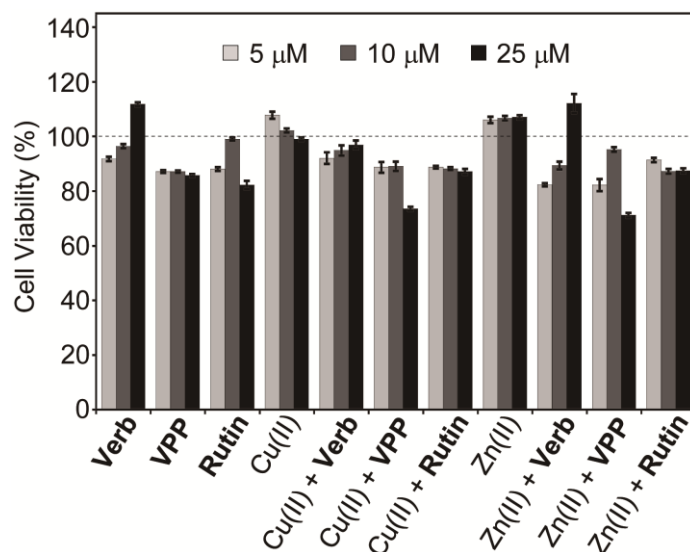
Figure A.7. Cytotoxicity of **Verbascoside** (**Verb**), **VPP**, and **Rutin** in the absence and presence of CuCl$_2$ or ZnCl$_2$. N2a cells treated with a metal chloride salt (CuCl$_2$ or ZnCl$_2$; 5 μM, 10 μM, or 25 μM) and a compound [**Verbascoside**, **VPP**, or **Rutin** (5 μM, 10 μM, or 25 μM)] were incubated for 24 h at 37 °C. Cell viability was determined by the MTT assay. Values of cell viability (%) were calculated compared to that of cells treated with DMSO only (0-1%, v/v). Error bars represent the standard error from three independent experiments.

Appendix B

Supporting Information for Chapter 3

B.1. Supplementary Figures
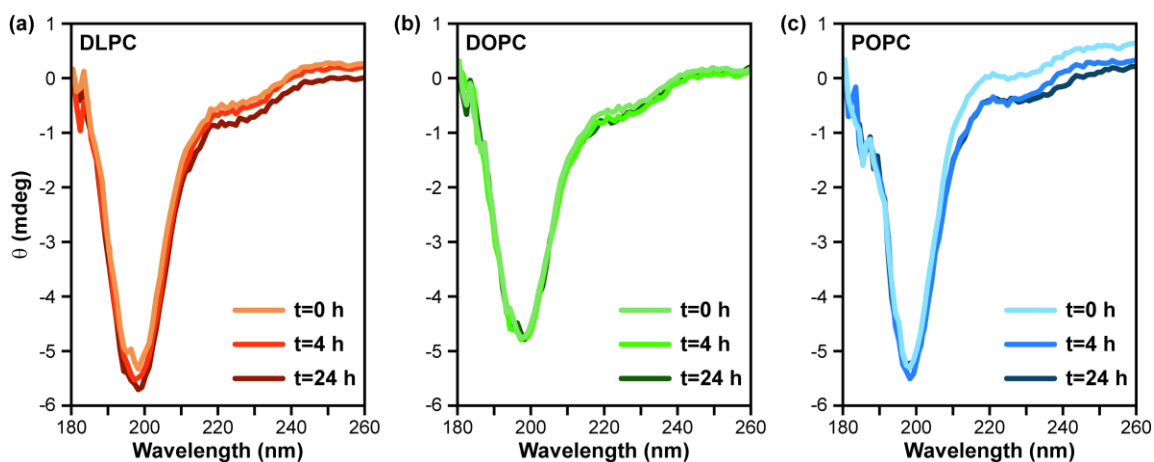
Figure B.1. Conformational analysis of Aβ$_{40}$ upon incubation with lipids for at least 24 h by CD. When Aβ$_{40}$ (20 μM) was co-incubated with 0.2 equiv (4 μM) LUVs composed of (a) DLPC, (b) DOPC, or (c) POPC at different time intervals. The random coil structure persisted in the presence of all three bilayers over the experimental timescale of 24 h.
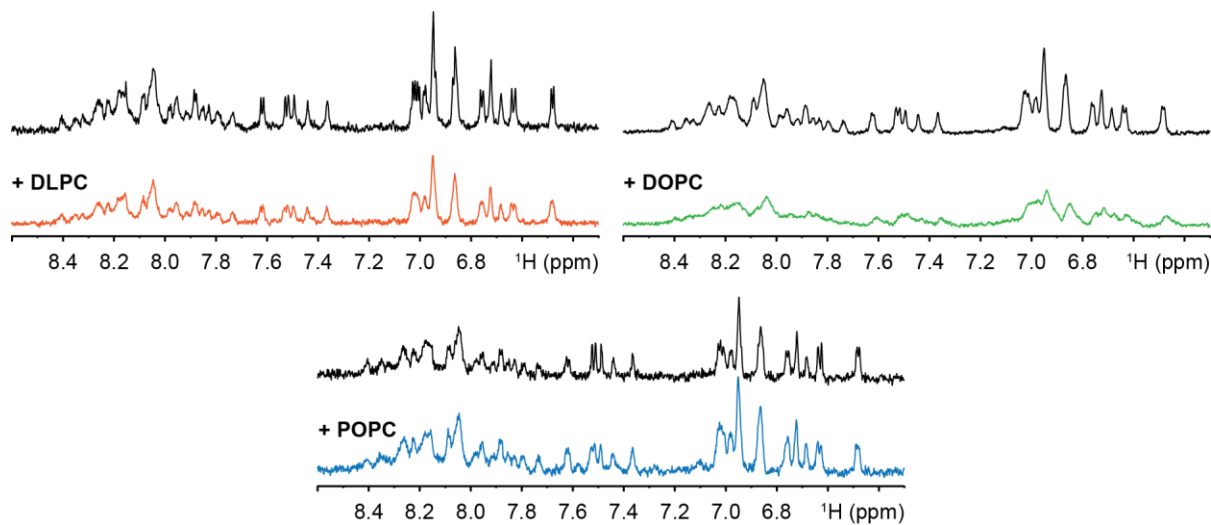
Figure B.2. Effect of LUVs on lipid-bound and –unbound states of peptide. $A\beta_{40}$ undergoes a fast-mediate exchange in the presence of substoichiometric lipid concentrations. The amide and aromatic regions of the ^{1}H region of $A\beta_{40}$ (80 µM) NMR spectra broaden in the presence of low concentrations of LUVs (14 µM lipid; colored spectra) relative to the lipid-free spectra (black), indicative of an exchange between lipid-bound and -unbound states of the peptide.
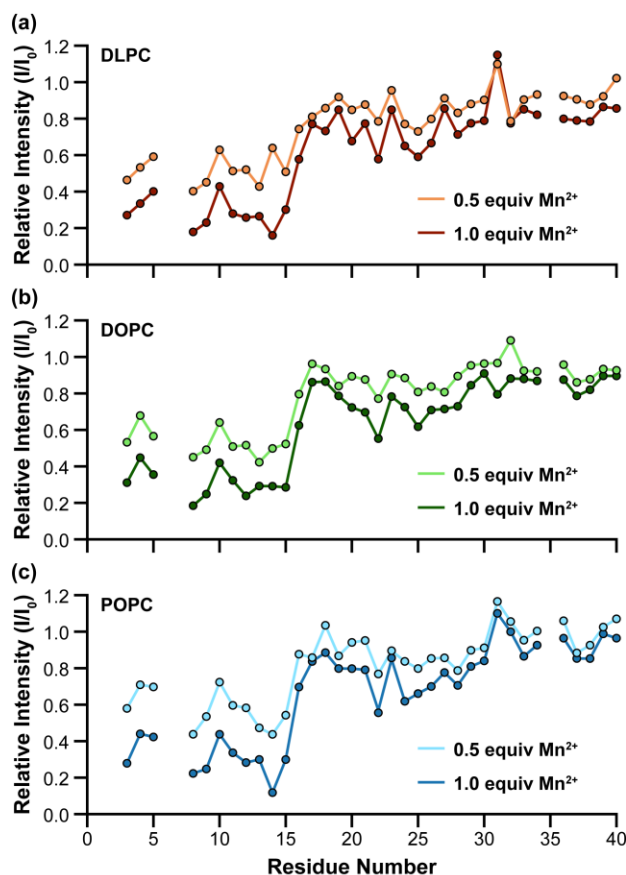
Figure B.3. Paramagnetic quenching of the peptide signal. A solution of uniformly ^{15}N-labeled Aβ$_{40}$ (80 μM) in the presence of LUVs (0.2 equiv, 16 μM) containing either (a) DLPC, (b) DOPC, or (c) POPC was titrated with a solution of MnCl$_2$ and the residue signal intensity was monitored by 2D SOFAST-HMQC (Bruker 600 MHz spectrometer, equipped with cryoprobe at 10 °C). The quenching of residue specific signal is indicative of exposure to buffer while maintenance of the initial intensity suggests the membrane interaction and protection from paramagnetic quenching.
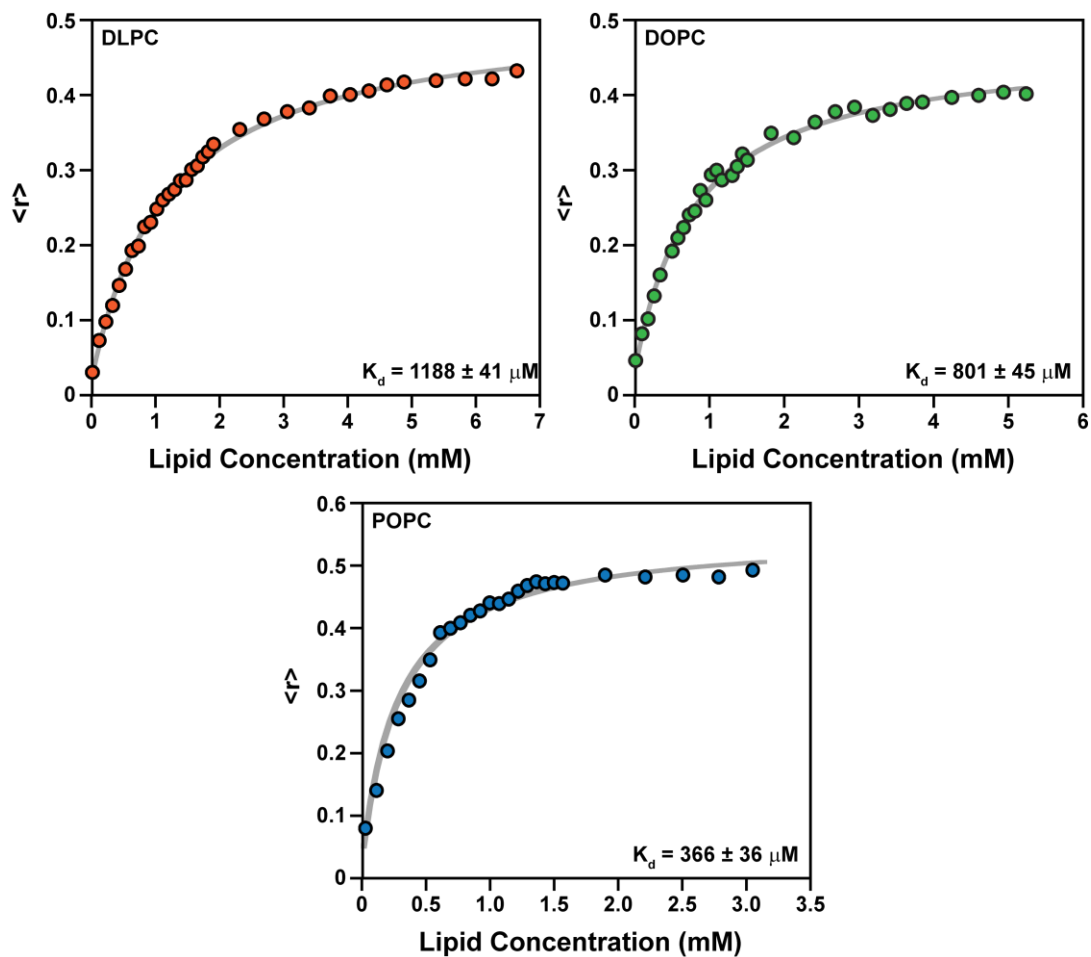
Figure B.4. Binding affinities of Aβ_{40} to lipid bilayers based on fluorescence polarization. 100 nm LUVs (DLPC, DOPC, and POPC) were titrated into 1 μM HiLyte 647-Aβ_{40} and the fluorescence polarization was monitored. Anisotropy values were converted to fraction bound and fit to obtain binding affinities of Aβ_{40} for the various bilayers.
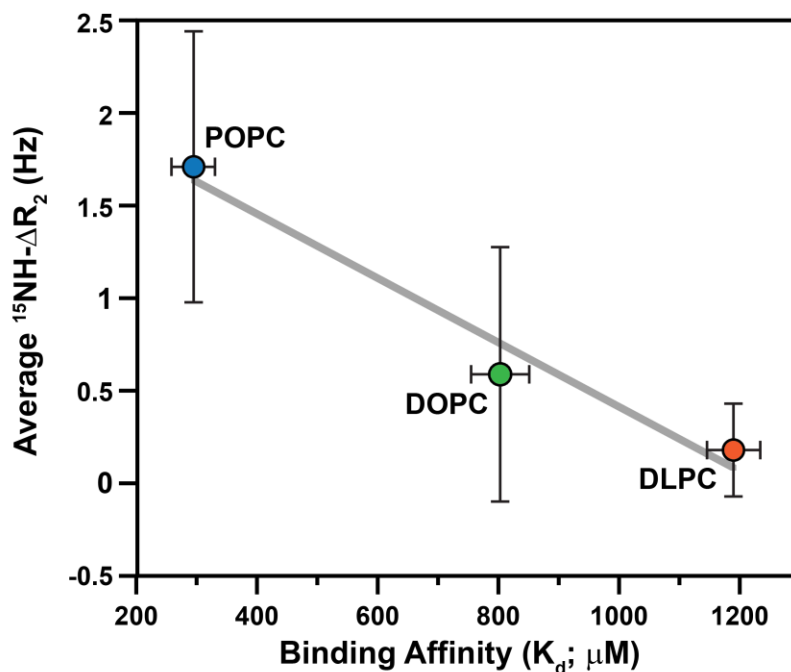
Figure B.5. Correlation between backbone flexibility and membrane affinity. There is a linear correlation between the average ΔR_2 and the binding affinity of the $A\beta_{40}$ peptide in the presence of each bilayer. The R_2 experiments of $A\beta_{40}$ with and without LUVs were performed on a Bruker 600 MHz spectrometer at 10 °C. The tighter the binding affinity (K_d) indicates the larger the ΔR_2, indicative of the reduced ensemble flexibility.

Appendix C

# Supporting Information for Chapter 4

C.1. Supplementary Figures
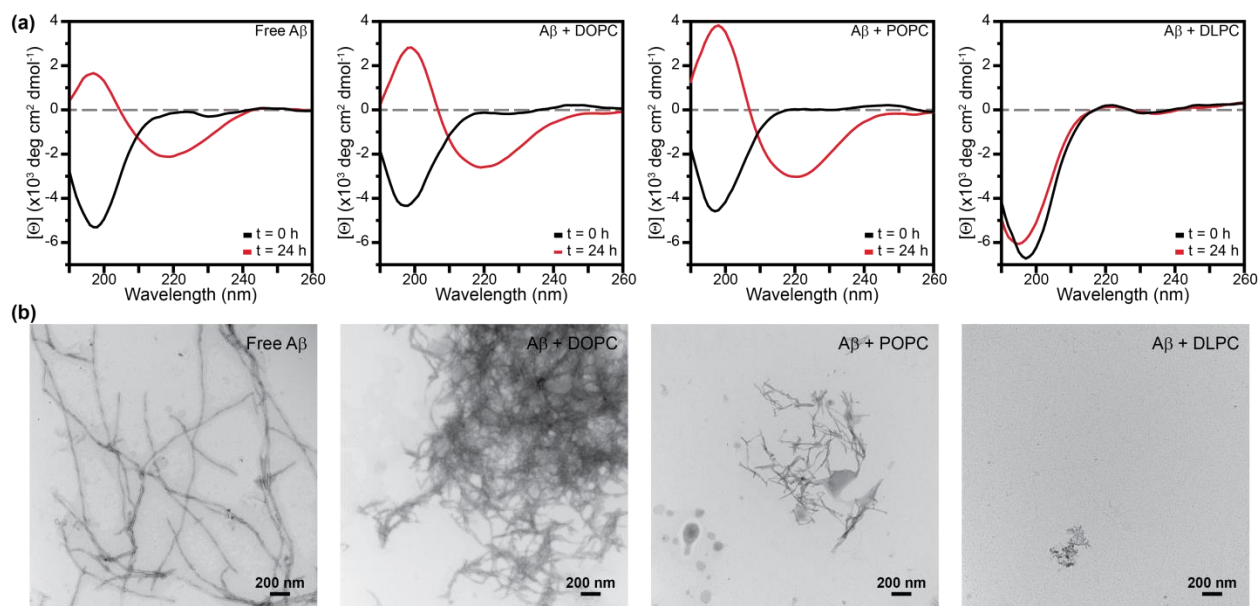
Figure C.1. Aβ aggregate secondary structure and morphology. (a) Aβ (30 μM) fibrils grown for 24 h in the absence and presence of DOPC, POPC, or DLPC LUVs (300 μM lipid) were compared to freshly prepared, monomeric Aβ by CD. (b) TEM images were acquired of the end stage aggregates after 24 h incubation for each sample used in CD analysis.
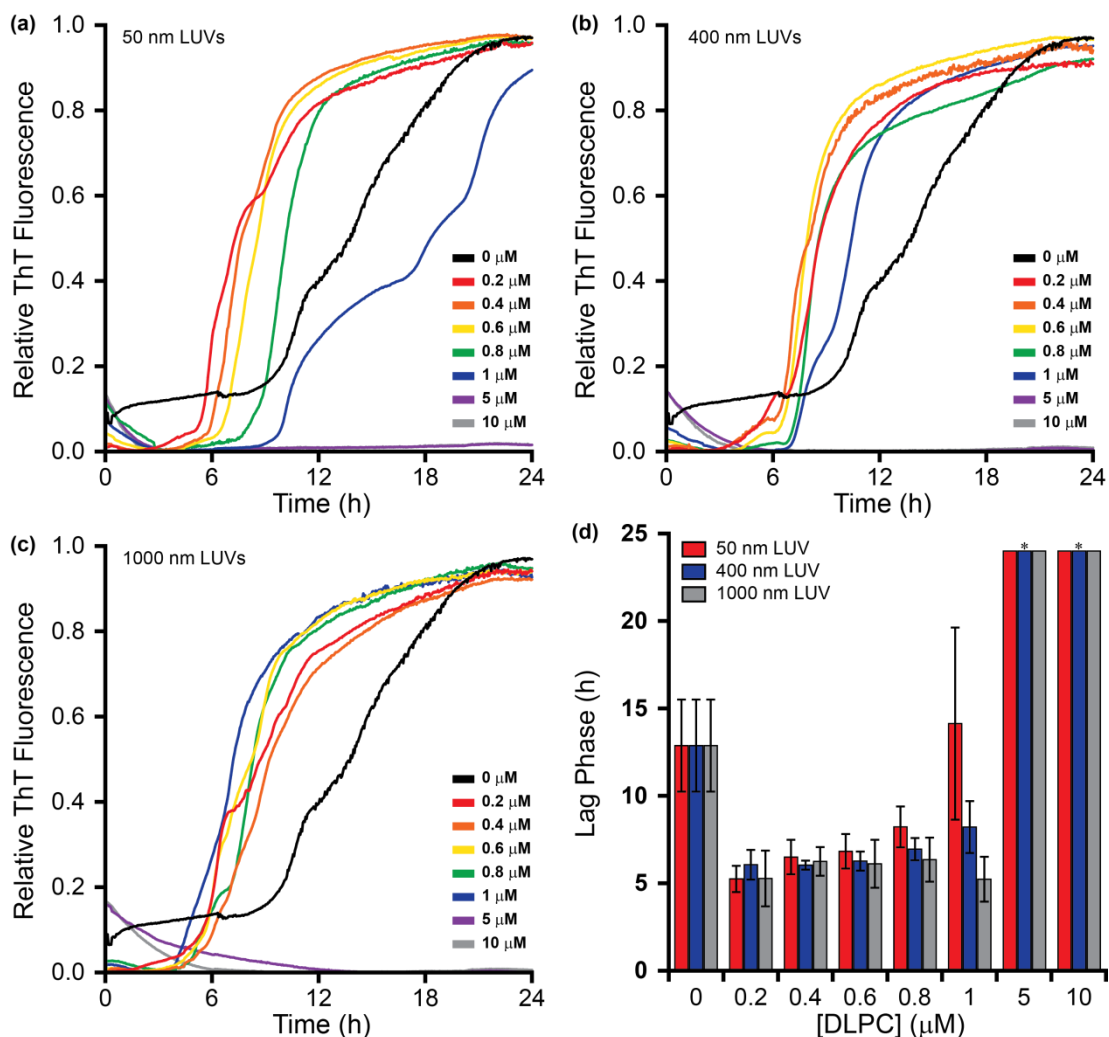
Figure C.2. Role of liposome curvature on DLPC inhibitory activity. LUVs of (a) 50 nm, (b) 400 nm, and (c) 1000 nm were incubated with monomeric Aβ (10 μM) at varying concentrations under aggregation promoting conditions. The kinetics of aggregation were monitored by ThT (20 μM) and the averages of three independent traces are presented. Conditions noted by * exhibited lag phases longer than 24 h which could not be fit within the experimental constraints. (d) Individual aggregation curves were fit to calculate the lag phase of aggregation as a function of DLPC concentration for all three LUV sizes. Values presented represent the average lag phase from three independent trials; error bars represent the standard deviation of three separate experiments.
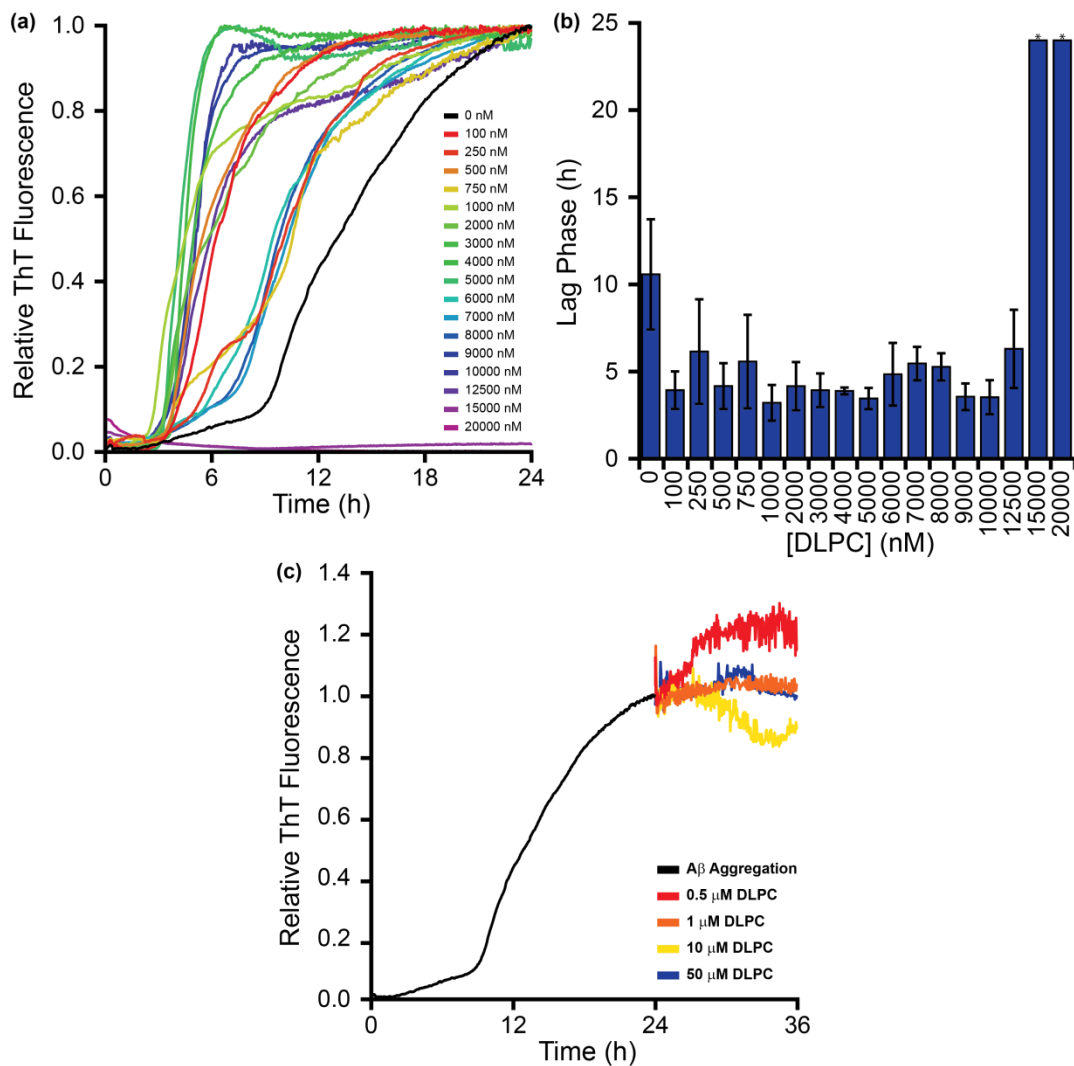
Figure C.3. Efficacy of free DLPC. (a) ThT probed the dose dependent ability of free DLPC to modulate the fibrillation of Aβ. Curves represent the average of three independent traces. (b) Individual aggregation curves were fit to calculate the lag phase of aggregation as a function of free DLPC concentration. Values presented represent the average lag phase; error bars represent the standard deviation of three separate experiments. Conditions noted by * exhibited lag phases longer than 24 h which could not be fit within the experimental constraints. (c) Free DLPC was added to preformed fibrils after 24 h incubation and the change in ThT fluorescence was monitored as a function of time.
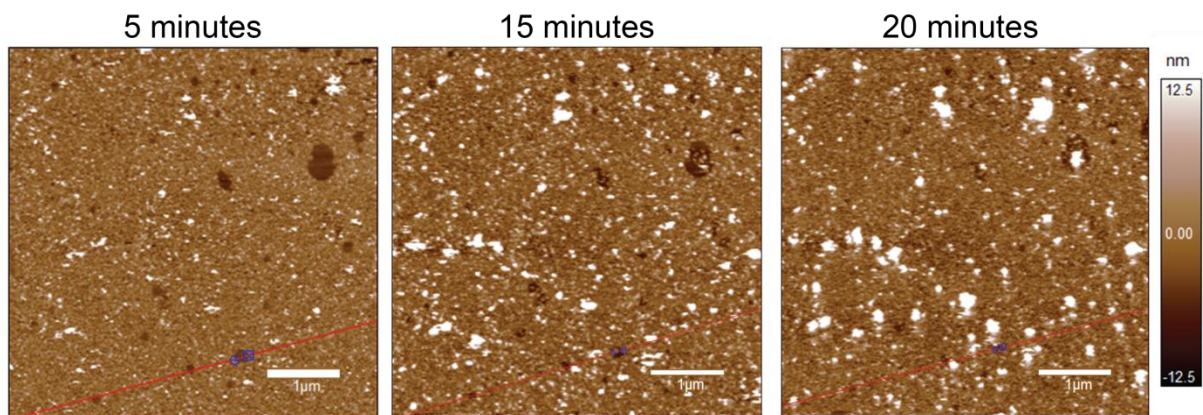
Figure C.4. AFM on DLPC SLBs at early time points. AFM measurements of the same 5 x 5 µm region of a DLPC SLB were taken at early time intervals.
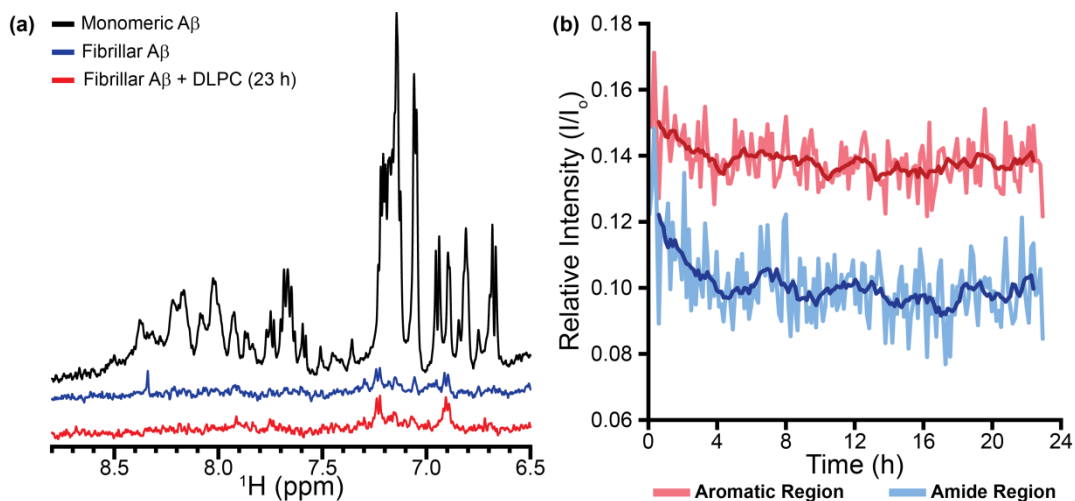
Figure C.5. Monomer observation during fiber remodeling. (a) The 1D ^{1}H spectrum of freshly prepared Aβ (50 μM) was observed prior to fibrillation. After 24 h, the fibrillar sample was again observed prior to the addition of DLPC LUVs (500 μM). (b) The 1D ^{1}H spectrum was subsequently observed at 8 minute intervals for 23 h. The relative intensity (compared to freshly prepared monomeric Aβ) of both the more flexible aromatic region (red) and the more rigid amide region (blue) were plotted versus time. The dark lines represent the moving average over a 40 minute interval.